

Robust Model Identification Methods for Nonlinear Second-Order Plant Models for Underwater Vehicles

by

Tyler Paine

A thesis submitted to The Johns Hopkins University
in conformity with the requirements for the degree of
Master of Science in Engineering

Baltimore, Maryland

May, 2018

© 2018 by Tyler Paine

All rights reserved

Abstract

This thesis addresses the problem of plant parameter model identification for nonlinear finite-dimensional second-order plant models for underwater vehicles from experimental data. These models are necessary for predictive simulation studies, model-based control algorithms, and model-based approaches to fault detection. The structure of these dynamical models can be derived using first principles, but the model parameters such as mass, drag, and thrust coefficients must be determined experimentally. This thesis provides solutions to several parts of this problem.

First, this thesis reports a derivation of a finite dimensional second-order using Newtonian dynamics. The general form of these equation of motion are widely accepted in the research literature, yet their full and detailed derivation using Newtonian dynamics is often omitted. This thesis seeks to address this lacuna.

Second, this thesis reports an extension of an adaptive identifier (AID) to underactuated, three degree of freedom underwater vehicles. Results of a simulation study are reported. Additionally, the same AID is extended to simultaneously identify plant and control parameters for six degree of freedom underwater vehicles. Another extension of the same AID is reported for plant models with diagonal mass and drag matrices. Stability proofs are reported for all new AIDs.

Finally, this thesis reports a new algorithm to estimate the parameters of dynamical plants using framework of the random sample consensus (RANSAC) algorithm. This new algorithm is shown in simulation to outperform traditional least squares parameter identification methods with respect to accuracy when observational data is corrupted by non-Gaussian noise.

Thesis Adviser

Louis Whitcomb
Professor
Department of Mechanical Engineering
Johns Hopkins University

Acknowledgments

I can trace any ability I have, however limited they all may be, to one or more mentors who have taught me along the way. This particular work is a product the mentorship I received from several people. They did not need to devote extra time to help me, but they did, and I am grateful to each of them for it.

In chronological order they are:

- Mr. Whiteman, my middle school mathematics teacher.
- Dr. Daniel Miller, my undergraduate statics and dynamics professor at Montana State University.
- Joel Galles, my first professional engineering mentor at the Naval Undersea Warfare Center Division Keyport.
- Dr. Louis Whitcomb, my masters program advisor at Johns Hopkins University and the advisor of this thesis.

Their time and effort is not lost on me, and I hope I can fully repay it in kind by being a mentor to others.

Errata

The original thesis was submitted to the library at Johns Hopkins University in May 2018. This version can be found here: <https://jscholarship.library.jhu.edu/handle/1774.2/59285>

Corrections and clarifications made after initial submission are listed by date.

June 2020:

- Equation 2.23 and associated sentence were corrected to include the contribution of the body force to the moment as seen in the world frame.
- Equations 2.54 through 2.60 were corrected to properly show the cancellation of terms in the change of world to body frames. The original argument was wrong, but the results were the same.
- Discussion was added to better explain the effects of added mass on the Coriolis forces. In particular why rotational Coriolis forces can appear even with only translational velocities are present. This discussion was added to existing observations in a new subsection 2.6.1.
- The 3-DOF velocity vector was added to the expressions in 2.145, 2.146, and 2.148 for clarity. The associated sentences were updated accordingly.

Thank you to Dr. Louis Whitcomb and Abhimanyu Shah for help with these corrections.

Please email me at tpaine1@jhu.edu if you find more errors. Thank you!

Table of Contents

Table of Contents	vi
List of Tables	ix
List of Figures	x
1 Introduction	1
2 Dynamics of Underwater Vehicles	4
2.1 Rigid Body Kinematics in the Body Fixed COM Frame	7
2.2 Rigid Body Kinematics in the Body Fixed “L” Frame	12
2.3 Hydrodynamic EOM in the Body Fixed COM Frame	14
2.4 Hydrodynamic EOM in the Body Fixed “L” Frame	18
2.5 Rigid Body EOM	24
2.6 Complete 6-DOF EOM in the Body Fixed “L” Frame	25
2.6.1 Structural Observations of 6-DOF EOM	26
2.7 Complete 3-DOF EOM in the Body Fixed “L” Frame	30
3 Adaptive Identification of Plant and Actuation Parameters of Underactuated UUVs	37
3.1 Introduction	37
3.2 Literature Review	38

3.3	Adaptive Identification of 3-DOF UUV Plant Parameters	41
3.3.1	Problem Statements	41
3.3.2	AID Extension to 3-DOF UUV Plants	42
3.3.2.1	AID Results in Simulation Studies of Fully Actuated 3-DOF UUVs	45
3.3.2.2	AID Results in Simulated, Underactuated, 3-DOF UUV	48
3.3.3	Discussion	50
3.4	Adaptive Identification of Plant and Actuation Parameters for 6-DOF UUVs	51
3.4.1	Problem Statements	51
3.4.2	AID of Plant and Actuation Parameters for Fully Coupled 6-DOF UUVs . . .	53
3.4.3	Extension of AID to 6-DOF UUV Plants with Diagonal Mass and Drag Matrices	57
4	Identification of Dynamical UUV Plants with Random Sample Consensus (RANSAC)	61
4.1	Introduction	61
4.2	Literature Review	62
4.2.1	Advances in the RANSAC Algorithm	62
4.2.2	Reported Implementations of the RANSAC Algorithm	63
4.3	Methodology	64
4.3.1	Check if the Solution is Well Defined	65
4.3.2	Preliminary Test	67
4.3.3	Forward Simulation and Model Fit Error	67
4.3.4	Inlier Classification and Early Exit Criteria	68
4.3.5	Parameter Identification Methods	69
4.4	Simulated 1-DOF Experimental Setup	71
4.5	Results	73

4.5.1	Simulated 1-DOF Data	73
4.5.2	Discussion	74
5	Conclusion	76
5.1	Future Work	77
	Appendices	78
A	On the Relationship Between “Derivative” and “Integral” Methods used in Least Squares	
	Parameter Estimation of Dynamical Plant Models	79
A.1	Regressor Matrix Formulation using “Derivative Method”	80
A.2	Regressor Matrix Formulation using “Integral Method”	82
A.3	Relationship Between the Nullspaces of the “Derivative Method” and “Integral Method”	84
	Bibliography	89
	CV	93

List of Tables

3.1	Standard Deviation σ of Added Noise	46
3.2	Mean Absolute Error of Simulated, Fully Actuated 3-DOF UUV Plant Using Identified Parameters	48
3.3	Mean Absolute Error of Simulated, Underactuated 3-DOF UUV Plant Using Identified Parameters	48

List of Figures

2.1	Illustration of coordinate frames	6
3.1	Simulation of the fully actuated, JHU ROV in three degrees of freedom with measurement noise	47
3.2	Simulation of the underactuated, JHU ROV in three degrees of freedom with measurement noise	49
3.3	Evaluation of the Lyapunov function in simulation of both a fully actuated (V_{FA}) and under actuated (V_{UA}) three degree of freedom (3-DOF) unmanned underwater vehicle (UUV)	50
4.1	Mean absolute error of plant velocities when using parameters identified from data with an increasing ratio of measurement outliers	74
4.2	One degree of freedom plant velocity in forward simulation using parameters identified by each method. Fraction of outliers = 0.13	75

Chapter 1

Introduction

The undersea environment continues to be an active area of interest for its natural resources, strategic military opportunities, many scientific frontiers, and a growing tourism industry. This environment is extreme and in many cases inaccessible to humans directly. For these reasons, unmanned underwater vehicles (UUVs) are designed and operated to extend our access to the subsea environment. Modern UUVs have a long history starting in 1866 with the invention of the first mechanically controlled, self-propelled submersible torpedo [16] which was followed by widespread use of simple guided torpedoes in World War I. Since World War I, UUVs have continued to become more capable and many different types of UUVs are currently deployed on scientific explorations, used to build and maintain critical undersea infrastructure, and utilized during national defense operations.

State-of-the-art UUVs are often equipped with large instrumentation suites to measure velocities, depth, and attitude along with other signals, and employ on-board computers to deploy algorithms for navigation, control, and other autonomous behaviors. There are a wide range of reported actuation methods of modern UUVs including conventional thrusters, control surfaces and other bio-inspired mechanisms [44], [27], [20], and [6]. However, operational performance of UUVs is often contingent on accurate identification of dynamical plant and actuation models that are unique to the configuration of each vehicle. Accurate model identification is required for

predictive simulation studies, the design and tuning of model-based UUV navigation and control algorithms, and model-based approaches to fault detection.

The general structure of the finite-dimensional dynamical plant model for UUVs is widely accepted, and a complete derivation of the equations of motion (EOM) is presented in Chapter 2. Additionally, the structure of many types of control models have been reported and experimentally verified by several researchers such as those in [41], [27], and [6]. However, all plant and actuator parameters such as added mass, drag, and control fin coefficients must be determined experimentally.

There are several reported approaches to estimating these plant and actuator parameters, sometimes called parameter identification or model fitting. These approaches include least squares methods, adaptive methods, Kalman filters and their nonlinear extensions, and other machine learning or neural net methods. This thesis reports two new approaches to estimating parameters of both UUV plants and actuator models; one approach extends a previously reported adaptive identifier (AID) to estimate actuator-model parameters in addition to plant parameters of underactuated UUVs, and the second approach implements a random sample consensus (RANSAC) algorithm for robust estimation of dynamical models. Both new approaches offer advantages over other existing methods. The AID extension enables the AID to estimate more parameters, and the algorithm based on the RANSAC framework provides more robust estimation in the from experimental data with non-Gaussian noise.

This thesis is organized in the following manner: Chapter 2 presents the derivation of the widely accepted EOM applicable to all underwater vehicles using Newtonian dynamics. EOM are reported for both the general six degree of freedom (6-DOF) class of UUVs and the three degree of freedom (3-DOF) class of UUVs with motion in only the surge, sway, and heading directions. Chapter 3 reports an extension of the AID reported in [36] for underactuated vehicles in 3-DOF. Performance of this extension is evaluated in a simulation study of a 3-DOF UUV. Chapter 3 also reports an extension of the AID to simultaneously evaluate the control parameter

identification for 6-DOF unmanned underwater vehicles (UUVs). Preliminary proofs of stability are reported for all new AIDs. Finally, Chapter 4 presents a new algorithm based on the RANSAC framework entitled "Dynamical Plant Identification using RANSAC" (DIRANSAC) that is designed to identify dynamical plant parameters in the presence of noisy experimental data with outliers. The performance of the DIRANSAC algorithm is evaluated in a simulated study of a one degree of freedom (1-DOF) UUV.

Chapter 2

Dynamics of Underwater Vehicles

This chapter presents a derivation of the six degree of freedom (6-DOF) equations of motion (EOM) for fully submerged underwater vehicles using classical Newtonian dynamics. This entire chapter draws substantially from published work on the dynamics of rigid-body underwater vehicles done by Steve Martin, Louis Whitcomb,[31], Thor Fossen [12], and others as cited. This derivation and the resulting final dynamical equations for underwater vehicles are not new. However, this section aims to present a complete and thorough derivation of these often-cited dynamical equations. Often only the final results are published without disclaimers and without stating the underlying assumptions. The step-by-step derivation of the EOM presented here allows for the possibility of several structural observations.

Many mathematical models and derivations of the EOM of underwater vehicles are reported. The first finite-dimensional mathematical models for underwater vehicles were developed at the US Navy's David Taylor Model Basin beginning in the 1950s [13] [14]. In 1961 Imlay in [23] reported an expansion of these models to include more complete definitions of added mass. Revisions to these early mathematical models were reported in 1979 by Feldman [9], and these revisions include the clarification on the definition of notation, coordinate systems, and sign convention. These early mathematical models were reported without derivation.

Sagatun in [12] reports a derivation of the EOM for marine vehicles using Lagrangian Dynamics, and Fossen in [12] reports an approach using the quasi-Lagrangian approach. In addition,

McFarland in [37] approaches the problem by making extensive use of the properties of the Special Euclidean group $SE(3)$ and the associated Lie Algebra $se(3)$. These other approaches have several advantages, including the use of generalized coordinates in Lagrangian formulations and manifolds in $SE(3)$ formulations. The reader is referred to these studies for additional details.

The Newtonian approach builds from familiar first principles, starting with Newton's second law which states that the sum of the forces, $\sum {}^w f$, acting on the vehicle is equal to the time derivative of linear momentum

$$\sum {}^w \vec{f} = \frac{d}{dt} [{}^w M {}^w \dot{x}] = {}^w \dot{M} {}^w \dot{x} + {}^w M {}^w \ddot{x}, \quad (2.1)$$

where ${}^w M \in \mathbb{R}^{3 \times 3}$ is the vehicle mass matrix and ${}^w \dot{x} \in \mathbb{R}^3$ its linear velocity, both as seen in the world frame denoted by the superscript "w". Newton's second law also states that the sum of the moments, $\sum {}^w t$, is equal to the time derivative of angular momentum of a rigid body about the origin of the world frame

$$\sum {}^w \vec{t} = \frac{d}{dt} [{}^w I {}^w \vec{\omega} + {}^w x \times {}^w M {}^w \dot{x}] \quad (2.2)$$

$$= {}^w \dot{I} {}^w \vec{\omega} + {}^w I {}^w \dot{\vec{\omega}} + {}^w \dot{x} \times {}^w M {}^w \dot{x} + {}^w x \times \frac{d}{dt} [{}^w M {}^w \dot{x}], \quad (2.3)$$

where ${}^w I \in \mathbb{R}^{3 \times 3}$ is the moment of inertia matrix of the vehicle and ${}^w \omega \in \mathbb{R}^3$ its angular velocity. The vector cross product is denoted as \times and its relationship to the $J(\cdot)$ operator is defined in (2.11).

Upon inspection of (2.1) and (2.3) we can see that all the terms are defined to be relative to a world frame which is assumed to be an inertial reference frame. This is an essential assumption mandated by Newton's first law. However, we will find it advantageous to rewrite (2.1) and (2.3) to contain only velocities as measured relative to the body frame of the vehicle and the time derivative of these so called body velocities. The body frame is not an inertial frame of reference and may seem awkward at first, but this arrangement affords some key conveniences. First this formulation allows for the mass and inertia matrices to be defined such that they are constant. It

is also convenient for many underwater vehicles to be instrumented with sensors that directly measure motions relative to the body frame.

With this goal in mind, we define the following coordinate frames in Fig 2.1:

- The world frame “ w ” is an inertial frame of reference.
- The body frame “ b ” is a body fixed frame coincident with the center of mass (COM) and aligned along the principal axis.
- The body frame “ L ” is an arbitrary body fixed frame, with the same orientation as the “ b ” frame but offset from the “ b ” frame by the vector ℓ . In practice a common location of the “ L ” frame is the center of pressure.

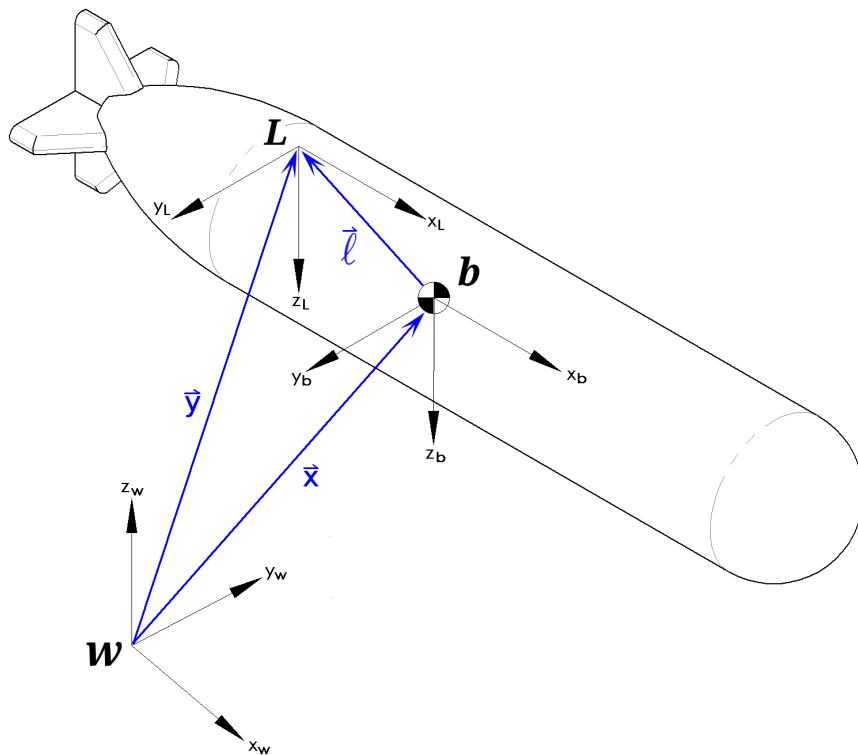


Figure 2.1: Illustration of coordinate frames

The remainder of this Chapter is organized as follows: Section 2.1 reports a derivation of rigid body kinematics in the body center of mass frame. Section 2.2 reports a derivation of rigid

body kinematics in the “ L ” frame not coincident with the center of mass. Section 2.3 reports a derivation of the hydrodynamics of underwater vehicles relative to the “ b ” or COM frame. Section 2.4 reports a derivation of the hydrodynamics of underwater vehicles relative relative to the “ L ” frame. Section 2.5 reports a derivation of the rigid body dynamics of underwater vehicles. Section 2.6 reports a complete derivation of of the EOM of 6-DOF underwater vehicles by combining the hydrodynamic and rigid body terms. Finally, Section 2.7 reports a derivation of the common three degree of freedom (3-DOF) class of vehicles where only the surge, sway, and heading of the vehicle are considered.

2.1 Rigid Body Kinematics in the Body Fixed COM Frame

In Fig 2.1 ${}^w x(t)$ is the vector from the origin of the world frame to the origin of the COM frame of the vehicle relative to, or as measured in, the world frame. We denote the COM frame as the “ b ” frame. The orientation or attitude of the vehicle relative to the world frame is defined by the vector $\vec{a}(t)$. We use Euler Angles to parameterize the orientation of the underwater vehicle which have an intuitive interpretation of roll pitch and yaw, but they exhibit a singularity at pitch angles of $\pm\pi/2$. However, this orientation is rare for many underwater vehicles. We define the non-inertial body velocity ${}^b v_x$ as the velocity of the underwater vehicle in the “ w ” frame (denoted as $\dot{x}(t)$) projected instantaneously on the body fixed frame b . Mathematically,

$${}^b v_x = {}^b_w R(\vec{a}) {}^w \dot{x}(t), \quad (2.4)$$

where the subscript x refers to the vector from the world frame to the “ b ” frame. The coordinate transformation ${}^b_w R(\vec{a})$ describes the orientation of vectors in the world frame as they appear in the b frame. ${}^b_w R(\vec{a})$ is clearly a function of $\vec{a}(t)$, and regardless of the chosen parameterization of $\vec{a}(t)$, ${}^b_w R(\vec{a})$ is always a member of the group of rigid body rotations $SO(3)$. The group $SO(3)$ is defined as

$$SO(3) = \{R \in \mathbb{R}^3 : R^T R = I, \det(R) = +1, \} \quad (2.5)$$

The inverse of the rotation matrix ${}^b_w R(\vec{a})$ is defined by the properties of group $SO(3)$ as

$${}^b_w R^{-1}(\vec{a}) = {}^b_w R^T(\vec{a}) = {}^w_b R(\vec{a}). \quad (2.6)$$

Here ${}^w_b R(\vec{a})$ can be physically interpreted as a rotation matrix that describes the orientation of vectors in the body frame as they appear in the world frame. Secondly, there is an important relationship between the $\frac{d}{dt} [{}^w_b R(\vec{a})]$ and the angular velocity of the COM frame. We start with the inverse property of $SO(3)$ and take the time derivative to yield

$${}^w_b R(\vec{a}) {}^w_b R^T(\vec{a}) = I \quad (2.7)$$

$$\frac{d}{dt} [{}^w_b R(\vec{a}) {}^w_b R^T(\vec{a})] = \frac{d}{dt} I \quad (2.8)$$

$${}^w_b \dot{R}(\vec{a}) {}^w_b R^T(\vec{a}) + {}^w_b R(\vec{a}) {}^w_b \dot{R}^T(\vec{a}) = 0 {}^w_b \dot{R}(\vec{a}) {}^w_b R^T(\vec{a}) = - \left({}^w_b \dot{R}(\vec{a}) {}^w_b R^T(\vec{a}) \right)^T. \quad (2.9)$$

Clearly ${}^w_b \dot{R}(\vec{a}) {}^w_b R^T(\vec{a})$ is skew symmetric. We define the instantaneous angular velocity of the body as seen in the world frame denoted as ${}^w \vec{\omega} = [\omega_{x_o}; \omega_{y_o}; \omega_{z_o}]$ to be

$$J({}^w \vec{\omega}) = {}^w_b \dot{R}(\vec{a}) {}^w_b R^T(\vec{a}), \quad (2.10)$$

where the mapping $J : \mathbb{R}^3 \mapsto SK(3) \in \mathbb{R}^{3 \times 3}$ defined as

$$J \left(\begin{array}{c} a \\ b \\ c \end{array} \right) = \begin{bmatrix} 0 & -c & b \\ c & 0 & -a \\ -b & a & 0 \end{bmatrix}. \quad (2.11)$$

The operator J is often described as the skew symmetric operator and is related to vector cross product operation (denoted as \times) where $\vec{a} \times \vec{b} = J(\vec{a})\vec{b}$.

We define the instantaneous body angular velocity as the spacial velocity projected onto the b frame

$$J({}^b \vec{\omega}) = {}^w_b R^T(\vec{a}) {}^w_b \dot{R}(\vec{a}). \quad (2.12)$$

Furthermore the relationship between ${}^w\vec{\omega}$ and ${}^b\vec{\omega}$ is

$$J({}^b\vec{\omega}) = {}^wR^T(\vec{a}) J({}^w\vec{\omega}) {}^wR(\vec{a}) \quad (2.13)$$

or

$${}^b\vec{\omega} = {}^wR^T(\vec{a}) {}^w\vec{\omega}. \quad (2.14)$$

We also note for all $R \in SO(3)$ that R distributes over the cross product thus $\forall p_1, p_2 \in \mathbb{R}^3$

$$R(p_1 \times p_2) = Rp_1 \times Rp_2 \quad (2.15)$$

$$RJ(p_1)p_2 = J(Rp_1)Rp_2. \quad (2.16)$$

Returning again to (2.1) and (2.3) we note that these equations contain linear acceleration ${}^w\ddot{x}$ and the angular acceleration ${}^w\dot{\vec{\omega}}$ of the vehicle both referenced to the world frame “ w ”. Again it will be advantageous to express these terms as the time derivatives of linear body velocities ${}^b\dot{v}_x$ and angular body velocities ${}^b\dot{\vec{\omega}}$.

We start with finding an expression for ${}^w\ddot{x}$ by multiplying both sides of (2.4) by ${}^wR(\vec{a})$, rearranging and taking the time derivative, and substituting in (2.12) which yields

$$\frac{d}{dt} {}^w\dot{x}(t) = \frac{d}{dt} [{}^wR(\vec{a}) {}^b\dot{v}_x] \quad (2.17)$$

$${}^w\ddot{x}(t) = {}^w\dot{R}(\vec{a}) {}^b\dot{v}_x + {}^wR(\vec{a}) {}^b\ddot{v}_x \quad (2.18)$$

$$= {}^wR(\vec{a}) J({}^b\vec{\omega}) {}^b\dot{v}_x + {}^wR(\vec{a}) {}^b\ddot{v}_x \quad (2.19)$$

$$= {}^wR(\vec{a}) \left(J({}^b\vec{\omega}) {}^b\dot{v}_x + {}^b\ddot{v}_x \right). \quad (2.20)$$

An expression for ${}^b\dot{\vec{\omega}}$ is found by taking the time derivative of (2.14) to yield

$${}^b\dot{\vec{\omega}} = {}^wR(\vec{a}) {}^w\dot{\vec{\omega}}. \quad (2.21)$$

Force and moment vectors on the left side of (2.1) and (2.3) respectively can also be defined relative

to the body frame as

$${}^w \vec{f} = {}^w R(\vec{a}) {}^b \vec{f} \quad (2.22)$$

$${}^w \vec{t} = {}^w R(\vec{a}) {}^b \vec{t} + J({}^w x) {}^w \vec{f}. \quad (2.23)$$

The sum of moments in the world frame includes the contribution from the forces acting on the vehicle body at the moment arm ${}^w x$.

Lastly expressions for ${}^w \dot{M}$ and ${}^w \dot{I}$ can be found by first noting the following similarity relationship between the “ w ” and “ b ” frame,

$${}^w M = {}^b R^T(\vec{a}) {}^b M {}^b R(\vec{a}) \quad (2.24)$$

$${}^w I = {}^b R^T(\vec{a}) {}^b I {}^b R(\vec{a}), \quad (2.25)$$

where ${}^w I$ and ${}^w M$ are both positive definite symmetric (PDS), time varying matrices expressed relative to the “ w ” frame coordinate system. By matrix similarity ${}^b I$ and ${}^b M$ are also both PDS matrices, but expressed relative to the “ b ” frame coordinate system. ${}^b I$ and ${}^b M$ are assumed to be constant, or equivalently the mass and the inertia of many underwater vehicles do not change when measured relative to a body fixed frame. This time invariance assumption can be justified for many classes of unmanned underwater vehicles (UUVs).

The similarity relationship in (2.24) and (2.25) is widely accepted and can be quickly justified using a simple example. Say we define an inertial frame “ j ” and ${}^j \vec{\zeta}$ is the acceleration a body the with a mass matrix ${}^j M$ subject to a net force ${}^j \vec{f}$ with the superscript j denoting all are relative to the “ j ” frame. From Newton’s second law the three are related by

$${}^j \vec{f} = {}^j M {}^j \vec{\zeta} \quad (2.26)$$

We assume there is another reference frame “ k ” and the rotation matrix ${}^k R$ is the transformation between frame “ j ” and frame “ k ”. Both the force and acceleration vectors can be expressed in the

“ k ” frame as ${}^k\vec{f} = {}^kR {}^j\vec{f}$ and ${}^k\vec{\zeta} = {}^kR {}^j\vec{\zeta}$, respectively. Substituting these into (2.26) and using a property of $SO(3)$ yields

$${}^jR {}^k\vec{f} = {}^jM {}^jR {}^k\vec{\zeta} \quad (2.27)$$

$${}^k\vec{f} = {}^jR^T {}^jM {}^jR {}^k\vec{\zeta} \quad (2.28)$$

$${}^k\vec{f} = {}^kM {}^k\vec{\zeta}. \quad (2.29)$$

This similarity transformation is still applicable even if the coordinate frames “ j ” and “ k ” are non-inertial coordinate frames.

Since bI and bM are both assumed time invariant, we use the product rule to get time derivatives of (2.24) and (2.25) as

$${}^w\dot{M} = {}^bR^T(\vec{a}) {}^bM {}^bR(\vec{a}) + {}^bR^T(\vec{a}) {}^bM {}^b\dot{R}(\vec{a}) \quad (2.30)$$

$${}^w\dot{I} = {}^bR^T(\vec{a}) {}^bI {}^bR(\vec{a}) + {}^bR^T(\vec{a}) {}^bI {}^b\dot{R}(\vec{a}). \quad (2.31)$$

Substituting (2.12) yields

$${}^w\dot{M} = {}^bR^T(\vec{a}) J({}^b\omega) {}^bM {}^bR(\vec{a}) + {}^bR^T(\vec{a}) {}^bM J({}^b\omega)^T {}^bR(\vec{a}) \quad (2.32)$$

$${}^w\dot{I} = {}^bR^T(\vec{a}) J({}^b\omega) {}^bI {}^bR(\vec{a}) + {}^bR^T(\vec{a}) {}^bI J({}^b\omega)^T {}^bR(\vec{a}). \quad (2.33)$$

2.2 Rigid Body Kinematics in the Body Fixed “L” Frame

It can be advantageous to write the EOM for underwater vehicles in an arbitrary body fixed frame that is not the COM or “b” frame. We will denote this arbitrary frame as the “L” frame. There are several reasons one might find this change of frame helpful. First, it can be difficult to measure dimensions relative to the center of mass that are needed for sensor offset kinematics and alignment. Additionally, it is common in naval engineering to write the EOM of a vessel relative to the ship’s pivot point, or the point on an underactuated vessel which the ship pivots about during turning maneuvers. Seo in [46] reviews the definition of the pivot point in surface vessels, which may also be applicable to underactuated underwater vehicles. It is also common practice to utilize body frames that are not located at the center of mass when in designing control algorithms. An example may be found in the trajectory tracking controllers reported in [30].

In a similar manner as (2.4) we define the translational body velocity of the “L” frame to be the instantaneous projection of ${}^w\dot{y}$ onto the body frame. Mathematically,

$${}^b v_y = {}^b_w R(\vec{a}) {}^w \dot{y}, \quad (2.34)$$

where the subscript y denotes the position vector y and the superscript b denotes the body frame. In this derivation the orientation of the “L” frame will be defined to be the same as the orientation of the “b” frame. To state this explicitly

$${}^w_L R(\vec{a}) = {}^w_b R(\vec{a}) {}^b_L R \quad (2.35)$$

$$= {}^w_b R(\vec{a}) I_{3 \times 3} \quad (2.36)$$

$$= {}^w_b R(\vec{a}). \quad (2.37)$$

For convenience we will continue to use the notation for the “b” frame in transformations between the world and body frames. However, if there is a time invariant transformation between the two frames “L” and “b”, or mathematically ${}^b_L R \neq I_{3 \times 3}$, then the following derivation would need to be

modified accordingly to reflect (2.35) and

$${}^w_L \dot{R}(\vec{a}) = {}^w_b \dot{R}(\vec{a}) {}^b_L R. \quad (2.38)$$

Similar to (2.21) differentiating (2.34) yields

$${}^w \ddot{y} = {}^w_b R(\vec{a}) \left(J({}^b \vec{\omega}) {}^b v_y + {}^b \dot{v}_y \right). \quad (2.39)$$

The position of the “L” frame relative to the “b” frame is

$${}^w y = {}^w x + {}^w_b R(\vec{a}) {}^b \ell. \quad (2.40)$$

We need an expression for ${}^b v_y$. Taking the time derivative yields

$${}^w \dot{y} = {}^w \dot{x} + {}^w_b \dot{R}(\vec{a}) {}^b \ell \quad (2.41)$$

$$= {}^w \dot{x} + {}^w_b R(\vec{a}) J({}^b \omega) {}^b \ell \quad (2.42)$$

$$= {}^w \dot{x} + {}^w_b R(\vec{a}) J^T({}^b \ell) {}^b \omega. \quad (2.43)$$

Substituting in (2.4) and (2.34) and multiply by ${}^w_b R^T(\vec{a})$ results in

$${}^w_b R(\vec{a}) {}^b v_y = {}^w_b R(\vec{a}) {}^b v_x + {}^w_b R(\vec{a}) J^T({}^b \ell) {}^b \omega \quad (2.44)$$

$${}^b v_y = {}^b v_x + J^T({}^b \ell) {}^b \omega, \quad (2.45)$$

or equivalently,

$${}^b v_x = {}^b v_y + J({}^b \ell) {}^b \vec{\omega}. \quad (2.46)$$

The expression for the time derivative of ${}^b v_x$ can be found by simply taking the time derivative of both sides which results in

$${}^b \dot{v}_x = {}^b \dot{v}_y + J({}^b \ell) {}^b \dot{\vec{\omega}}. \quad (2.47)$$

And lastly, we note that the mass matrix in the “L” frame is equivalent to the mass matrix in the “b” frame, *i.e.* ${}^\ell M = {}^b M$. This is a consequence of (2.24) and the assumption (2.37). We will use ${}^b M$

for convenience. The relationship between the moment of inertia in the “ L ” frame and the moment of inertia in the “ b ” frame is defined using the generalized principal axis theorem [24], thus

$${}^\ell I = {}^b I + J^T({}^b \ell) {}^b M J({}^b \ell). \quad (2.48)$$

2.3 Hydrodynamic EOM in the Body Fixed COM Frame

The hydrodynamics of underwater vehicles relative to the “ b ” frame can be completed by returning to the definitions of Newton’s Second Law in (2.1) and (2.3). In the case of hydrodynamics the matrices ${}^w M$ and ${}^w I$ contain terms often referred to as added mass, mass ascension, apparent mass, virtual mass and hydrodynamic added mass in the naval dynamics literature [31] [12] [22]. We will consider them to be positive definite symmetric (PDS). Additionally, we define the net hydrodynamic force and moment acting on the vehicle to be ${}^w \vec{f}_H$ and ${}^w \vec{t}_H$, respectively.

Starting with the linear degrees of freedom we can substitute (2.32), (2.4), (2.24), and (2.20) into (2.1), thus

$$\begin{aligned} {}^w \vec{f}_H &= {}^b_w R^T(\vec{a}) J({}^b \omega) {}^b M {}^b_w R(\vec{a}) {}^b_w R^T(\vec{a}) {}^b v_x + {}^b_w R^T(\vec{a}) {}^b M J({}^b \omega)^T {}^b_w R(\vec{a}) {}^b_w R^T(\vec{a}) {}^b v_x \\ &\quad + {}^b_w R^T(\vec{a}) {}^b M {}^b_w R(\vec{a}) {}^b_w R(\vec{a}) \left(J({}^b \vec{\omega}) {}^b v_x + {}^b \dot{v}_x \right) \end{aligned} \quad (2.49)$$

$$\begin{aligned} &= {}^b_w R^T(\vec{a}) J({}^b \omega) {}^b M {}^b v_x + {}^b_w R^T(\vec{a}) {}^b M J({}^b \omega)^T {}^b v_x \\ &\quad + {}^b_w R^T(\vec{a}) {}^b M J({}^b \vec{\omega}) {}^b v_x + {}^b_w R^T(\vec{a}) {}^b M {}^b \dot{v}_x \end{aligned} \quad (2.50)$$

$$= {}^b_w R^T(\vec{a}) \left(J({}^b \omega) {}^b M {}^b v_x + {}^b M {}^b \dot{v}_x \right). \quad (2.51)$$

Substituting in (2.22) to the left hand side and multiplying on the left by ${}^b_w R(\vec{a})$ results in

$${}^b_w R(\vec{a}) {}^b \vec{f}_H = {}^b_w R^T(\vec{a}) \left(J({}^b \omega) {}^b M {}^b v_x + {}^b M {}^b \dot{v}_x \right) \quad (2.52)$$

$${}^b \vec{f}_H = J({}^b \omega) {}^b M {}^b v_x + {}^b M {}^b \dot{v}_x. \quad (2.53)$$

For the rotational degrees of freedom we consider (2.3) and (2.23). Using the definition (2.1) the term ${}^w x \times \frac{d}{dt} [{}^w M^w \dot{x}]$ can be canceled as

$${}^w_b R(\vec{a}) {}^b \vec{t} + J({}^w x) {}^w \vec{f} = {}^w I^w \vec{\omega} + {}^w I^w \dot{\vec{\omega}} + {}^w \dot{x} \times {}^w M^w \dot{x} + \cancel{{}^w x \times \frac{d}{dt} [{}^w M^w \dot{x}]} \quad (2.54)$$

$${}^w_b R(\vec{a}) {}^b \vec{t} = {}^w I^w \vec{\omega} + {}^w I^w \dot{\vec{\omega}} + {}^w \dot{x} \times {}^w M^w \dot{x} \quad (2.55)$$

We substitute (2.33), (2.14), (2.25), (2.21), (2.4), and (2.24) into (2.3), and note that $J^T({}^b \omega) {}^b \omega = 0$, and utilize the distributive property of $SO(3)$ in (2.16). These steps result in

$$\begin{aligned} {}^w_b R(\vec{a}) {}^b \vec{t}_H &= {}^b_w R^T(\vec{a}) J({}^b \omega) {}^b I {}^b_w R(\vec{a}) {}^w_b R(\vec{a}) {}^b \omega + {}^b_w R^T(\vec{a}) {}^b I J({}^b \omega)^T {}^b_w R(\vec{a}) {}^w_b R(\vec{a}) {}^b \omega \\ &\quad + {}^b_w R^T(\vec{a}) {}^b I {}^b_w R(\vec{a}) {}^w_b R(\vec{a}) {}^b \dot{\omega} + {}^b_w R^T(\vec{a}) {}^b v_x \times {}^b_w R^T(\vec{a}) {}^b M {}^b_w R(\vec{a}) {}^b_w R^T(\vec{a}) {}^b v_x \end{aligned} \quad (2.56)$$

$$\begin{aligned} &= {}^b_w R^T(\vec{a}) J({}^b \omega) {}^b I {}^b \omega + {}^b_w R^T(\vec{a}) {}^b I J({}^b \omega)^T {}^b \omega \\ &\quad + {}^b_w R^T(\vec{a}) {}^b I {}^b \dot{\omega} + {}^b_w R^T(\vec{a}) {}^b v_x \times {}^b_w R^T(\vec{a}) {}^b M {}^b v_x \end{aligned} \quad (2.57)$$

$$= {}^b_w R^T(\vec{a}) \left(J({}^b \omega) {}^b I {}^b \omega + {}^b I {}^b \dot{\omega} + J({}^b v_x) {}^b_w R^T(\vec{a}) {}^b M {}^b v_x \right). \quad (2.58)$$

Multiplying on the left by ${}^b_w R(\vec{a})$ results in

$${}^b_w R(\vec{a}) {}^w_b R(\vec{a}) {}^b \vec{t}_H = {}^b_w R(\vec{a}) {}^b_w R^T(\vec{a}) \left(J({}^b \omega) {}^b I {}^b \omega + {}^b I {}^b \dot{\omega} + J({}^b v_x) {}^b_w R^T(\vec{a}) {}^b M {}^b v_x \right) \quad (2.59)$$

$${}^b \vec{t}_H = J({}^b \omega) {}^b I {}^b \omega + {}^b I {}^b \dot{\omega} + J({}^b v_x) {}^b_w R^T(\vec{a}) {}^b M {}^b v_x. \quad (2.60)$$

Equations (2.53) and (2.60) can be combined by using the fact that $J(b\omega) {}^b M {}^b v_x = J^T({}^b M {}^b v_x) {}^b \omega$ to yield

$$\begin{bmatrix} {}^b \vec{f}_H \\ {}^b \vec{t}_H \end{bmatrix} = \begin{bmatrix} {}^b M & \mathbf{0}_{3 \times 3} \\ \mathbf{0}_{3 \times 3} & {}^b I \end{bmatrix} \begin{bmatrix} {}^b \dot{v}_x \\ {}^b \dot{\omega} \end{bmatrix} + \begin{bmatrix} \mathbf{0}_{3 \times 3} & J^T({}^b M {}^b v_x) \\ J^T({}^b M {}^b v_x) & J^T({}^\ell I {}^b \dot{\omega}) \end{bmatrix} \begin{bmatrix} {}^b v_x \\ {}^b \dot{\omega} \end{bmatrix} \quad (2.61)$$

$$\begin{bmatrix} {}^b \vec{f}_H \\ {}^b \vec{t}_H \end{bmatrix} = {}^b M_A \begin{bmatrix} {}^b \dot{v}_x \\ {}^b \dot{\omega} \end{bmatrix} + {}^b C_A \begin{bmatrix} {}^b v_x \\ {}^b \dot{\omega} \end{bmatrix}. \quad (2.62)$$

Together the matrices

$${}^b M_A = \begin{bmatrix} {}^b M & \mathbf{0}_{3 \times 3} \\ \mathbf{0}_{3 \times 3} & {}^b I \end{bmatrix} \quad (2.63)$$

and

$${}^b C_A = \begin{bmatrix} \mathbf{0}_{3 \times 3} & J^T({}^b M {}^b v_x) \\ J^T({}^b M {}^b v_x) & J^T({}^\ell I {}^b \dot{\omega}) \end{bmatrix} \quad (2.64)$$

are often referred to as the added mass terms, which are considered radiation induced forces in naval architecture. Here the force and moment vectors ${}^b \vec{f}_H$ and ${}^b \vec{t}_H$ represent the hydrodynamic forces and moments acting on the vehicle. There are many hydrodynamic forces and moments that act on an underwater vehicle, but we consider those that dominate in the hydrodynamic EOM to be the drag terms and buoyancy terms. A discussion concerning the omitted effects of wind, currents, waves, and other external environmental forces is provided in [12].

Infinite-dimensional drag forces acting on underwater vehicles are typically modeled using quadratic drag terms. This model structure is confirmed in experimental results and conclusions in [31] and [37] and is widely used in the literature. Some authors consider other models for drag, and the most common alternative is to use a sum of linear drag and quadratic drag terms [31], [37], [12]. However, we only consider quadratic drag terms in this derivation. This is the most common model in literature and we can justify the omission of the linear drag term using first principles. Linear, or viscous resistance drag dominates systems with very low Reynolds numbers ($Re < 1$). Underwater vehicles of interest here have sizes on the order of m^3 and usually operate at higher Reynolds numbers.

We define the hydrodynamic drag to be the quadratic drag matrix

$${}^b DQ({}^b v_x, {}^b \vec{\omega}) = \sum_{i=1}^3 |v_{x_i}| D_i + \sum_{i=1}^3 |\vec{\omega}_{x_i}| D_i, \quad (2.65)$$

where each PDS drag matrix for the i^{th} degree of freedom ($i = 1, 2, \dots, 6$) is defined as

$${}^b D_i = \begin{bmatrix} {}^b D_{i,1,1} & {}^b D_{i,1,2} & {}^b D_{i,1,3} & {}^b D_{i,1,4} & {}^b D_{i,1,5} & {}^b D_{i,1,6} \\ {}^b D_{i,2,1} & {}^b D_{i,2,2} & {}^b D_{i,2,3} & {}^b D_{i,2,4} & {}^b D_{i,2,5} & {}^b D_{i,2,6} \\ {}^b D_{i,3,1} & {}^b D_{i,3,2} & {}^b D_{i,3,3} & {}^b D_{i,3,4} & {}^b D_{i,3,5} & {}^b D_{i,3,6} \\ {}^b D_{i,4,1} & {}^b D_{i,4,2} & {}^b D_{i,4,3} & {}^b D_{i,4,4} & {}^b D_{i,4,5} & {}^b D_{i,4,6} \\ {}^b D_{i,5,1} & {}^b D_{i,5,2} & {}^b D_{i,5,3} & {}^b D_{i,5,4} & {}^b D_{i,5,5} & {}^b D_{i,5,6} \\ {}^b D_{i,6,1} & {}^b D_{i,6,2} & {}^b D_{i,6,3} & {}^b D_{i,6,4} & {}^b D_{i,6,5} & {}^b D_{i,6,6} \end{bmatrix}. \quad (2.66)$$

Buoyant forces are present in all underwater vehicles that displace water. The net buoyant force of a vehicle with dry mass m , water density ρ , and displaced volume ∇ is

$${}^w \vec{f}_b = {}^w \vec{f}_g - {}^w \vec{f}_{buoy} \quad (2.67)$$

$$= m {}^w \vec{g} - \rho \nabla {}^w \vec{g} \quad (2.68)$$

$$= (m - \rho \nabla) {}^w \vec{g}. \quad (2.69)$$

This formulation follows the convention that negatively buoyant vehicles will sink while positively buoyant vehicles will rise if the sign of the gravity vector ${}^w \vec{g}$ is negative downward. In the “ b ” frame these vectors are defined as

$${}^b \vec{f}_b = {}^b R(\vec{a}) {}^w \vec{f}_b \quad (2.70)$$

$$= {}^b R(\vec{a}) (m - \rho \nabla) {}^w \vec{g}. \quad (2.71)$$

If the center of mass and center of buoyancy are not collocated then these forces induce a righting moment on the vehicle. Define ${}^b r_{cb}$ to be the vector from the “ b ” frame to the center of

buoyancy. Therefore the net righting moment is

$${}^b\tau_b = J({}^br_{cb}) {}^b\vec{f}_{buoy} \quad (2.72)$$

$$= J({}^br_{cb}) {}^b_wR(\vec{a}) (-\rho\nabla)^w\vec{g}. \quad (2.73)$$

Let ${}^b\mathcal{G}(\vec{a})$ be the combined vector of buoyant forces (2.71) and righting moment (2.73) defined as

$${}^b\mathcal{G}(\vec{a}) = \left| \begin{array}{c} {}^b_wR(\vec{a})(m - \rho\nabla)^w\vec{g} \\ J({}^br_{cb}) {}^b_wR(\vec{a}) (-\rho\nabla)^w\vec{g} \end{array} \right| \quad (2.74)$$

Thus we can equate the hydrodynamic terms in the body “b” frame (2.61) to (2.65) and (2.74) as

$$\left| \begin{array}{c} {}^b\vec{f}_H \\ {}^b\vec{t}_H \end{array} \right| = - {}^bDQ({}^bv_x, {}^b\vec{\omega}) \left| \begin{array}{c} {}^bv_x \\ {}^b\vec{\omega} \end{array} \right| + \left| \begin{array}{c} {}^b_wR(\vec{a})(m - \rho\nabla)^w\vec{g} \\ J({}^br_{cb}) {}^b_wR(\vec{a}) (-\rho\nabla)^w\vec{g} \end{array} \right| \quad (2.75)$$

$$= \begin{bmatrix} {}^bM & 0_{3 \times 3} \\ 0_{3 \times 3} & {}^bI \end{bmatrix} \left| \begin{array}{c} {}^b\dot{v}_x \\ {}^b\dot{\vec{\omega}} \end{array} \right| + \begin{bmatrix} 0_{3 \times 3} & J^T({}^bM^b v_x) \\ J^T({}^bM^b v_x) & J^T({}^\ell I^b \vec{\omega}) \end{bmatrix} \left| \begin{array}{c} {}^bv_x \\ {}^b\vec{\omega} \end{array} \right|, \quad (2.76)$$

or, equivalently

$$0 = {}^bM_A \left| \begin{array}{c} {}^b\dot{v}_x \\ {}^b\dot{\vec{\omega}} \end{array} \right| {}^bC_A \left| \begin{array}{c} {}^bv_x \\ {}^b\vec{\omega} \end{array} \right| + {}^bDQ({}^bv_x, {}^b\vec{\omega}) \left| \begin{array}{c} {}^bv_x \\ {}^b\vec{\omega} \end{array} \right| - {}^b\mathcal{G}(\vec{a}). \quad (2.77)$$

2.4 Hydrodynamic EOM in the Body Fixed “L” Frame

Newton’s EOM in a coordinate frame non-coincident with the COM can be found by substituting (2.46) and (2.47) into (2.53), thus

$${}^\ell\vec{f}_H = {}^b\vec{f}_H \quad (2.78)$$

$$= J({}^b\vec{\omega}) {}^bM^b v_x + {}^bM^b \dot{v}_x \quad (2.79)$$

$$= J({}^b\vec{\omega}) {}^bM^b v_y + J({}^b\vec{\omega}) {}^bMJ({}^b\ell) {}^b\vec{\omega} + {}^bM^b \dot{v}_y + {}^bMJ({}^b\ell) {}^b\dot{\vec{\omega}}. \quad (2.80)$$

The torque applied to the body in the “L” frame is defined as the sum of the contribution from moments due to forces in the “b” frame and the net torque in the “b” frame. We note that the ${}^b\ell$

vector is defined relative to the “ b ” frame. Subsequent substitution of (2.80) and (2.60) yields

$${}^{\ell}\vec{t}_H = J^T({}^b\ell) {}^b\vec{f}_H + {}^b\vec{t}_H \quad (2.81)$$

$$\begin{aligned} &= J^T({}^b\ell) \left(J({}^b\vec{\omega}) {}^bM {}^bv_y + J({}^b\vec{\omega}) {}^bMJ({}^b\ell) {}^b\vec{\omega} + {}^bM {}^bv_y + {}^bMJ({}^b\ell) {}^b\dot{\vec{\omega}} \right) \\ &\quad + {}^bI {}^b\dot{\vec{\omega}} + J({}^b\vec{\omega}) {}^bI {}^b\vec{\omega} + J({}^bv_x) {}^bM {}^bv_x. \end{aligned} \quad (2.82)$$

Using the distributive property of cross products $J^T({}^b\ell)$ can be distributed as

$$\begin{aligned} {}^{\ell}\vec{t}_H &= J^T({}^b\ell) J({}^b\vec{\omega}) {}^bM {}^bv_y + J^T({}^b\ell) J({}^b\vec{\omega}) {}^bMJ({}^b\ell) {}^b\vec{\omega} + J^T({}^b\ell) {}^bM {}^bv_y \\ &\quad + J^T({}^b\ell) {}^bMJ({}^b\ell) {}^b\dot{\vec{\omega}} + {}^bI {}^b\dot{\vec{\omega}} + J({}^b\vec{\omega}) {}^bI {}^b\vec{\omega} + J({}^bv_x) {}^bM {}^bv_x. \end{aligned} \quad (2.83)$$

The last term, $J({}^bv_x) {}^bM {}^bv_x$, can be defined as a function of bv_y and ${}^b\vec{\omega}$. Using the relationship (2.46) the last term becomes

$$J({}^bv_x) {}^bM {}^bv_x = J({}^bv_y + J({}^b\ell) {}^b\vec{\omega}) {}^bM ({}^bv_y + J({}^b\ell) {}^b\vec{\omega}) \quad (2.84)$$

$$= J({}^bv_y + J({}^b\ell) {}^b\vec{\omega}) ({}^bM {}^bv_y + {}^bMJ({}^b\ell) {}^b\vec{\omega}) \quad (2.85)$$

$$= ({}^bv_y + J({}^b\ell) {}^b\vec{\omega}) \times ({}^bM {}^bv_y + {}^bMJ({}^b\ell) {}^b\vec{\omega}). \quad (2.86)$$

We can expand this expression following the distributive property of the cross product over addition, *i.e.* $p_1 \times (p_2 + p_3) = (p_1 \times p_2) + (p_1 \times p_3)$. Note for all vectors $p_1, p_2, p_3, p_4 \in \mathbb{R}^3$,

$$(p_1 + p_2) \times (p_3 + p_4) = (p_1 + p_2) \times p_3 + (p_1 + p_2) \times p_4 \quad (2.87)$$

$$= -p_3 \times (p_1 + p_2) - p_4 \times (p_1 + p_2) \quad (2.88)$$

$$= -(p_3 \times p_1) - (p_3 \times p_2) - (p_4 \times p_1) - (p_4 \times p_2) \quad (2.89)$$

$$= (p_1 \times p_3) + (p_2 \times p_3) + (p_1 \times p_4) + (p_2 \times p_4). \quad (2.90)$$

Thus the term $J({}^b v_x) {}^b M {}^b v_x$ becomes

$$\begin{aligned}
({}^b v_y + J({}^b \ell) {}^b \vec{\omega}) \times ({}^b M {}^b v_y + {}^b M J({}^b \ell) {}^b \vec{\omega}) &= - ({}^b M {}^b v_y \times {}^b v_y) - ({}^b M {}^b v_y \times J({}^b \ell) {}^b \vec{\omega}) \\
&\quad - ({}^b M J({}^b \ell) {}^b \vec{\omega} \times {}^b v_y) - ({}^b M J({}^b \ell) {}^b \vec{\omega} \times J({}^b \ell) {}^b \vec{\omega}) \\
&\quad = J({}^b v_y) {}^b M {}^b v_y + J(J({}^b \ell) {}^b \vec{\omega}) {}^b M {}^b v_y \\
&\quad + J({}^b v_y) {}^b M J({}^b \ell) {}^b \vec{\omega} + J(J({}^b \ell) {}^b \vec{\omega}) {}^b M J({}^b \ell) {}^b \vec{\omega}. \quad (2.92)
\end{aligned}$$

Thus the EOM for angular degrees of freedom can be expressed as a function of ${}^b v_y$ and ${}^b \vec{\omega}$ (and their time derivatives) as

$$\begin{aligned}
{}^\ell \vec{t}_H &= J^T({}^b \ell) J({}^b \vec{\omega}) {}^b M {}^b v_y + J^T({}^b \ell) J({}^b \vec{\omega}) {}^b M J({}^b \ell) {}^b \vec{\omega} + J^T({}^b \ell) {}^b M \dot{v}_y \\
&\quad + J^T({}^b \ell) {}^b M J({}^b \ell) \dot{{}^b \vec{\omega}} + {}^b I \dot{{}^b \vec{\omega}} + J({}^b \vec{\omega}) {}^b I \dot{{}^b \vec{\omega}} \\
&\quad + J({}^b v_y) {}^b M {}^b v_y + J(J({}^b \ell) {}^b \vec{\omega}) {}^b M {}^b v_y + J({}^b v_y) {}^b M J({}^b \ell) {}^b \vec{\omega} \\
&\quad + J(J({}^b \ell) {}^b \vec{\omega}) {}^b M J({}^b \ell) {}^b \vec{\omega}. \quad (2.93)
\end{aligned}$$

The two terms $J^T({}^b \ell) J({}^b \vec{\omega}) {}^b M J({}^b \ell) {}^b \vec{\omega}$ and $J(J({}^b \ell) {}^b \vec{\omega}) {}^b M J({}^b \ell) {}^b \vec{\omega}$ can be combined using the fact that cross products satisfy the Jacobi Identity (2.94). We find it more clear to manipulate the Jacobi Identity first and then directly substitute these terms such that the result allows use of the parallel axis theorem, specifically,

$$p_1 \times (p_2 \times p_3) + p_2 \times (p_3 \times p_1) + p_3 \times (p_1 \times p_2) = 0 \quad \forall p_1, p_2, p_3 \in \mathbb{R}^3 \quad (2.94)$$

$$p_1 \times (p_2 \times p_3) - p_2 \times (p_1 \times p_3) - (p_1 \times p_2) \times p_3 = 0 \quad (2.95)$$

$$-p_1 \times (p_2 \times p_3) + (p_1 \times p_2) \times p_3 = -p_2 \times (p_1 \times p_3). \quad (2.96)$$

We directly substitute in the two terms $J^T(^b\ell)J(^b\vec{\omega})^bMJ(^b\ell)^b\vec{\omega}$ and $J(J(^b\ell)^b\vec{\omega})^bMJ(^b\ell)^b\vec{\omega}$ noting

$$p_1 = {}^b\ell \quad p_2 = {}^b\vec{\omega} \quad p_3 = {}^bMJ(^b\ell)^b\vec{\omega}$$

to yield

$$J^T(^b\ell)J(^b\vec{\omega})^bMJ(^b\ell)^b\vec{\omega} + J(J(^b\ell)^b\vec{\omega})^bMJ(^b\ell)^b\vec{\omega} = -J(^b\vec{\omega})J(^b\ell)^bMJ(^b\ell)^b\vec{\omega} \quad (2.97)$$

$$= J(^b\vec{\omega})J^T(^b\ell)^bMJ(^b\ell)^b\vec{\omega}. \quad (2.98)$$

We substitute this result back into the EOM for angular degrees of freedom (2.83) to result in

$$\begin{aligned} {}^\ell\vec{I}_H &= J^T(^b\ell)J(^b\vec{\omega})^bM^bv_y + J^T(^b\ell)^bM^b\dot{v}_y \\ &+ J^T(^b\ell)^bMJ(^b\ell)^b\dot{\vec{\omega}} + {}^bI^b\dot{\vec{\omega}} + J(^b\vec{\omega})J^T(^b\ell)^bMJ(^b\ell)^b\vec{\omega} + J(^b\vec{\omega})^bI^b\vec{\omega} \\ &+ J(^bv_y)^bM^bv_y + J(J(^b\ell)^b\vec{\omega})^bM^bv_y + J(^bv_y)^bMJ(^b\ell)^b\vec{\omega}. \end{aligned} \quad (2.99)$$

The expression for the inertia matrix relative to the "L" frame, ${}^\ell I$, was defined in (2.48). We substitute in the general principal axis theorem (2.48) into (2.99) to yield

$$\begin{aligned} {}^\ell\vec{I}_H &= J^T(^b\ell)J(^b\vec{\omega})^bM^bv_y + J^T(^b\ell)^bM^b\dot{v}_y \\ &+ {}^\ell I^b\dot{\vec{\omega}} + J(^b\vec{\omega}){}^\ell I^b\vec{\omega} \\ &+ J(^bv_y)^bM^bv_y + J(J(^b\ell)^b\vec{\omega})^bM^bv_y + J(^bv_y)^bMJ(^b\ell)^b\vec{\omega}. \end{aligned} \quad (2.100)$$

The Jacobi Identity can be used again to combine the two terms $J^T(^b\ell)J(^b\vec{\omega})^bM^bv_y$ and $J(J(^b\ell)^b\vec{\omega})^bM^bv_y$. Taking the same form as (2.96) we can substitute directly by

$$p_1 = {}^b\ell \quad p_2 = {}^b\vec{\omega} \quad p_3 = {}^bM^bv_y$$

to yield

$$J^T({}^b\ell)J({}^b\vec{\omega}){}^bM{}^bv_y + J(J({}^b\ell){}^b\vec{\omega}){}^bM{}^bv_y = -J({}^b\vec{\omega})J({}^b\ell){}^bM{}^bv_y \quad (2.101)$$

$$=J(J({}^b\ell){}^bM{}^bv_y){}^b\vec{\omega} \quad (2.102)$$

We substitute this result back into the EOM for angular degrees of freedom (2.100) to yield

$$\begin{aligned} {}^\ell\vec{t}_H &= J^T({}^b\ell){}^bM{}^bv_y + {}^\ell I{}^b\dot{\vec{\omega}} + J({}^b\vec{\omega}){}^\ell I{}^b\vec{\omega} + J({}^bv_y){}^bM{}^bv_y \\ &+ J({}^bv_y){}^bMJ({}^b\ell){}^b\vec{\omega} + J(J({}^b\ell){}^bM{}^bv_y){}^b\vec{\omega}. \end{aligned} \quad (2.103)$$

We combine equations (2.80) and (2.103) as

$$\begin{aligned} \begin{bmatrix} {}^\ell\vec{f}_H \\ {}^\ell\vec{t}_H \end{bmatrix} &= \begin{bmatrix} {}^bM & {}^bMJ({}^b\ell) \\ J^T({}^b\ell){}^bM & {}^\ell I \end{bmatrix} \begin{bmatrix} {}^bv_y \\ {}^b\vec{\omega} \end{bmatrix} \\ &+ \begin{bmatrix} \mathbf{0}_{3 \times 3} & J^T({}^bM{}^bv_y + {}^bMJ({}^b\ell){}^b\vec{\omega}) \\ J^T({}^bM{}^bv_y + {}^bMJ({}^b\ell){}^b\vec{\omega}) & J^T({}^\ell I{}^b\vec{\omega} + J^T({}^b\ell){}^bM{}^bv_y) \end{bmatrix} \begin{bmatrix} {}^bv_y \\ {}^b\vec{\omega} \end{bmatrix}. \end{aligned} \quad (2.104)$$

We define the ‘‘added mass’’ matrix

$${}^\ell M_A = \begin{bmatrix} {}^bM & {}^bMJ({}^b\ell) \\ J^T({}^b\ell){}^bM & {}^\ell I \end{bmatrix} \quad (2.105)$$

and the ‘‘added mass’’ Coriolis matrix

$${}^\ell C_A = \begin{bmatrix} \mathbf{0}_{3 \times 3} & J^T({}^bM{}^bv_y + {}^bMJ({}^b\ell){}^b\vec{\omega}) \\ J^T({}^bM{}^bv_y + {}^bMJ({}^b\ell){}^b\vec{\omega}) & J^T({}^\ell I{}^b\vec{\omega} + J^T({}^b\ell){}^bM{}^bv_y) \end{bmatrix}. \quad (2.106)$$

We note that ${}^\ell M_A$ is symmetric and ${}^\ell C_A$ is skew symmetric. We can write (2.104) as

$$\begin{bmatrix} {}^\ell\vec{f}_H \\ {}^\ell\vec{t}_H \end{bmatrix} = {}^\ell M_A \begin{bmatrix} {}^bv_y \\ {}^b\dot{\vec{\omega}} \end{bmatrix} + {}^\ell C_A \begin{bmatrix} {}^bv_y \\ {}^b\vec{\omega} \end{bmatrix}. \quad (2.107)$$

As in Section 2.4 we define the quadratic drag matrix ${}^\ell DQ({}^bv_y, {}^b\vec{\omega})$ to be

$${}^\ell DQ({}^bv_y, {}^b\vec{\omega}) = \sum_{i=1}^3 |{}^bv_{y_i}| {}^\ell D_i + \sum_{i=1}^3 |{}^b\vec{\omega}_i| {}^\ell D_i. \quad (2.108)$$

Each negative semidefinite drag matrix for the i^{th} degree of freedom ($i = 1, 2, \dots, 6$) is defined as

$${}^\ell D_i = \begin{bmatrix} {}^\ell D_{i,1} & {}^\ell D_{i,2} & {}^\ell D_{i,3} & {}^\ell D_{i,4} & {}^\ell D_{i,5} & {}^\ell D_{i,6} \\ {}^\ell D_{i,1} & {}^\ell D_{i,2} & {}^\ell D_{i,3} & {}^\ell D_{i,4} & {}^\ell D_{i,5} & {}^\ell D_{i,6} \\ {}^\ell D_{i,3,1} & {}^\ell D_{i,3,2} & {}^\ell D_{i,3,3} & {}^\ell D_{i,3,4} & {}^\ell D_{i,3,5} & {}^\ell D_{i,3,6} \\ {}^\ell D_{i,4,1} & {}^\ell D_{i,4,2} & {}^\ell D_{i,4,3} & {}^\ell D_{i,4,4} & {}^\ell D_{i,4,5} & {}^\ell D_{i,4,6} \\ {}^\ell D_{i,5,1} & {}^\ell D_{i,5,2} & {}^\ell D_{i,5,3} & {}^\ell D_{i,5,4} & {}^\ell D_{i,5,5} & {}^\ell D_{i,5,6} \\ {}^\ell D_{i,6,1} & {}^\ell D_{i,6,2} & {}^\ell D_{i,6,3} & {}^\ell D_{i,6,4} & {}^\ell D_{i,6,5} & {}^\ell D_{i,6,6} \end{bmatrix}. \quad (2.109)$$

The buoyancy term $\mathcal{G}(\vec{a})$ is structurally different in the “L” frame. The buoyant force term remains the same but the righting moment is different. Define ${}^\ell r_{cb}$ to be the vector from the “L” frame to the center of buoyancy and note ${}^b \ell$ is as before the vector from the center of gravity to the “L” frame. Thus the righting moment is

$${}^\ell \tau_b = J({}^\ell r_{cb}) {}^b \vec{f}_{buoy} - J({}^b \ell) {}^b \vec{f}_g \quad (2.110)$$

$$= J({}^\ell r_{cb}) {}^b_w R(\vec{a}) (-\rho \nabla)^w \vec{g} - J({}^b \ell) {}^b_w R(\vec{a}) (m)^w \vec{g}. \quad (2.111)$$

We can write all the hydrodynamic terms in the body “L” frame as

$$\begin{aligned} \begin{bmatrix} {}^\ell \vec{f}_H \\ {}^\ell \vec{t}_H \end{bmatrix} &= \begin{bmatrix} {}^b M & {}^b MJ({}^b \ell) \\ J^T({}^b \ell) {}^b M & {}^\ell I \end{bmatrix} \begin{bmatrix} {}^b \dot{v}_y \\ {}^b \dot{\omega} \end{bmatrix} \\ &+ \begin{bmatrix} 0_{3 \times 3} & J^T({}^b M {}^b v_y + {}^b MJ({}^b \ell) {}^b \dot{\omega}) \\ J^T({}^b M {}^b v_y + {}^b MJ({}^b \ell) {}^b \dot{\omega}) & J^T({}^\ell I {}^b \dot{\omega} + J^T({}^b \ell) {}^b M {}^b v_y) \end{bmatrix} \begin{bmatrix} {}^b v_y \\ {}^b \dot{\omega} \end{bmatrix} \end{aligned} \quad (2.112)$$

$$= -{}^\ell DQ({}^b v_y, {}^b \dot{\omega}) \begin{bmatrix} {}^b v_y \\ {}^b \dot{\omega} \end{bmatrix} - \left| J({}^\ell r_{cb}) {}^b_w R(\vec{a}) (-\rho \nabla)^w \vec{g} + J({}^b \ell) {}^b_w R(\vec{a}) (m)^w \vec{g} \right|. \quad (2.113)$$

We define

$${}^\ell \mathcal{G}(\vec{a}) = \left| J({}^\ell r_{cb}) {}^b_w R(\vec{a}) (-\rho \nabla)^w \vec{g} - J({}^b \ell) {}^b_w R(\vec{a}) (m)^w \vec{g} \right|. \quad (2.114)$$

Thus (2.113) is simplified to

$$0 = {}^\ell M_A \begin{bmatrix} {}^b \dot{v}_y \\ {}^b \dot{\omega} \end{bmatrix} + {}^\ell C_A \begin{bmatrix} {}^b v_y \\ {}^b \dot{\omega} \end{bmatrix} + {}^\ell DQ({}^b v_y, {}^b \dot{\omega}) \begin{bmatrix} {}^b v_y \\ {}^b \dot{\omega} \end{bmatrix} + {}^\ell \mathcal{G}(\vec{a}). \quad (2.115)$$

2.5 Rigid Body EOM

In general, the derivation of the EOM using rigid-body dynamics follows the derivation of the hydrodynamic EOM in Section 2.3 and Section 2.4 with two differences.

First the body mass matrix, ${}^b M_{RB}$, is just a scalar mass multiplied by the identity $mI_{3 \times 3}$ (dropping the w). From (2.24) and the inverse property of $SO(3)$ we see

$${}^b M_{RB} = {}^b R(\vec{a}) {}^w M_w^b R^T(\vec{a}) = {}^b R(\vec{a}) {}^w m I_{3 \times 3} {}^b R^T(\vec{a}) = m I_{3 \times 3}. \quad (2.116)$$

This similarity extends to the EOM written in both the “ b ” and “ L ” frames where we note

$${}^\ell M_{RB} = {}^b M_{RB} = m I_{3 \times 3}. \quad (2.117)$$

The second difference is the replacement of hydrodynamic rotational inertia ${}^w I$ with the rigid body inertia, ${}^w I_{RB}$. Both ${}^w I$ and ${}^w I_{RB}$ are PDS, but unlike the added mass inertia ${}^\ell I$, closed form expressions for ${}^w I_{RB}$ exist for many simple geometric shapes.

For the rigid body dynamics we define the external applied forces and moments to be \vec{f} and $\vec{\tau}$ respectively. These forces are applied to the vehicle from thrusters or control surfaces which are not already accounted for in the hydrodynamic derivation. For example, similar to (2.104), the rigid body dynamics in the “ L ” frame is defined as

$$\begin{aligned} \begin{bmatrix} {}^\ell \vec{f} \\ {}^\ell \vec{\tau} \end{bmatrix} &= \begin{bmatrix} m I_{3 \times 3} & m I_{3 \times 3} J^{(b \ell)} \\ J^T({}^{b \ell}) m I_{3 \times 3} & {}^\ell I_{RB} \end{bmatrix} \begin{bmatrix} {}^b \vec{v}_y \\ {}^b \vec{\omega} \end{bmatrix} \\ &+ \begin{bmatrix} 0_{3 \times 3} & J^T(m {}^b v_y + m J^{(b \ell)} {}^b \vec{\omega}) \\ J^T(m {}^b v_y + m J^{(b \ell)} {}^b \vec{\omega}) & J^T({}^\ell I_{RB} {}^b \vec{\omega} + J^T({}^{b \ell}) m {}^b v_y) \end{bmatrix} \begin{bmatrix} {}^b v_y \\ {}^b \vec{\omega} \end{bmatrix}. \end{aligned} \quad (2.118)$$

Note that the kernel of the term $J^T(m {}^b v_y)$ in the lower left entry in the Coriolis matrix in (2.118) is the $span({}^b v_y)$. This term can be ignored, but is retained herein for clarity on the simplification steps to follow.

In a similar manner we define ${}^\ell M_{RB}$ and ${}^\ell C_{RB}$ to be the rigid body mass and inertia matrices respectively. Therefore we can express the rigid body dynamics in the “L” frame as

$$\begin{bmatrix} {}^\ell \vec{f} \\ {}^\ell \vec{\tau} \end{bmatrix} = {}^\ell M_{RB} \begin{bmatrix} {}^b \dot{v}_y \\ {}^b \dot{\vec{\omega}} \end{bmatrix} + {}^\ell C_{RB} \begin{bmatrix} {}^b v_y \\ {}^b \vec{\omega} \end{bmatrix}. \quad (2.119)$$

2.6 Complete 6-DOF EOM in the Body Fixed “L” Frame

As reported in [12] and [7], it is common to assume that the hydrodynamics and rigid-body dynamics can be linearly superimposed to define the complete EOM of underwater vehicles. For the derivation of EOM in the “L” frame we add together the dynamics defined in (2.115) and (2.119) as

$$\begin{aligned} 0 = & \quad {}^\ell M_A \begin{bmatrix} {}^b \dot{v}_y \\ {}^b \dot{\vec{\omega}} \end{bmatrix} + {}^\ell C_A \begin{bmatrix} {}^b v_y \\ {}^b \vec{\omega} \end{bmatrix} + {}^\ell DQ({}^b v_y, {}^b \vec{\omega}) \begin{bmatrix} {}^b v_y \\ {}^b \vec{\omega} \end{bmatrix} - {}^\ell \mathcal{G}(\vec{a}) \\ + & \quad \begin{bmatrix} {}^\ell \vec{f} \\ {}^\ell \vec{\tau} \end{bmatrix} = \quad {}^\ell M_{RB} \begin{bmatrix} {}^b \dot{v}_y \\ {}^b \dot{\vec{\omega}} \end{bmatrix} + {}^\ell C_{RB} \begin{bmatrix} {}^b v_y \\ {}^b \vec{\omega} \end{bmatrix} \end{aligned}$$

We combine the mass matrices in (2.113) and (2.118) to yield

$$\begin{aligned} & \begin{bmatrix} {}^b M & {}^b M J({}^b \ell) \\ J^T({}^b \ell) {}^b M & {}^\ell I \end{bmatrix} + \begin{bmatrix} m I_{3 \times 3} & m I_{3 \times 3} J({}^b \ell) \\ J^T({}^b \ell) m I_{3 \times 3} & {}^\ell I_{RB} \end{bmatrix} \\ & = \begin{bmatrix} {}^b M + m I_{3 \times 3} & ({}^b M + m I_{3 \times 3}) J({}^b \ell) \\ J^T({}^b \ell) ({}^b M + m I_{3 \times 3}) & {}^\ell I + {}^\ell I_{RB} \end{bmatrix}. \end{aligned} \quad (2.120)$$

Taking ${}^b M_t = {}^b M + m I_{3 \times 3}$, ${}^\ell I_t = {}^\ell I + {}^\ell I_{RB}$, and $M_\ell = {}^b M_t J({}^b \ell)$ yields

$$\begin{bmatrix} {}^b M_t & M_\ell \\ M_\ell^T & {}^\ell I_t \end{bmatrix}. \quad (2.121)$$

The mass matrix is symmetric since $M_\ell^T = J^T({}^b \ell) ({}^b M_t)^T$ and $({}^b M_t)^T = {}^b M_t$ are symmetric.

The hydrodynamics and rigid body Coriolis matrices in (2.113) and (2.118) can be added together as

$$\begin{aligned} & \begin{bmatrix} 0_{3 \times 3} & J^T({}^b M {}^b v_y + {}^b M J({}^b \ell) {}^b \vec{\omega}) \\ J^T({}^b M {}^b v_y + {}^b M J({}^b \ell) {}^b \vec{\omega}) & J^T({}^\ell I {}^b \vec{\omega} + J^T({}^b \ell) {}^b M {}^b v_y) \end{bmatrix} \\ & + \begin{bmatrix} 0_{3 \times 3} & J^T(m {}^b v_y + m J({}^b \ell) {}^b \vec{\omega}) \\ J^T(m {}^b v_y + m J({}^b \ell) {}^b \vec{\omega}) & J^T({}^\ell I_{RB} {}^b \vec{\omega} + J^T({}^b \ell) m {}^b v_y) \end{bmatrix}. \end{aligned} \quad (2.122)$$

Again taking ${}^b M_t = {}^b M + m I_{3 \times 3}$, ${}^\ell I_t = {}^\ell I + {}^\ell I_{RB}$, and $M_\ell = {}^b M_t J({}^b \ell)$ the expression for the total Coriolis matrix is

$$\begin{bmatrix} 0_{3 \times 3} & J^T({}^b M_t {}^b v_y + M_\ell {}^b \vec{\omega}) \\ J^T({}^b M_t {}^b v_y + M_\ell {}^b \vec{\omega}) & J^T({}^\ell I_t {}^b \vec{\omega} + M_\ell^T {}^b v_y) \end{bmatrix}. \quad (2.123)$$

This formulation is skew symmetric and equivalent to (2.125) in [12]. Other parameterizations where the Coriolis matrix is not skew symmetric are possible, however it is always possible to assemble the Coriolis matrix such that $\dot{M} - C(v)$ is a skew symmetric matrix [38].

We combine all hydrodynamic and rigid body terms together to yield the following EOM for 6-DOF underwater vehicles:

$$\begin{aligned} \begin{bmatrix} {}^\ell \vec{f} \\ {}^\ell \vec{\tau} \end{bmatrix} &= \begin{bmatrix} {}^b M_t & M_\ell \\ M_\ell^T & {}^\ell I_t \end{bmatrix} \begin{bmatrix} {}^b \dot{v}_y \\ {}^b \dot{\vec{\omega}} \end{bmatrix} \\ & + \begin{bmatrix} 0_{3 \times 3} & J^T({}^b M_t {}^b v_y + M_\ell {}^b \vec{\omega}) \\ J^T({}^b M_t {}^b v_y + M_\ell {}^b \vec{\omega}) & J^T({}^\ell I_t {}^b \vec{\omega} + M_\ell^T {}^b v_y) \end{bmatrix} \begin{bmatrix} {}^b v_y \\ {}^b \vec{\omega} \end{bmatrix} + {}^\ell DQ({}^b v_y, {}^b \vec{\omega}) \begin{bmatrix} {}^b v_y \\ {}^b \vec{\omega} \end{bmatrix} - {}^\ell \mathcal{G}(\vec{a}) \end{aligned} \quad (2.124)$$

This formulation is consistent with that reported in [12].

2.6.1 Structural Observations of 6-DOF EOM

We can make a few structural observations. First in the definition above ${}^b M_t$ and ${}^\ell I_t$ are both 3×3 matrices. The body-frame hydrodynamic added-mass matrix, ${}^b M$, and the body-frame added-inertia matrix, ${}^\ell I$, are not necessarily diagonal. For rigid bodies it is true that the mass matrix $m I_{3 \times 3}$ and inertia matrix ${}^\ell I_{RB}$ will be diagonal when the frame of reference is aligned along the principal

axis. In fact, this basis for the “ b ” frame was chosen during the derivation of the rigid body EOM with this simplicity in mind. However, if this frame of reference is chosen, then the hydrodynamic added mass matrix bM_A and inertial matrix ${}^\ell I$ will not necessarily be diagonal. Both bM_A and ${}^\ell I$ are considered real PDS and are therefore diagonalizable by real unitary matrices, or in other words there is some similarity transform in using a member of $SO(3)$ to a frame where each of the hydrodynamic mass and inertia matrices are diagonal (it is not clear if such a frame exists where they are both diagonal). However these two “principal” bases, one for the rigid body and the other added mass, are most likely not the same for an underwater vehicles unless symmetry is present. To state this explicitly, in the “ b ” basis frame:

1. ${}^bM = R_M D_M R_M^T$ where D_M is diagonal and $R_M \neq I_{3 \times 3}$
2. ${}^bI = R_I D_I R_I^T$ where D_I is diagonal and $R_I \neq I_{3 \times 3}$
3. ${}^bM_{RB} = m I_{3 \times 3}$
4. ${}^w I_{RB}$ is diagonal

As a result, the combined mass and inertia matrices can only be considered real PDS because the sum of a diagonal matrix with real positive entries and a PDS matrix is PDS.

Another observation can be found in the off diagonal terms of the combined mass matrix where $M_\ell = {}^bM_t J({}^b\ell)$. Clearly these blocks contain information about the vector ${}^b\ell$ which may be difficult to measure in practice. However the dynamical model of a vehicle described in (2.124) can be identified using methods reported in [28], [33], or [37], using the “ L ” frame to be some frame of reference that is easy to measure. After the dynamical model is identified, the vector from the “ L ” frame to the center of mass ${}^b\ell$ could be estimated from the off diagonal terms of the mass matrix. The estimate may serve as a confirmation of the accuracy of the model. A similar approach may make it possible to estimate the location of the pivot point of a ship, which has been shown to exist [46], but which is also difficult to measure directly.

Yet another observation can be made in the off-diagonal blocks of the Coriolis matrix in 2.124. In particular, the lower left off-diagonal block contains the term $J^T({}^bM_t{}^b v_y)$. This term, when multiplied by the corresponding portion of the body velocity vector ${}^b v_y$, results in non-zero Coriolis forces in the angular degrees of freedom from only translational velocities. This is true even if the reference frame is the “b” frame located at the COM (the vector $\ell = 0$, and thus $M_\ell = {}^bM_t J({}^b\ell) = 0$). At face value this seems incorrect given intuition about rigid-body dynamics. However, this is correct, and is related to the assumptions about added mass. If and only if all the eigenvalues of the PDS combined added-mass matrix bM_t are equal, then there will be no Coriolis forces in the angular degrees of freedom as a result of this term. The proof is given as follows:

FACT: ${}^bM_t \in \mathbb{R}^{3 \times 3}$ is positive definite symmetric (PDS). $J^T({}^bM_t{}^b v_y){}^b v_y = 0 \Leftrightarrow$ all eigenvalues of bM_t are equal.

PROOF:

- $J^T({}^bM_t{}^b v_y){}^b v_y = 0 \Leftrightarrow$ all eigenvalues of bM_t are equal.

bM_t is symmetric and is therefore diagonalizable by a real unitary matrix R_m as ${}^bM_t = R_m^T D_m R_m$. By assumption $D_m = s_m I_{3 \times 3}$, $s_m \in \mathbb{R}_+$. Therefore

$$\begin{aligned}
 J^T({}^bM_t{}^b v_y){}^b v_y &= \\
 J^T(R_m^T D_m R_m{}^b v_y){}^b v_y &= \\
 J^T(R_m^T s_m I_{3 \times 3} R_m{}^b v_y){}^b v_y &= \\
 s_m J^T(R_m^T R_m{}^b v_y){}^b v_y &= \\
 s_m J^T(I_{3 \times 3}{}^b v_y){}^b v_y &= \\
 s_m J^T({}^b v_y){}^b v_y &= 0
 \end{aligned}$$

- $J^T({}^bM_t {}^b v_y) {}^b v_y = 0 \Rightarrow$ all eigenvalues of bM_t are equal.

Again bM_t is symmetric and is therefore diagonalizable by a real unitary matrix R_m as ${}^bM_t = R_m^T D_m R_m$ and $R_m {}^bM_t R_m^T = D_m$. All the eigenvalues $\lambda_1, \lambda_2, \lambda_3$ of bM_t are the diagonal entries of the diagonal matrix D_m . By definition of unitary matrices $R_m^T R_m = I_{3 \times 3}$

$$J^T({}^bM_t {}^b v_y) {}^b v_y = 0$$

$$J({}^b v_y) {}^bM_t {}^b v_y = 0 \quad (\text{anticommutative property of cross products})$$

$$R_m^T R_m J({}^b v_y) {}^bM_t {}^b v_y = 0$$

$$R_m^T J(R_m {}^b v_y) R_m {}^bM_t {}^b v_y = 0 \quad (\text{disributive property of cross products 2.16})$$

$$R_m^T J(R_m {}^b v_y) R_m {}^bM_t R_m^T R_m {}^b v_y = 0$$

$$R_m^T J(R_m {}^b v_y) D_m R_m {}^b v_y = 0$$

$$R_m^T J({}^m v_y) D_m {}^m v_y = 0 \quad (\text{without loss of generality } {}^m v_y = R_m {}^b v_y)$$

$$|R_m^T J({}^m v_y) D_m {}^m v_y|_2 = |0|_2 \quad |*|_2 \text{ denotes the } l_2 \text{ norm.}$$

$${}^m v_y^T D_m^T J^T({}^m v_y) R_m R_m^T J({}^m v_y) D_m {}^m v_y = 0$$

$${}^m v_y^T D_m^T J^T({}^m v_y) J({}^m v_y) D_m {}^m v_y = 0$$

$$|J({}^m v_y) D_m {}^m v_y|_2 = 0.$$

We use the definition of the geometric magnitude of cross product, $|a \times b|_2 = |a|_2 |b|_2 |\sin(\theta)|$

where θ is the angle between vectors a and b . Then

$$|{}^m v_y|_2 |D_m {}^m v_y|_2 |\sin(\theta_m)| = 0.$$

Ignore the trivial solution ${}^m v_y = 0$. All the eigenvalues of ${}^b M_t$ are positive and nonzero because ${}^b M_t$ is PDS. Thus all diagonal entries in D_m ($\lambda_1, \lambda_2, \lambda_3$) are positive and $D_m \neq 0_{3 \times 3}$. As a consequence $|\sin(\theta_m)| = 0$. By definition of the *sin* function, the angle θ_m between vectors ${}^m v_y$ and $D_m {}^m v_y$ is equal to 0 or π (or $n\pi$). Using geometric reasoning, $\theta_m = 0$ or π implies the $D_m {}^m v_y \parallel {}^m v_y$. Thus matrix D_m only scales the magnitude of the vector ${}^m v_y$ and does not change the orientation. Therefore $\lambda_1 = \lambda_2 = \lambda_3 = s_m$ and $D_m {}^m v_y \parallel {}^m v_y = s_m I_{3 \times 3} {}^m v_y \parallel {}^m v_y = s_m {}^m v_y \parallel {}^m v_y \rightarrow D_m = s_m I_{3 \times 3}$, and since ${}^b M_t$ is PDS $s_m \in \mathbb{R}_+$

The same results directly follow for rigid body motion where ${}^b M_t = m I_{3 \times 3}$. This is mentioned in the commentary after (2.118).

In general, all the eigenvalues of the combined added-mass matrix ${}^b M_t$ are not assumed to be equal. Unequal eigenvalues are expected if the vehicle does not exhibit the same added mass properties about all three cardinal planes. In the case of torpedo shaped vehicle, the same added mass properties can be expected about two planes (in the sway and heave degrees of freedom), but not all three.

2.7 Complete 3-DOF EOM in the Body Fixed “L” Frame

The 6-DOF equations reported in (2.124) can be pared down to 3-DOF equations by eliminating the degrees of freedom that are not considered. Here we consider the structure of ${}^b M$ and ${}^\ell I$ in the common 3-DOF class of vehicles with two translational degrees of freedom often referred to as surge and sway and one rotational degree of freedom often known as yaw or heading.

To observe some structure in the 6-DOF EOM we define ${}^b M_t$ and ${}^\ell I$ from (2.124) as

$${}^b M_t = \begin{bmatrix} {}^b m_{11} & {}^b m_{12} & {}^b m_{13} \\ {}^b m_{12} & {}^b m_{22} & {}^b m_{23} \\ {}^b m_{13} & {}^b m_{23} & {}^b m_{33} \end{bmatrix} \quad (2.125)$$

$${}^\ell I = \begin{bmatrix} i_{11} & i_{12} & i_{13} \\ i_{12} & i_{22} & i_{23} \\ i_{13} & i_{23} & i_{33} \end{bmatrix}. \quad (2.126)$$

The vector from the body “ b ” frame to the “ L ” frame, ${}^b\ell$, only exists in one plane in this 3-DOF model. As an aside, if the “ L ” frame is to be considered to be the center of pressure (using naval architecture terminology) and the vehicle exhibits port-starboard symmetry then ℓ_y will be approximately equal to 0. However, for this 3-DOF configuration we consider

$${}^b\ell = \begin{bmatrix} \ell_x \\ \ell_y \\ 0 \end{bmatrix}. \quad (2.127)$$

Thus $M_\ell = {}^bM_t J({}^b\ell)$ can be expressed as

$$M_\ell = \begin{bmatrix} {}^b m_{11} & {}^b m_{12} & {}^b m_{13} \\ {}^b m_{12} & {}^b m_{22} & {}^b m_{23} \\ {}^b m_{13} & {}^b m_{23} & {}^b m_{33} \end{bmatrix} \begin{bmatrix} 0 & 0 & \ell_y \\ 0 & 0 & -\ell_x \\ -\ell_y & \ell_x & 0 \end{bmatrix} \quad (2.128)$$

$$= \begin{bmatrix} -{}^b m_{13}\ell_y & {}^b m_{13}\ell_x & ({}^b m_{11}\ell_y - {}^b m_{12}\ell_x) \\ -{}^b m_{23}\ell_y & {}^b m_{23}\ell_x & ({}^b m_{12}\ell_y - {}^b m_{22}\ell_x) \\ -{}^b m_{33}\ell_y & {}^b m_{33}\ell_x & ({}^b m_{13}\ell_y - {}^b m_{23}\ell_x) \end{bmatrix}. \quad (2.129)$$

For simplicity we define the plant velocities as

$${}^b v_y = \begin{bmatrix} v_1 \\ v_2 \\ v_3 \end{bmatrix} \quad \text{and} \quad {}^b \omega = \begin{bmatrix} v_4 \\ v_5 \\ v_6 \end{bmatrix}. \quad (2.130)$$

The entire 6x6 mass matrix can be assembled and we can partition it from this 6-DOF mass matrix expression

$$\begin{bmatrix} {}^b M_t & M_\ell \\ M_\ell^T & \ell I_t \end{bmatrix} \begin{vmatrix} \dot{v}_1 \\ \dot{v}_2 \\ 0 \\ 0 \\ 0 \\ \dot{v}_6 \end{vmatrix} \quad (2.131)$$

to this 3-DOF mass matrix expression

$$\begin{bmatrix} {}^b m_{11} & {}^b m_{12} & ({}^b m_{11} \ell_y - {}^b m_{12} \ell_x) \\ {}^b m_{12} & {}^b m_{22} & ({}^b m_{12} \ell_y - {}^b m_{22} \ell_x) \\ ({}^b m_{11} \ell_y - {}^b m_{12} \ell_x) & ({}^b m_{12} \ell_y - {}^b m_{22} \ell_x) & i_{33} \end{bmatrix} \begin{vmatrix} \dot{v}_1 \\ \dot{v}_2 \\ \dot{v}_6 \end{vmatrix}. \quad (2.132)$$

To simply further, we can define ${}^b \bar{M}_t$ and ${}^b \ell_{3DOF}$ as

$${}^b \bar{M}_t = \begin{bmatrix} {}^b m_{11} & {}^b m_{12} \\ {}^b m_{12} & {}^b m_{22} \end{bmatrix} \quad (2.133)$$

$${}^b \ell_{3DOF} = \begin{vmatrix} \ell_x \\ \ell_y \end{vmatrix}. \quad (2.134)$$

Also we define the mapping $J_2 : \mathbb{R} \mapsto SK(2) \in \mathbb{R}^{2 \times 2}$ as

$$J_2(c) = \begin{bmatrix} 0 & -c \\ c & 0 \end{bmatrix}. \quad (2.135)$$

Using the definitions (2.133), (2.134) and (2.135) we can define ${}^b \bar{M}_\ell$ as

$$\begin{aligned} {}^b \bar{M}_\ell &= {}^b \bar{M}_t J_2^T(1) {}^b \ell_{3DOF} \\ &= \begin{bmatrix} {}^b m_{11} & {}^b m_{12} \\ {}^b m_{12} & {}^b m_{22} \end{bmatrix} \begin{bmatrix} 0 & 1 \\ -1 & 0 \end{bmatrix} \begin{vmatrix} \ell_x \\ \ell_y \end{vmatrix}. \end{aligned} \quad (2.136)$$

Thus the 3-DOF mass matrix in (2.132) can be rewritten as

$$\begin{bmatrix} {}^b \bar{M}_t & {}^b \bar{M}_\ell \\ {}^b \bar{M}_\ell^T & I_{33} \end{bmatrix}. \quad (2.137)$$

The same process can be repeated for the Coriolis matrix. The only blocks of the 6-DOF Coriolis matrix that contribute to the 3-DOF model are the off diagonal blocks. This is obvious upon

examination of the structure present in the 6-DOF model which has the form

$$\begin{bmatrix} 0 & 0 & 0 & 0 & C_{15} & -C_{16} \\ 0 & 0 & 0 & -C_{15} & 0 & C_{26} \\ 0 & 0 & 0 & C_{16} & -C_{26} & 0 \\ 0 & C_{15} & -C_{16} & 0 & C_{45} & -C_{46} \\ -C_{15} & 0 & C_{26} & -C_{45} & 0 & C_{56} \\ C_{16} & -C_{26} & 0 & C_{46} & -C_{56} & 0 \end{bmatrix} \begin{bmatrix} v_1 \\ v_2 \\ 0 \\ 0 \\ 0 \\ v_6 \end{bmatrix}. \quad (2.138)$$

We use the definitions (2.125) and (2.134) and the terms in the off-diagonal blocks of the 6-DOF Coriolis matrix, $J^T({}^b M_t {}^b v_y + M_{\ell 2} {}^b \vec{\omega})$, can be written out as

$$\begin{aligned} {}^b M_t {}^b v_y &= \begin{bmatrix} {}^b m_{11} & {}^b m_{12} & {}^b m_{13} \\ {}^b m_{12} & {}^b m_{22} & {}^b m_{23} \\ {}^b m_{13} & {}^b m_{23} & {}^b m_{33} \end{bmatrix} \begin{bmatrix} v_1 \\ v_2 \\ 0 \end{bmatrix} \\ &= \begin{bmatrix} {}^b m_{11} v_1 + {}^b m_{12} v_2 \\ {}^b m_{12} v_1 + {}^b m_{22} v_2 \\ {}^b m_{13} v_1 + {}^b m_{23} v_2 \end{bmatrix} \end{aligned} \quad (2.139)$$

$$\begin{aligned} M_{\ell} {}^b \vec{\omega} &= \begin{bmatrix} -{}^b m_{13} \ell_y & {}^b m_{13} \ell_x & ({}^b m_{11} \ell_y - {}^b m_{12} \ell_x) \\ -{}^b m_{23} \ell_y & {}^b m_{23} \ell_x & ({}^b m_{12} \ell_y - {}^b m_{22} \ell_x) \\ -{}^b m_{33} \ell_y & {}^b m_{33} \ell_x & ({}^b m_{13} \ell_y - {}^b m_{23} \ell_x) \end{bmatrix} \begin{bmatrix} 0 \\ 0 \\ v_6 \end{bmatrix} \\ &= \begin{bmatrix} ({}^b m_{11} \ell_y - {}^b m_{12} \ell_x) v_6 \\ ({}^b m_{12} \ell_y - {}^b m_{22} \ell_x) v_6 \\ ({}^b m_{13} \ell_y - {}^b m_{23} \ell_x) v_6 \end{bmatrix}. \end{aligned} \quad (2.140)$$

Upon inspection of (2.138) only the terms in the e_1 and e_2 basis vector position will enter into this 3-DOF formulation, thus the 1,3 and 2,3 entries in the 3-DOF Coriolis matrix are

$$\begin{bmatrix} -{}^b m_{12} v_1 - {}^b m_{22} v_2 - ({}^b m_{12} \ell_y - {}^b m_{22} \ell_x) v_6 \\ {}^b m_{11} v_1 + {}^b m_{12} v_2 + ({}^b m_{11} \ell_y - {}^b m_{12} \ell_x) v_6 \end{bmatrix}. \quad (2.141)$$

This can be shown to be equivalent to

$$\begin{bmatrix} 0 & -1 \\ 1 & 0 \end{bmatrix} \begin{bmatrix} {}^b m_{11} & {}^b m_{12} \\ {}^b m_{12} & {}^b m_{22} \end{bmatrix} \begin{bmatrix} v_1 \\ v_2 \end{bmatrix} + \begin{bmatrix} 0 & -1 \\ 1 & 0 \end{bmatrix} \begin{bmatrix} {}^b m_{11} & {}^b m_{12} \\ {}^b m_{12} & {}^b m_{22} \end{bmatrix} \begin{bmatrix} 0 & 1 \\ -1 & 0 \end{bmatrix} \begin{bmatrix} \ell_x \\ \ell_y \end{bmatrix} v_6. \quad (2.142)$$

We use the definition of ${}^b \bar{M}_t$ in (2.133) and ${}^b \bar{M}_{\ell}$ in (2.136) and the mapping (2.135) to simplify the 1,3 and 2,3 entries in the 3-DOF Coriolis matrix to

$$J_2(1) {}^b \bar{M}_t \begin{bmatrix} v_1 \\ v_2 \end{bmatrix} + J_2(v_6) {}^b \bar{M}_{\ell}. \quad (2.143)$$

The 3,1 and 3,2 entries in the 3-DOF Coriolis matrix are the negative transpose of the 1,3 and 2,3 entries defined in (2.143), and thus

$$\begin{aligned} & - \left[J_2(1)^b \bar{M}_t \begin{vmatrix} v_1 \\ v_2 \end{vmatrix} + J_2(v_6)^b \bar{M}_\ell \right]^T \\ & = |v_1 \quad v_2|^b \bar{M}_t J_2(1) + {}^b \bar{M}_\ell^T J_2(v_6). \end{aligned} \quad (2.144)$$

The 3-DOF Coriolis matrix (and the 3-DOF velocity vector) can be assembled using (2.143) and (2.144) to match the Coriolis matrix in [33] as

$$\begin{bmatrix} 0_{2 \times 2} & J_2(1)^b \bar{M}_t \begin{vmatrix} v_1 \\ v_2 \end{vmatrix} + J_2(v_6)^b \bar{M}_\ell \\ |v_1 \quad v_2|^b \bar{M}_t J_2(1) + {}^b \bar{M}_\ell^T J_2(v_6) & 0 \end{bmatrix} \begin{vmatrix} v_1 \\ v_2 \\ v_6 \end{vmatrix}. \quad (2.145)$$

This formulation of the Coriolis is still skew symmetric. Another equivalent way to express the 3-DOF Coriolis matrix (and the 3-DOF velocity vector) is to rearrange the terms as

$$\begin{bmatrix} J_2(v_6)^b \bar{M}_t & J_2(v_6)^b \bar{M}_\ell \\ |v_1 \quad v_2|^b \bar{M}_t J_2(1) & {}^b \bar{M}_\ell^T J_2(1) \begin{vmatrix} v_1 \\ v_2 \end{vmatrix} \end{bmatrix} \begin{vmatrix} v_1 \\ v_2 \\ v_6 \end{vmatrix}. \quad (2.146)$$

Here the 3,3 entry is a scalar and therefore it is equivalent to its transpose

$$\left[{}^b \bar{M}_\ell^T J_2(1) \begin{vmatrix} v_1 \\ v_2 \end{vmatrix} \right]^T = |v_1 \quad v_2| J_2(-1)^b \bar{M}_\ell. \quad (2.147)$$

Therefore another equivalent formulation of the Coriolis matrix (and the 3-DOF velocity vector) is

$$\begin{bmatrix} J_2(v_6)^b \bar{M}_t & J_2(v_6)^b \bar{M}_\ell \\ |v_1 \quad v_2|^b \bar{M}_t J_2(1) & |v_1 \quad v_2| J_2(-1)^b \bar{M}_\ell \end{bmatrix} \begin{vmatrix} v_1 \\ v_2 \\ v_6 \end{vmatrix}. \quad (2.148)$$

The Coriolis matrix can be parameterized and organized many different ways. This is because the Coriolis term, which includes both the Coriolis matrix and the velocity vector, is inherently a vector-valued function. However, it is always possible to assemble the Coriolis matrix such that $\dot{M} - C(v)$ is a skew symmetric matrix [38]. In a similar manner we can pare down the drag matrix ${}^\ell DQ(v_1, v_2, v_6)$ to be

$${}^\ell DQ(v_1, v_2, v_6) = |v_1| D_1 + |v_2| D_2 + |v_6| D_6. \quad (2.149)$$

Each PDS drag matrix for the i^{th} degree of freedom ($i = 1, 2, 6$) is defined as

$${}^\ell D_i = \begin{bmatrix} {}^\ell D_{i,1,1} & {}^\ell D_{i,1,2} & {}^\ell D_{i,1,3} \\ {}^\ell D_{i,2,1} & {}^\ell D_{i,2,2} & {}^\ell D_{i,2,3} \\ {}^\ell D_{i,3,1} & {}^\ell D_{i,3,2} & {}^\ell D_{i,3,3} \end{bmatrix}. \quad (2.150)$$

In conclusion, the dynamical EOM of a 3-DOF underwater vehicle with degrees of freedom in surge, sway, and yaw are

$$\begin{aligned}
\begin{bmatrix} {}^\ell f_1 \\ {}^\ell f_2 \\ {}^\ell \tau_6 \end{bmatrix} &= \begin{bmatrix} {}^b \bar{M}_t & {}^b \bar{M}_\ell \\ {}^b \bar{M}_\ell^T & I_{33} \end{bmatrix} \begin{bmatrix} \dot{v}_1 \\ \dot{v}_2 \\ \dot{v}_6 \end{bmatrix} \\
&+ \begin{bmatrix} & & & & & \\ & & 0_{2 \times 2} & & & \\ & & & J_2(1) {}^b \bar{M}_t & & \\ & & & & & J_2(v_6) {}^b \bar{M}_\ell \\ & & & & & \\ & & & & & 0 \end{bmatrix} \begin{bmatrix} v_1 \\ v_2 \\ v_6 \end{bmatrix} \\
&+ {}^\ell DQ(v_1, v_2, v_3) \begin{bmatrix} v_1 \\ v_2 \\ v_6 \end{bmatrix}.
\end{aligned} \tag{2.151}$$

This is equivalent to

$$\begin{aligned}
\begin{bmatrix} {}^\ell f_1 \\ {}^\ell f_2 \\ {}^\ell \tau_6 \end{bmatrix} &= \begin{bmatrix} {}^b \bar{M}_t & {}^b \bar{M}_\ell \\ {}^b \bar{M}_\ell^T & I_{33} \end{bmatrix} \begin{bmatrix} \dot{v}_1 \\ \dot{v}_2 \\ \dot{v}_6 \end{bmatrix} + \begin{bmatrix} & & & & & \\ & & J_2(v_6) {}^b \bar{M}_t & & & \\ & & & & & J_2(v_6) {}^b \bar{M}_\ell \\ & & & & & \\ & & & & & \\ & & & & & \end{bmatrix} \begin{bmatrix} v_1 \\ v_2 \\ v_6 \end{bmatrix} \\
&+ {}^\ell DQ(v_1, v_2, v_3) \begin{bmatrix} v_1 \\ v_2 \\ v_6 \end{bmatrix}.
\end{aligned} \tag{2.152}$$

Buoyant forces do not enter into this particular 3-DOF formulation, but some authors [33] include additional bias terms to account for unmodeled thruster dynamics, and other unmodeled dynamics such as cable tethers.

Chapter 3

Adaptive Identification of Plant and Actuation Parameters of Underactuated UUVs

3.1 Introduction

This chapter reports a novel adaptive identification algorithm for the estimation of parameters for unmanned underwater vehicles (UUVs) underwater vehicle plant dynamical models from experimental data in which a fully-submerged UUV performs dynamic maneuvers. This adaptive identifier (AID) approach is inspired by the AID approach originally reported in McFarland and Whitcomb [36], for the case of fully-actuated UUVs. Specifically, Chapter 3 reports the following new results:

1. A preliminary proof of an extension of [36] to identify both actuation parameters and plant parameters for six degree of freedom (6-DOF) UUVs simultaneously.
2. A preliminary simulation study that indicates that the AID in [36] can be extended to underactuated three degree of freedom (3-DOF) UUVs.
3. AID algorithm and proof of an extension of [36] for 6-DOF UUV plants with diagonal mass and drag matrices.

The remainder of this chapter is organized as follows: Section 3.2 provides a review of literature

on parameter identification of UUVs. Section 3.3 reports a proof of the extension of [36] for underactuated 3-DOF UUV plants of the form addressed in [32]. Subsections 3.3.2.1 and 3.3.2.2 report the results of numerical simulations for both fully actuated and underactuated 3-DOF UUVs. Section 3.4 reports a proof of an extension of [36] to estimate actuation parameters of 6-DOF UUVs simultaneously. Section 3.4.3 reports a proof of an extension of [36] to 6-DOF UUV plants with diagonal mass and drag matrices.

3.2 Literature Review

Several methods for the experimental identification of dynamical plant parameters for UUVs have been reported. They broadly fall into one of the following categories: least squares linear regression, adaptive estimation, Kalman filter variants, and machine learning (ML) or neural net (NN) techniques.

- **Least Squares**

Hegrenaes *et al.* in [18] describes a constrained least squares method for 3-DOF parameter identification of the "HUGIN 4500" UUV during sea trials in the Oslo-fjord, Norway. The approach identifies the control surface parameters as defined in [41] and the model parameter simultaneously. A cross validation with experimental results is reported.

Martin and Whitcomb in [29] report experimental identification and validation of a 6-DOF model of the fully actuated Johns Hopkins University (JHU) remotely operated vehicle (ROV) using both total least squares and ordinary least squares. They report a comparative experimental evaluation of several candidate plant models and conclude that the fully coupled quadratic drag model perform better than corresponding decoupled drag models for this class of underwater vehicles.

Experimental parameter identification for underactuated gliders are reported by Graver *et al.* in [15] The authors only report methods for estimating parameters that are observable in steady glide which eliminates the need for body accelerations.

Ridao *et al.* in [42] compares identification of a fully actuated decoupled 3-DOF model parameters for the “URIS UU” vehicle using least squares and a second method which involves numerical integration to avoid derivatives of body velocity signals which can be difficult to obtain in experiments. Appendix A reports a result that indicates that with a sufficiently small dt these two methods are actually equivalent and are therefore subject to the same noise and numerical inaccuracies.

Naterajan *et al.* in [40] reports offline experimental parameter identification of the under-actuated 6-DOF “DAGON” UUV by first identifying the thruster model parameters, then identifying the vehicle drag and mass parameters.

- **Adaptive Estimation**

An approach to adaptive identification of UUV plant parameters was first reported by Smallwood and Whitcomb in [48] for fully-actuated multi-degree of freedom UUVs, but is limited to fully diagonal plant models in which the dynamics of each degree of freedom is fully decoupled and independent from the dynamics of other degrees of freedom. McFarland and Whitcomb in [36] report an AID for fully coupled, fully actuated 6-DOF UUVs. Neither AID requires body acceleration signals. Both provide Lyapunov stability proofs and experimental results for the fully actuated JHU ROV are compared with those found using ordinary least squares. These adaptive estimation techniques require knowledge of thruster dynamics and involve tuning adaptation gains for best performance.

- **Kalman Filters**

The authors in [49] report an EKF estimation of 1 DOF dynamics of an underactuated, torpedo shaped body using experimental data.

In [43] Sabet *et al.* identify some dynamical model parameters of a 6-DOF torpedo shaped UUV in simulation using Cubature and Transformed Unscented Kalman Filters. Performance is compared with previously reported Extended Kalman Filters which are limited by linearization of the nonlinear dynamical system. The authors estimate control input coefficients for the control surfaces as formulated in [41] but assume the thrust coefficient and mass terms are known.

- **Machine Learning (ML) and Neural Net (NN) Methods**

In [55] Wehbe *et al.* reports a study of several machine learning (ML) methods for identifying the decoupled drag in the Sway and Yaw DOF of the “Leng” torpedo shaped UUV. They conclude that kernel based nonlinear estimators (SVR, KRR, GPR) yield better estimations for hydrodynamic damping terms of underwater vehicles than neural net (NN) or least square estimations. However, the prohibitively long computational time required to complete the ML and NN estimates.

Another study [54] reports the use of NN in drag parameter identification of UUVs. The authors in [54] report the method to be robust to noise and to be able to correctly identify time varying drag parameters with online learning. The authors report a numerical simulation study but no experimental evaluation.

In [56] Wu *et al.* report a symbolic regression method for UUV parameters based on genetic algorithms and genetic programming. Using simulated 6-DOF data, the authors compare identification using a symbolic regression and Levenberg-Marquardt least squares.

Online reinforcement learning is proposed by Karras *et al.* in [26] to identify the parameters

of an underactuated UUV. The method is derivative-free, and four degree of freedom (x, y, z , heading) experimental results are reported.

All ML/NN approaches reviewed assume knowledge of thruster and control surface models. In addition, significant computational time and training data is needed to complete estimates using ML and NN methods.

3.3 Adaptive Identification of 3-DOF UUV Plant Parameters

3.3.1 Problem Statements

The equations of motion (EOM) for fully coupled, 3-DOF (surge, sway, and heading) UUVs are reported in Chapter 2.7. They have the form

$$\tau = u(t) = M\dot{v} + C(M, v)v - D(v)v + b_a, \quad (3.1)$$

where $\tau = u(t) \in \mathbb{R}^3$ is the vector of forces (in surge and sway) and moments (in heading) acting on the body. $\tau = [f_1; f_2; t_6]$. $v \in \mathbb{R}^3$ is the body velocity (the velocity of the body projected into the body coordinate frame). $v = [v_1; v_2; v_6]$. $\dot{v} \in \mathbb{R}^3$ is the derivative of the body velocity. $\dot{v} = [\dot{v}_1; \dot{v}_2; \dot{v}_6]$. The mass matrix M , Coriolis matrix $C(M, v)$, and the quadratic drag matrix $D(v)$ are defined in Chapter 2. This formulation assumes all drag matrices are negative semi-definite and thus a minus sign appears in (3.1). Some authors such as in [33] will define the drag matrix as positive definite and change the sign accordingly. In either case, the drag term must result in damping, or the dissipation of energy of the system.

The term $b_a \in \mathbb{R}^3$ is the sum of buoyancy and bias terms. Entries of the bias term b_a can be parameterized as

$$b_a = \begin{bmatrix} b_1 \\ b_2 \\ b_6 \end{bmatrix}. \quad (3.2)$$

Some entries in the b_a vector can be neglected in some conditions, but all entries are considered

herein. Buoyant forces are not present in this particular 3-DOF arrangement, but vehicle configurations and thrusters often have bias. One example of this is reported in [33] where the authors report a non-zero bias they conclude is related to the forces from a tether.

3.3.2 AID Extension to 3-DOF UUV Plants

In [36] McFarland and Whitcomb report a new AID for fully actuated 6-DOF UUVs. This AID approach is adapted and extended herein to estimate parameters of a 3-DOF UUV. The remainder of this section reports these extensions in bold.

- Plant:

$$\tau = M\dot{v} + C(M, v)v - D(v)v + \mathbf{b}_a \quad (3.3)$$

- Task: Design parameter update laws for \hat{v} , \hat{M} , \hat{D}_i , and $\hat{\mathbf{b}}_a$ such that $\lim_{t \rightarrow \infty} \Delta v(t) = \vec{0}$, $\lim_{t \rightarrow \infty} \hat{M}(t) = \vec{0}$, $\lim_{t \rightarrow \infty} \hat{D}_i(t) = \vec{0}$, and $\lim_{t \rightarrow \infty} \hat{\mathbf{b}}_a(t) = \vec{0}$. Additionally, design the parameter update laws such that signals are bounded.

- Error Coordinates:

- $\Delta v(t) = \hat{v}(t) - v(t)$
- $\Delta M(t) = \hat{M}(t) - M$
- $\Delta D_i(t) = \hat{D}_i(t) - D_i$
- $\Delta \mathbf{b}_a(t) = \hat{\mathbf{b}}_a(t) - \mathbf{b}_a$

- Parameter Update Laws (removing the explicit notation for time dependence):

$$\dot{\hat{v}} = \hat{M}^{-1} \left(-C(\hat{M}, v)v + D(v)v - b_a + \tau \right) + \alpha \Delta v \quad (3.4)$$

$$\dot{\hat{M}} = \frac{\gamma_1}{2} (\psi_1 v^T + v \psi_1^T + \Delta v \psi_2^T + \psi_2 \Delta v^T) \quad (3.5)$$

$$\dot{\hat{D}}_i = -\gamma_2 |v_i| \Delta v^T \quad (3.6)$$

$$\dot{\hat{b}}_a = \gamma_3 \Delta v \quad (3.7)$$

Where

- $\psi_1 = ad_{SE(2)}(v)^T \Delta v$
- The adjoint operator $ad_{SE(2)}$ is defined as

$$ad_{SE(2)}(v) = \begin{bmatrix} \mathbf{0} & -v_6 & \mathbf{0} \\ v_6 & \mathbf{0} & \mathbf{0} \\ -v_2 & v_1 & \mathbf{0} \end{bmatrix} \quad (3.8)$$

- $\psi_2 = \dot{\hat{v}} + \alpha \Delta v$
- Adaptation gains $\alpha, \gamma_1, \gamma_2, \gamma_3 \in \mathbb{R}_+$
- $\hat{M}(t_0)$ is positive definite symmetric (PDS)
- $\hat{v}(t_0) = v(t_0)$
- $\exists \epsilon \in \mathbb{R}_+$ such that $\mathcal{T}(t_0)^{1/2} + \epsilon \leq \lambda_3$ where

$$\begin{aligned} \mathcal{T}(t_0) = & \|\Delta M(t_0)\|_F^2 + \frac{\gamma_1}{\gamma_2} \sum_{i=1}^3 \|\Delta D_i(t_0)\|_F^2 \\ & + \frac{\gamma_1}{\gamma_3} \|\Delta b_a(t_0)\|^2 \end{aligned} \quad (3.9)$$

- System and Stability Proof:

A proof for convergence of estimates \hat{v} , \hat{M} , and \hat{D}_i , $i = 1, 2, 3$, to true plant values is reported in [36]. We provide one additional term in the Lyapunov function to show convergence of

the bias term estimate \hat{b}_a to the true bias term b_a . Consider the Lyapunov candidate function

$$V(t) = \frac{1}{2} \Delta v^T M \Delta v + \frac{1}{2\gamma_1} \text{tr}(\Delta M \Delta M^T) \quad (3.10)$$

$$+ \frac{1}{2\gamma_2} \sum_{i=1}^3 \text{tr}(\Delta D_i \Delta D_i^T) + \frac{1}{2\gamma_3} \Delta \mathbf{b}_a^T \Delta \mathbf{b}_a.$$

. In a procedure similar to methods reported in [36], we develop the following velocity error dynamics expression

$$M \Delta \dot{v} = M(\dot{\hat{v}} - \dot{v})$$

$$= \alpha M \Delta v - \Delta M \psi_2 - \text{ad}(v) \Delta M v \quad (3.11)$$

$$+ \left(\sum_{i=1}^6 |v_i| \Delta D_i \right) v - \Delta \mathbf{b}_a.$$

The Lyapunov function candidate (3.10) is:

- positive definite
- radially unbounded
- equal zero if and only if $\Delta v = \vec{0}$, $\Delta M = 0_{3 \times 3}$, $\Delta D_i = 0_{3 \times 3} \forall i$, **and** $\Delta \mathbf{b}_a = \vec{0}$.

The time derivative of (3.10) is

$$\dot{V}(t) = \frac{1}{2} \left(\dot{\Delta v}^T M \Delta v + \Delta v^T M \dot{\Delta v} \right) + \frac{1}{\gamma_1} \text{tr}(\Delta M \dot{\Delta M}^T) + \frac{1}{\gamma_2} \sum_{i=1}^3 \text{tr}(\Delta D_i \dot{\Delta D}_i^T) \quad (3.12)$$

$$+ \frac{1}{\gamma_3} \dot{\Delta \mathbf{b}}_a^T \Delta \mathbf{b}_a.$$

We first substitute in (3.11) and the parameter updates laws (3.4)-(3.6). The result is

$$\dot{V}(t) = -\alpha \Delta v^T M \Delta v - \frac{1}{2} \Delta v^T \Delta \mathbf{b}_a - \frac{1}{2} \Delta \mathbf{b}_a^T \Delta v + \frac{1}{\gamma_3} \dot{\Delta \mathbf{b}}_a^T \Delta \mathbf{b}_a \quad (3.13)$$

$$= -\alpha \Delta v^T M \Delta v - \Delta v^T \Delta \mathbf{b}_a + \frac{1}{\gamma_3} \dot{\Delta \mathbf{b}}_a^T \Delta \mathbf{b}_a. \quad (3.14)$$

And finally we substitute the parameter update law (3.7) to yield

$$\dot{V}(t) = -\alpha \Delta v^T M \Delta v. \quad (3.15)$$

As reported in [36], this expression is negative definite in Δv and negative semidefinite in the error coordinates Δv , ΔM , ΔD_i , and $\Delta \mathbf{b}_a$.

We note from [36] that with v , Δv , ΔM , ΔD_i , and $\Delta \mathbf{b}_a$ bounded and M , D_i , and \mathbf{b}_a constant, it is implied that \hat{v} , \hat{M} , \hat{D}_i , and $\hat{\mathbf{b}}_a$ are bounded. Additionally it can be shown that M^{-1} is bounded using the same approach as that in [36] and thus $\dot{\Delta v}$ is bounded. Additionally $\Delta v \in \mathcal{L}_2$ and bounded $\dot{\Delta v}$ implies that $\lim_{t \rightarrow \infty} \Delta v = \vec{0}$

Since the parameter update equation (3.30) is bounded and $\lim_{t \rightarrow \infty} \Delta v = \vec{0}$ this implies that $\lim_{t \rightarrow \infty} \dot{M} = \vec{0}$, $\lim_{t \rightarrow \infty} \dot{D}_i = \vec{0} \forall i$, and $\lim_{t \rightarrow \infty} \dot{\mathbf{b}}_a = \vec{0}$. We conclude the estimator's angular and linear velocities asymptotically converge to the velocities of the actual vehicle and the estimated parameters converge to the constant values.

3.3.2.1 AID Results in Simulation Studies of Fully Actuated 3-DOF UUVs

Studies of a simulated UUV plant were conducted, and the "true" parameters were chosen to match those of the JHU ROV that were experimentally identified in [32]. In a similar manner as the methods reported in [32], open loop control input was used to excite all 3 DOF in simulation. Specifically, the control input was

$$\begin{bmatrix} f_1 \\ f_2 \\ \tau_6 \end{bmatrix} = \begin{bmatrix} 10 * \sin(0.25 * t) \text{ (N)} \\ 50 * \sin(0.35 * t) \text{ (N)} \\ 200 * \sin(0.3 * t) \text{ (N-m)} \end{bmatrix}. \quad (3.16)$$

Vehicle parameters were identified using both the AID method and Ordinary Least Squares (OLS) for comparison. White Gaussian noise was added to both the body velocity and the time derivative body velocity in an effort to mimic expected experimental sensor noise. The specific noise characteristics are provided in Table 3.1.

Thirty minutes of plant excitation was simulated for the identification process. One could

Table 3.1: Standard Deviation σ of Added Noise

Signal	σ	Signal	σ
$v_1(t)$		$\dot{v}_1(t)$	
$v_2(t)$	$0.01 \frac{m}{s}$	$\dot{v}_2(t)$	$0.1 \frac{m}{s^2}$
$v_6(t)$		$\dot{v}_6(t)$	

optimize the choice of control inputs to increase excitation, thereby reducing the simulation time required to identify parameters. However, such an effort was outside of the scope of this study.

The set of adaptation gains used in simulation studies was:

$$a = 2.5 \quad (3.17)$$

$$\gamma_1 = 950 \quad (3.18)$$

$$\gamma_2 = 1200 \quad (3.19)$$

$$\gamma_3 = 8.5 \quad (3.20)$$

After the adaptive identification process was complete, another simulation was completed to validate the accuracy of the identified parameters. In the validation simulation the UUV plant with the identified parameter set was subjected to the same initial condition and control signal. The accuracy of the identified model was reported as the mean absolute error (MAE) between the velocities of the simulated plant with the true parameters and the velocities of the simulated plant with the identified parameters.

The results are shown in Figure 3.1. The forward simulation with the true parameter values is noted as “v_true”, the simulation with the OLS identified parameters is noted as “v_ls” and the simulation with the adaptively identified parameters is noted as “v_ad”. Figure 3.1 shows just over 200 seconds of a 30-minute simulation. 100 simulation runs were completed to provide statistically significant results. The random noise added to each signal as reported in Table 3.1 was different

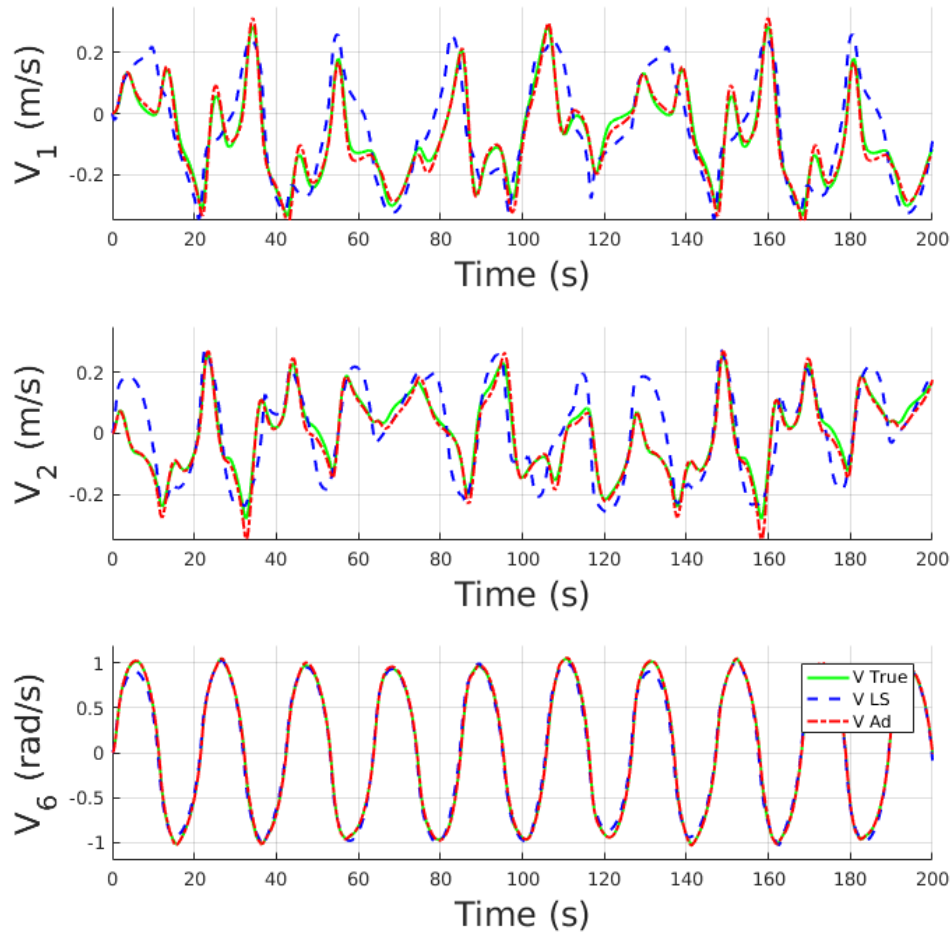


Figure 3.1: Simulation of the fully actuated, JHU ROV in three degrees of freedom with measurement noise for each simulation run, but all simulation runs used the same adaptive gains. The mean absolute errors were then averaged over all 100 simulation runs.

The MAE of the simulated, fully actuated 3-DOF UUV plant using identified parameters from both AID and OLS methods was summarized in Table 3.2. The MAE in velocities of the simulated UUV with the adaptively identified parameters was lower than the MAE of the simulated UUV with the parameters identified using OLS.

Table 3.2: Mean Absolute Error of Simulated, Fully Actuated 3-DOF UUV Plant Using Identified Parameters

DOF	AD ID PLANT	LS ID PLANT
v_1	0.016 <i>m/s</i>	0.076 <i>m/s</i>
v_2	0.015 <i>m/s</i>	0.066 <i>m/s</i>
v_6	0.010 <i>rad/s</i>	0.048 <i>rad/s</i>

Table 3.3: Mean Absolute Error of Simulated, Underactuated 3-DOF UUV Plant Using Identified Parameters

DOF	AD ID PLANT	LS ID PLANT
v_1	0.016 <i>m/s</i>	0.059 <i>m/s</i>
v_2	0.012 <i>m/s</i>	0.062 <i>m/s</i>
v_6	0.011 <i>rad/s</i>	0.030 <i>rad/s</i>

3.3.2.2 AID Results in Simulated, Underactuated, 3-DOF UUV

The 3-DOF UUV simulation was repeated but using a simple underactuated plant model in which surge and yaw are actuated, but the sway (lateral) degree of freedom has no direct control authority, i.e. $f_2 = 0$. As with the fully actuated UUV, the parameters of the underactuated UUV plant were estimated using both the AID and least squares. The same adaptive gains (3.17)-(3.20) were used, although further optimization is possible. The same validation process was performed by simulating the identified model of the underactuated UUV subject to the same initial state and control inputs. The results are shown in Figure 3.2.

As before 100 simulation runs of the underactuated UUV were completed to get statistically significant results. Each simulation had different random noise which is characterized in Table 3.1. The MAE of the simulated, underactuated 3-DOF UUV plant using identified parameters from both AID and least squares methods was summarized in Table 3.3. As reported for the fully actuated UUV, the adaptively identified underactuated UUV plant was found to have a lower MAE than the UUV plant identified using OLS in simulation studies.

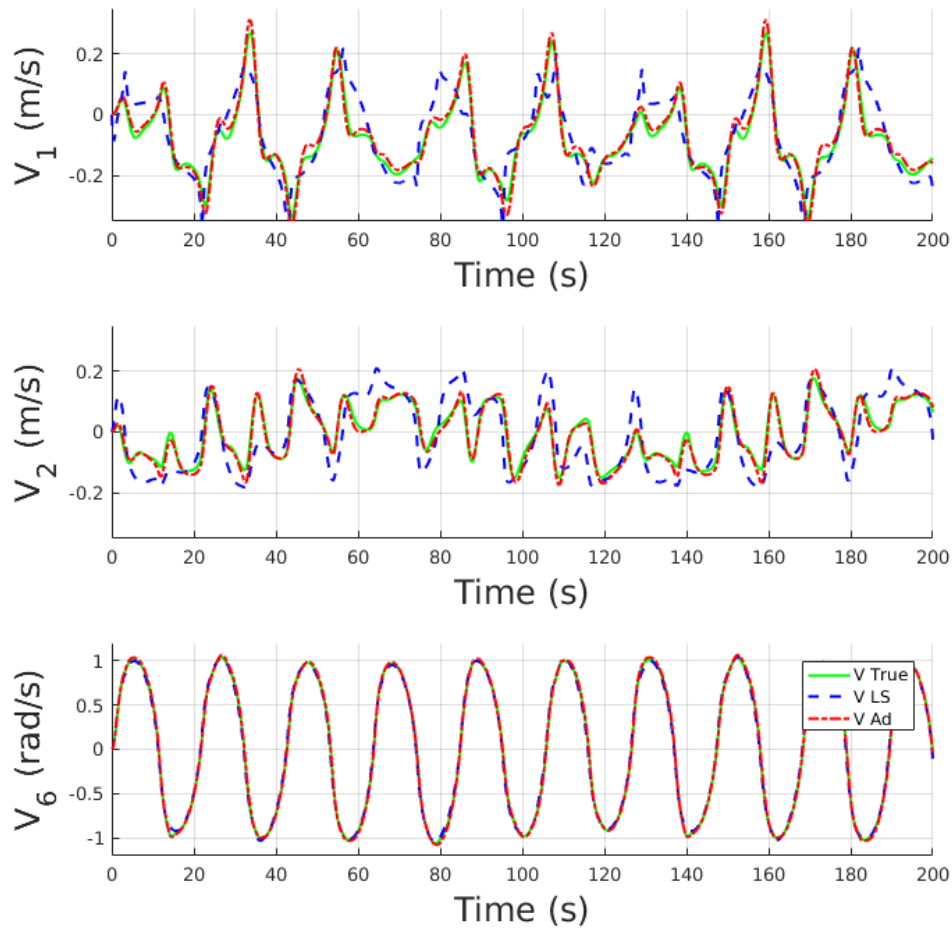


Figure 3.2: Simulation of the underactuated, JHU ROV in three degrees of freedom with measurement noise

Figure 3.3 provides a plot of the value of the Lyapunov function $V(t)$ during one simulation run of the fully actuated UUV and one simulation run of the underactuated UUV. As seen in Figure 3.3, $V_{UA}(t)$ does not decrease as fast as $V_{FA}(t)$. This was expected as the simulated motion in the v_2 direction for this underactuated plant is not as large as the simulated motion of fully actuated plant. As a consequence, there is less persistent excitation in the sway v_2 degree of freedom, and more time is required for the parameter estimates to converge to the “true” values.

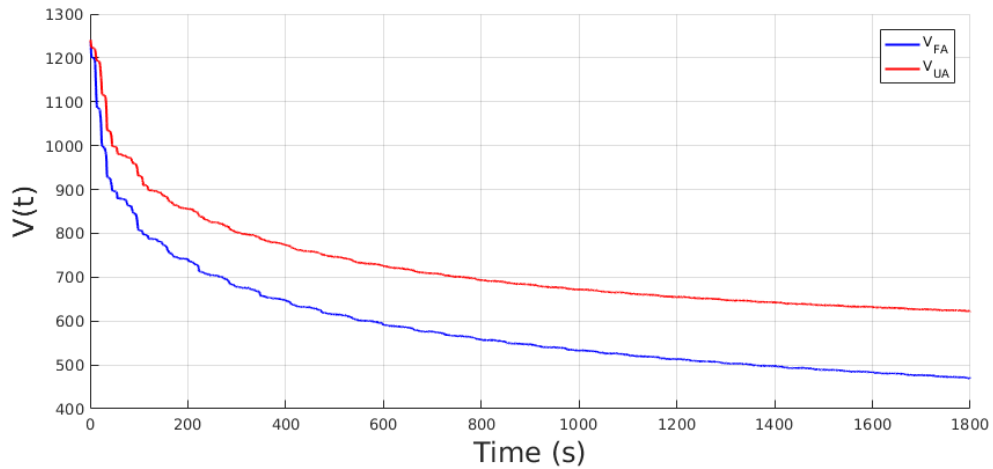


Figure 3.3: Evaluation of the Lyapunov function in simulation of both a fully actuated (V_{FA}) and under actuated (V_{UA}) 3-DOF UUV

Additionally, although it may appear that $\lim_{t \rightarrow \infty} V_{UA}(t) \neq 0$, or that $V_{UA}(t)$ is bounded below by some positive non-zero number, it was confirmed that if the simulation is run to $4e5$ seconds (530 days) the value of $V_{UA}(t)$ decreases to less than $0.5 \text{ kg m}^2/\text{s}^2$. Obviously this length of time is unreasonable and the control and adaptive gains could be better optimized, but the result of this experiment suggests that the estimated parameters of underactuated vehicles eventually converge to the true values in simulation.

3.3.3 Discussion

These results indicate that the AID for fully actuated 6-DOF UUVs reported in [36] can be used for adaptive identification of underactuated 3-DOF UUV plant parameters. In both cases the UUV plant using AID parameters performed better in simulation than the the UUV plant using the parameters identified using OLS methods. This was likely because Gaussian noise was added to the derivative of the body velocity, a signal that the AID estimates, but the OLS uses directly. As with any adaptive identifier, parameter convergence requires persistent excitation in all degrees of freedom [39], but these results demonstrate that control authority in all degrees of freedom is not required to achieve parameter convergence. The inherent coupling of motion between degrees of freedom can be sufficient to meet this persistent excitation criteria.

3.4 Adaptive Identification of Plant and Actuation Parameters for 6-DOF UUVs

3.4.1 Problem Statements

The following section presents an extension of the AID reported in [36] that simultaneously adaptively identifies both plant and control vector parameters of fully coupled 6-DOF UUVs. This result may be extended to underactuated UUVs as a logical consequence of the simulation study in Section 3.3.

The control actuators or actuation available for many UUVs is often modeled as a function of one or more unknown parameters, such as propeller coefficients and lift and drag coefficients of control surfaces, which we will refer to as actuation parameters, and known signals such as angular velocity of propellers, position of control surfaces, and velocity of vehicle relative to the water. Control of a UUV is traditionally achieved using some combination of thrusters and actuated control surfaces, but control of UUVs using bio-inspired methods is demonstrated in [44], [27], [20], and [6]. Regardless of the specific method of actuation, the control actuation available to most UUVs can be modeled as a function of unknown actuation parameters and known plant states and known control signals.

Although the structures of many of these control functions are well studied and experimentally verified in the literature [41], the actuation parameters must be determined experimentally for each UUV. The following parameter identification method is applicable to a wide range of fully actuated and underactuated UUVs of the form

$$M\dot{v} = -C(v)v - D(v)v - \mathcal{G}(\vec{a}) + \tau(v, \vec{a}, \xi), \quad (3.21)$$

where $v \in \mathbb{R}^6$ is a vector containing the linear and angular body velocity as defined in Chapter 2, $v = [v_1; v_2; v_3; v_4; v_5; v_6]$. For convenience we also define the body linear velocity $v = [v_1; v_2; v_3] \in \mathbb{R}^3$ and the body angular velocity $\omega = [v_4; v_5; v_6] \in \mathbb{R}^3$. $\dot{v} \in \mathbb{R}^6$ is the derivative of body velocity, $\dot{v} = [\dot{v}_1; \dot{v}_2; \dot{v}_3; \dot{v}_4; \dot{v}_5; \dot{v}_6]$. The vector \vec{a} is the body attitude vector as defined in Chapter 2. The mass

matrix M , Coriolis matrix $C(v)$, quadratic drag matrix $D(v)$, and $\mathcal{G}(\vec{a})$ are defined in Chapter 2. The control vector $\tau(v, \vec{a}, \xi) \in \mathbb{R}^6$ is defined as the vector of body-forces that are a result of body velocity v , attitude of the vehicle \vec{a} , and p control inputs such as fin angle and propeller speed denoted as $\xi \in \mathbb{R}^p$. If the actuation parameters enter linearly into $\tau(v, \vec{a}, \xi)$ then the control vector can be factored as

$$\tau(v, \vec{a}, \xi) = G_a(v, \vec{a}, \xi)\theta_a. \quad (3.22)$$

Where $G_a(v, \vec{a}, \xi) \in \mathbb{R}^{6 \times n}$ is the (usually) non-linear regressor matrix and $\theta_a \in \mathbb{R}^n$ is the parameter vector that contains the actuator parameters to be identified. Examples of these terms include lift and drag coefficients of the control surfaces and propeller coefficients. Substituting (3.22) into (3.21) results in

$$M\dot{v} = -C(v)v - D(v)v - \mathcal{G}(\vec{a}) + G_a(v, \vec{a}, \xi)\theta_a. \quad (3.23)$$

The following AID is can accommodate any vehicle control configuration that satisfies two conditions:

1. The parameters to be identified which make up θ_a must enter linearly into $\tau(v, \vec{a}, \xi)$
2. The function $G_a(v, \vec{a}, \xi) \in \mathcal{C}^1$ and is bounded for bounded v , \vec{a} , and ξ . In the sequel we will give conditions under which these signals can be proven to remain bounded.

This AID extension comes with an additional caveat. Since all terms on both sides of (3.23) contain parameters to be estimated and these parameters enter linearly, the estimate of the set of parameters is only defined up to scale. This is analogous to the limitations of the Nullspace Based Least Squares (NBLS) parameter identification method defined in Section 4.3.5.

3.4.2 AID of Plant and Actuation Parameters for Fully Coupled 6-DOF UUVs

This section extends the results of Section 3.3 to include control parameter identification of 6-DOF UUVs. New extensions to the AID reported in [36] are reported in bold for clarity.

- Plant: Using the definition of the drag matrix $D(v) = \sum_{i=1}^6 |v_i| \hat{D}_i$, the plant is of the form:

$$M\dot{v} = -C(v)v - \left(\sum_{i=1}^6 |v_i| \hat{D}_i \right) v - \mathcal{G}(\vec{a}) + \mathbf{G}_a(v, \vec{a}, \xi) \theta_a \quad (3.24)$$

- Task: Design parameter update laws for $\hat{v}(t)$, $\hat{M}(t)$, $\hat{D}_i(t)$, $\hat{g}(t)$, $\hat{b}(t)$, and $\hat{\theta}_a(t)$ such that $\lim_{t \rightarrow \infty} \Delta v(t) = \vec{0}$, $\lim_{t \rightarrow \infty} \hat{M}(t) = 0_{6 \times 6}$, $\lim_{t \rightarrow \infty} \hat{D}_i(t) = 0_{6 \times 6}$, $\lim_{t \rightarrow \infty} \hat{g}(t) = 0$, $\lim_{t \rightarrow \infty} \hat{b}(t) = \vec{0}$, and $\lim_{t \rightarrow \infty} \hat{\theta}_a(t) = \vec{0}$

- Error Coordinates:

- $\Delta v(t) = \hat{v}(t) - v(t)$
- $\Delta M(t) = \hat{M}(t) - M$
- $\Delta D_i(t) = \hat{D}_i(t) - D_i$
- $\Delta g(t) = \hat{g}(t) - g$
- $\Delta b(t) = \hat{b}(t) - b$
- $\Delta \theta_a(t) = \hat{\theta}_a(t) - \theta_a$

- Parameter Update Laws:

$$\dot{\hat{v}} = \hat{M}^{-1} \left(-C(\hat{M}, v)v - \left(\sum_{i=1}^6 |v_i| \hat{D}_i \right) v - \mathcal{G}(\vec{a}) + G_a(v, \vec{a}, \xi) \hat{\theta}_a \right) - \alpha \Delta v \quad (3.25)$$

$$\dot{\hat{M}} = \frac{\gamma_1}{2} (\psi_1 v^T + v \psi_1^T + \Delta v \psi_2^T + \psi_2 \Delta v^T) \quad (3.26)$$

$$\dot{\hat{D}}_i = \gamma_2 |v_i| \Delta v v^T \quad (3.27)$$

$$\dot{\hat{g}} = \gamma_3 \Delta v^T R^T(\vec{a}) e_3 \quad (3.28)$$

$$\dot{\hat{b}} = -\gamma_4 J(\Delta \omega) R^T(\vec{a}) e_3 \quad (3.29)$$

$$\dot{\hat{\theta}}_a = -\gamma_5 \left(G_a(v, \vec{a}, \xi) \right)^T \Delta v \quad (3.30)$$

Where

- $G_a(v, \vec{a}, \xi) \hat{\theta}_a$ will be shown to be bounded in consequence of the boundedness of v , \vec{a} , ξ , and $\hat{\theta}_a$
- $C(\hat{M}, v)$ is the Coriolis matrix defined in Chapter 2.
- $\psi_1 = ad(v)^T \Delta v$
- $\psi_2 = \dot{\hat{v}} + \alpha \Delta v$
- $\alpha, \gamma_1, \gamma_2, \gamma_3, \gamma_4, \gamma_5 \in \mathbb{R}_+$
- $\hat{M}(t_0)$ is symmetric positive definite
- $\hat{v}(t_0) = v(t_0)$

The details of the much of the following stability proof are reported in [36] and are not reproduced here unless required for clarity on the extension for simultaneous identification of actuation

parameters. As in [36] we develop the velocity error dynamics expression

$$\begin{aligned}
M\dot{\Delta v} &= M(\dot{\phi} - \dot{v}) \\
&= \alpha M\Delta v - \Delta M\psi_2 - ad(v)\Delta Mv \\
&\quad - \left(\sum_{i=1}^6 |v_i| \Delta D_i \right) v - \Delta \mathcal{G}(R(\vec{a})) + \mathbf{G}_a(v, \vec{a}, \xi) \Delta \theta_a.
\end{aligned} \tag{3.31}$$

Now consider the Lyapunov function candidate

$$\begin{aligned}
V(t) &= \frac{1}{2} \Delta v^T M \Delta v + \frac{1}{2\gamma_1} \text{tr}(\Delta M \Delta M^T) + \frac{1}{2\gamma_2} \sum_{i=1}^6 \text{tr}(\Delta D_i \Delta D_i^T) \\
&\quad + \frac{1}{2\gamma_3} (\Delta g)^2 + \frac{1}{2\gamma_4} \Delta b^T \Delta b + \frac{1}{2\gamma_5} \Delta \theta_a^T \Delta \theta_a.
\end{aligned} \tag{3.32}$$

The Lyapunov candidate function (3.32) is:

- positive definite
- radially unbounded
- equal zero if and only if $\Delta v = \vec{0}$, $\Delta M = 0_{6 \times 6}$, $\Delta D_i = 0_{6 \times 6} \forall i$, $\Delta g = 0$, $\Delta b = \vec{0}$, **and** $\Delta \theta_a = \vec{0}$.

The time derivative of (3.32) is

$$\begin{aligned}
\dot{V}(t) &= \frac{1}{2} \left(\dot{\Delta v}^T M \Delta v + \Delta v^T M \dot{\Delta v} \right) + \frac{1}{\gamma_1} \text{tr}(\Delta M \dot{\Delta M}^T) + \frac{1}{\gamma_2} \sum_{i=1}^6 \text{tr}(\Delta D_i \dot{\Delta D}_i^T) \\
&\quad + \frac{1}{2\gamma_3} \Delta g \dot{\Delta g} + \frac{1}{\gamma_4} \Delta b^T \dot{\Delta b} + \frac{1}{\gamma_5} \Delta \theta_a^T \dot{\Delta \theta}_a.
\end{aligned} \tag{3.33}$$

This can be simplified using (3.31). Substituting (3.25)-(3.29) results in

$$\begin{aligned}\dot{V}(t) &= -\alpha\Delta v^T M\Delta v + \frac{1}{2}\Delta\theta_a^T \left(G(v, \vec{a}, \xi) \right)^T \Delta v + \frac{1}{2}\Delta v^T G(v, \vec{a}, \xi)\Delta\theta_a + \frac{1}{\gamma_5}\Delta\theta_a^T \Delta\dot{\theta}_a \quad (3.34) \\ &= -\alpha\Delta v^T M\Delta v + \Delta\theta_a^T \left(G(v, \vec{a}, \xi) \right)^T \Delta v + \frac{1}{\gamma_5}\Delta\theta_a^T \Delta\dot{\theta}_a.\end{aligned}$$

Finally substituting the parameter update law (3.30) results in

$$\dot{V}(t) = -\alpha\Delta v^T M\Delta v \quad (3.35)$$

This expression is negative definite in Δv and negative semidefinite in the error coordinates Δv , ΔM , ΔD_i , Δg , Δb , and $\Delta\theta_a$.

A proof that the smallest eigenvalue of \hat{M} is bounded away from zero is left as future work. We will assume this statement is true if the parameters are initialized close to the “true” values, which is confirmed in simulation studies.

We note from [36] that with v , Δv , ΔM , ΔD_i , Δg , Δb , and $G(v, \vec{a}, \xi)$, bounded and M , D_i , g , b , and θ_a constant, it is implied that \hat{v} , \hat{M} , \hat{D}_i , \hat{g} , \hat{b} , and $\hat{\theta}_a$ are bounded. If we assume that the smallest eigenvalue of \hat{M} is bounded away from zeros for all time then \hat{M}^{-1} is bounded and thus $\Delta\dot{v}$ is bounded. Additionally $\Delta v \in \mathcal{L}_2$ and bounded $\Delta\dot{v}$ implies that $\lim_{t \rightarrow \infty} \Delta v = \vec{0}$

Since the parameter update equation (3.30) is bounded and $\lim_{t \rightarrow \infty} \Delta v = \vec{0}$ this implies that $\lim_{t \rightarrow \infty} \dot{\hat{M}} = \vec{0}$, $\lim_{t \rightarrow \infty} \dot{\hat{D}}_i = \vec{0} \forall i$, $\lim_{t \rightarrow \infty} \dot{\hat{g}} = 0$, $\lim_{t \rightarrow \infty} \dot{\hat{b}} = \vec{0}$, and $\lim_{t \rightarrow \infty} \dot{\hat{\theta}}_a = \vec{0}$. Therefore the estimator’s angular and linear velocities asymptotically converge to the velocities of the actual vehicle and all estimated parameters converge to a common scalar multiple of their constant values [36].

3.4.3 Extension of AID to 6-DOF UUV Plants with Diagonal Mass and Drag Matrices

This section reports an extension of the AID reported in Section 3.4.2 to the class of UUV plants with diagonal mass and drag matrices. Smallwood and Whitcomb report the first AID for fully decoupled UUV plants in [48]. Their approach was to approximate the 6-DOF UUV plant model as six one degree of freedom (1-DOF) plant models where each degree of freedom is completely independent of all the others and they report a common AID applicable to all six 1-DOF plants. The AID presented here differs from [48] in that it includes coupling from Coriolis terms, but omits all linear damping terms.

Consider the case of plant models of UUVs of the form (3.21) where the mass M and drag D matrices in are diagonal. Specifically

$$M = \text{diag}([m_{11}; m_{22}; m_{33}; m_{44}; m_{55}; m_{66}]) \quad (3.36)$$

$$= \text{diag}(m) \quad (3.37)$$

and

$$D = \begin{bmatrix} |v_1|d_{11} & 0 & 0 & 0 & 0 & 0 \\ 0 & |v_2|d_{22} & 0 & 0 & 0 & 0 \\ 0 & 0 & |v_3|d_{33} & 0 & 0 & 0 \\ 0 & 0 & 0 & |v_4|d_{44} & 0 & 0 \\ 0 & 0 & 0 & 0 & |v_5|d_{55} & 0 \\ 0 & 0 & 0 & 0 & 0 & |v_6|d_{66} \end{bmatrix} \quad (3.38)$$

$$= \text{diag}(|v|) \text{diag}(d). \quad (3.39)$$

The total mass vector $m \in \mathbb{R}^6$ contains the sum of the added mass and rigid body terms and the total drag vector $d \in \mathbb{R}^6$ contains the scalar quadratic drag parameters for each degree of freedom.

- Task: Modify parameter update laws (3.26) (3.27) to adaptively identify $\hat{m}(t)$ and $\hat{d}(t)$ defined in (3.37) and (3.39) such that $\lim_{t \rightarrow \infty} \hat{m}(t) = \vec{0}$, $\lim_{t \rightarrow \infty} \hat{d}(t) = \vec{0}$,

- Modified Error Coordinates:

- $\Delta m(t) = \hat{m}(t) - m$

- $\Delta d(t) = \hat{d}(t) - d$

For convenience we will define $\Delta M = \text{diag}(\Delta m)$ and $\Delta D = \text{diag}(\Delta d)$.

- Parameter Update Laws:

$$\dot{\hat{m}} = \gamma_1 (v^T \text{diag}(\psi_1) + \psi_2^T \text{diag}(\Delta v))^T \quad (3.40)$$

$$\dot{\hat{d}} = \gamma_2 (\Delta v^T \text{diag}(|v|) \text{diag}(v))^T \quad (3.41)$$

Where

- $\text{diag}(\hat{m}(t_0))$ is PDS, or equivalently all entries in $\hat{m}(t_0)$ are positive

- System and Stability Proof

Consider the following Lyapunov function candidate

$$\begin{aligned} V(t) = & \frac{1}{2} \Delta v^T M \Delta v + \frac{1}{2\gamma_1} \Delta m^T \Delta m + \frac{1}{2\gamma_2} \Delta d^T \Delta d \\ & + \frac{1}{2\gamma_3} (\Delta g)^2 + \frac{1}{2\gamma_4} \Delta b^T \Delta b + \frac{1}{2\gamma_5} \Delta \theta_a^T \Delta \theta_a. \end{aligned} \quad (3.42)$$

As in Section 3.4.2 (3.42) is

- positive definite
 - radially unbounded
 - equal zero if and only if $\Delta v = \vec{0}$, $\Delta m = \vec{0}$, $\Delta d = \vec{0}$, $\Delta g = 0$, $\Delta b = \vec{0}$, and $\Delta \theta_a = \vec{0}$.

The time derivative of (3.42) is

$$\begin{aligned} \dot{V}(t) = & \frac{1}{2} \left(\dot{\Delta v}^T M \Delta v + \Delta v^T M \dot{\Delta v} \right) + \frac{1}{\gamma_1} \dot{\Delta m}^T \Delta m + \frac{1}{\gamma_2} \dot{\Delta d}^T \Delta d \\ & + \frac{1}{2\gamma_3} \Delta g \dot{\Delta g} + \frac{1}{\gamma_4} \Delta b^T \dot{\Delta b} + \frac{1}{\gamma_5} \Delta \theta_a^T \dot{\Delta \theta}_a. \end{aligned} \quad (3.43)$$

Substituting in (3.31) yields

$$\begin{aligned} \dot{V}(t) = & -\alpha \Delta v^T M \Delta v - \frac{1}{2} \left(v^T \Delta M \psi_1 + \psi_2^T \Delta M \Delta v \right) \\ & - \frac{1}{2} \left(\Delta v^T \Delta M \psi_2 + \psi_1^T \Delta M v \right) - \Delta v^T \text{diag}(|v|) \Delta D v \\ & - \Delta v^T \Delta \mathcal{G}(R(\vec{a})) + \Delta v^T G_a(v, \vec{a}, \xi) \Delta \theta_a + \frac{1}{\gamma_1} \dot{\Delta m}^T \Delta m + \frac{1}{\gamma_2} \dot{\Delta d}^T \Delta d \\ & + \frac{1}{2\gamma_3} \Delta g \dot{\Delta g} + \frac{1}{\gamma_4} \Delta b^T \dot{\Delta b} + \frac{1}{\gamma_5} \Delta \theta_a^T \dot{\Delta \theta}_a. \end{aligned} \quad (3.44)$$

Again we first substitute in the unmodified parameter update laws (3.28)-(3.30) for clarity.

This yields

$$\begin{aligned} \dot{V}(t) = & -\alpha \Delta v^T M \Delta v - \frac{1}{2} \left(v^T \Delta M \psi_1 + \psi_2^T \Delta M \Delta v \right) \\ & - \frac{1}{2} \left(\Delta v^T \Delta M \psi_2 + \psi_1^T \Delta M v \right) - \Delta v^T \text{diag}(|v|) \Delta D v \\ & + \frac{1}{\gamma_1} \dot{\Delta m}^T \Delta m + \frac{1}{\gamma_2} \dot{\Delta d}^T \Delta d. \end{aligned} \quad (3.45)$$

Note that for all vectors $y_1, y_2 \in \mathbb{R}^6$ $diag(y_1)y_2 = diag(y_2)y_1$ and $y_1^T diag(y_2) = y_2^T diag(y_1)$.

Thus

$$\begin{aligned} \dot{V}(t) = & -\alpha \Delta v^T M \Delta v - \left(v^T diag(\psi_1) + \psi_2^T diag(\Delta v) \right) \Delta m & (3.46) \\ & - \Delta v^T diag(|v|) diag(v) \Delta d \\ & + \frac{1}{\gamma_1} \Delta \dot{m}^T \Delta m + \frac{1}{\gamma_2} \Delta \dot{d}^T \Delta d. \end{aligned}$$

Finally, we substitute in the modified parameter update laws (3.40)-(3.41) to yield

$$\dot{V}(t) = -\alpha \Delta v^T M \Delta v. \quad (3.47)$$

This result for the stability of the modified AID for diagonal UUV plants shares the same properties as the result for the AID of fully coupled UUV plants reported in Section 3.4.2. The implication is that as previously, the estimate of unmodified parameters converge to constant values, and $\lim_{t \rightarrow \infty} \hat{m} = \vec{0}$ and $\lim_{t \rightarrow \infty} \hat{d} = \vec{0}$.

Chapter 4

Identification of Dynamical UUV Plants with Random Sample Consensus (RANSAC)

4.1 Introduction

This chapter presents an algorithm that uses the random sample consensus (RANSAC) framework for robust identification of parameters of dynamical systems. We call this algorithm Dynamical Plant Identification using RANSAC (DIRANSAC). The original RANSAC algorithm was developed to estimate transformation models between camera image planes using corresponding features from a set of observed data that contain outliers. RANSAC is a fundamental tool in the field of computer vision. At its most basic variant, RANSAC involves first randomly sampling the data to generate a hypothesis of the parameters to be identified, and then testing this hypothesis against the entire dataset [11]. RANSAC was designed to improve model fitting when using observational data corrupted by both Gaussian and non-Gaussian noise (commonly referred to as noisy data with outliers). Although the noise characteristics of dynamical plants are different than those of image feature correspondence, the author has found the RANSAC framework to improve the estimate of dynamical plant parameters in the presence of noisy observational data with outliers.

Such an approach can be advantageous in several instances. The plant parameters for complex dynamical systems, such as underwater vehicles whose underlying dynamics are infinite dimensional due to the effects of the viscous fluid in which they operate, are often identified from observed experimental data by fitting the data to approximate finite-dimensional models. As a result, the observational data collected in experiments will not fit the model exactly and the associated error will be non Gaussian, limiting the effectiveness of classic least squares approaches to parameter estimation of these plants. Additionally dynamical systems sometimes operate intermittently in two or more different regimes; in the case of underwater robotic vehicles one such regime dominates when the vehicle is at or near the surface and another when the vehicle is fully submerged [12]. By design DIRANSAC will fit a model that agrees with the majority of the observations, and the effect of data collected in other regimes will be minimized.

The remainder of this chapter is organized as follows: Section 4.2 first provides a review of literature on the original RANSAC algorithm and the many reported improvements on RANSAC currently used the field of computer vision. Section 4.2 then reports a review of literature in other fields besides computer vision that report implementations of the RANSAC algorithm to solve parameter estimation problems. Section 4.3 reports the new DIRANSAC algorithm. Section 4.4 reports the methodology for a simulation study to identify parameters of a simple one degree of freedom (1-DOF) unmanned underwater vehicle (UUV) dynamical plant using noisy observational data corrupted with outliers. Section 4.5 reports simulated results and a discussion of these results.

4.2 Literature Review

4.2.1 Advances in the RANSAC Algorithm

First published in 1981, the seminal RANSAC paper [11] has been cited over 19,000 times and is widely used in many applications in the field of computer vision. Many reported improvements on RANSAC have followed. A thorough survey of several notable improvements over the basic RANSAC algorithm is reported by Choi *et al.*, more than 15 years after the original paper [3].

The authors in [3] categorize the many reported improvements by their intended objective: to be accurate, to be fast, and to be robust. An overview of their findings is given as follows:

To Be Accurate: In an effort to be more accurate, other loss functions were proposed including M-estimator SAC (MSAC) and Maximum Likelihood SAC (MLE SAC) [51] as well as adding a local optimization step as in Locally Optimized RANSAC (LO-RANSAC) [4]. MSAC, MLE SAC, and the original RANSAC were all found to have similar accuracies in homography estimation, and LO-RANSAC was shown to offer improvements in accuracy at an additional computational cost.

To Be Fast: Methods have been proposed to increase speed by employing guided sampling like Guided MLE SAC [50] and Progressive SAC (PROSAC) [5], and partial evaluation methods such as Randomized RANSAC (R-RANSAC) [34] and Sequential Probability Ratio Test (SPRT) [35]. However, in theory guided MLE SAC and PROSAC can actually impair the global search. R-RANSAC and SPRT were shown to reduce computational time by only performing the verification process on the entire data set if the estimate passes the pretest.

To Be Robust: The robustness of the RANSAC algorithm can be improved using adaptive evaluation to adjust the inlier threshold such as Least Median of Squares (LMedS) [47] or MLE SAC using the estimate of the error variance (u-MLE SAC) [2], although these approaches experience problems if the expected inlier ratios are less than 0.5. Adaptive termination is also used in Maximum A Posterior Estimation SAC (MAPSAC) [10] to recompute the number of iterations required based on the observed inlier ratios.

4.2.2 Reported Implementations of the RANSAC Algorithm

Implementations of RANSAC-based algorithms are reported in fields other than computer vision.

Farahmand *et al.* proposes a novel “doubly robust” Kalman smoother to handle both state and measurement outliers in dynamical systems [8]. It is shown to perform comparably to RANSAC-Huber smoothers in dynamical trajectory tracking with measurement outliers ratios less than 50%, but shown to perform considerably better than RANSAC when subject to state outliers. In [8] the

authors propose a version that allows for on-line estimation. There are no reported improvements to the basic RANSAC algorithm used for comparison, and experiments with only a fixed number of hypothesis for are reported.

Schnabel in [45] reports an implementation of a RANSAC based algorithm to detect geometric shapes in point clouds. The authors fit models of different shapes and optimize the sampling process by increasing sampling of nearby data (in Cartesian space). The results demonstrates robust object detection using RANSAC in noisy point cloud data corrupted by outliers.

Some implementations of RANSAC in the field of biomedical research are reported. Uhercik *et al.* in [52] reports a RANSAC based algorithm for estimating parameters used in localization of surgical tools in 3-D ultrasound images. The results indicate improvements in computational time and accuracy over other existing methods when applied to both simulated and real ultrasound images. Kang *et al.* in [25] reports a RANSAC based algorithm to model the nonlinear phagocyte transmigration process and compares performance with least squares.

To the best of the author's knowledge this thesis is the first reported application of RANSAC to dynamical plant parameter estimation.

4.3 Methodology

The basic RANSAC algorithm was adapted to better estimate plant parameters in dynamical systems. Several improvements found in the literature were directly implemented in addition to improvements that follow from key observations by the author about the parameters of dynamical systems. The DIRANSAC algorithm was generalized for dynamical systems with q degrees of freedom and k control inputs where \mathcal{T} observations are available.

The inputs to DIRANSAC are observational data, known plant parameters, and DIRANSAC hyperparameters, or parameters that control the process of the algorithm and can be tuned for performance. The observational data consists of $\vec{t}_{ob} \in \mathbb{R}^{k \times \mathcal{T}}$, a vector of observed plant control inputs and $\vec{v}_{ob} \in \mathbb{R}^{q \times \mathcal{T}}$, a vector of observed plant velocities. All observational data must be

sampled at the same time, i.e. for every $\tau_{ob}(t_i)$ there is a corresponding $v_{ob}(t_i)$. All known plant parameters such as length and volume are denoted as Γ_{kn} . The inlier threshold $\epsilon \in \mathbb{R}^q$ is a hyperparameter that defines the distance threshold used to classify a data point as an inlier or outlier of the hypothesized estimate. The probability of success η is a hyperparameter that provides the acceptable lower limit of the likelihood that the solution that is returned is computed using only inliers. The initial guess of the inlier ratio is passed as I , which is best initialized to a low estimate. Lastly the hyperparameter m provides an estimate for the number of random observations that must be drawn to compute a well defined solution. A higher estimate of m is more conservative.

There are two outputs from DIRANSAC, the estimate of the parameter set with the lowest error θ_p , and the ratio of inliers for that parameter set I_e . An overview is presented in Algorithm 1.

4.3.1 Check if the Solution is Well Defined

Naturally the question arises as to how many samples should be randomly drawn to compute the estimate $\hat{\theta}_p$. There are analytical solutions for the number of samples required to estimate the fundamental matrix in computer vision applications, and the commonly used algorithm nominally uses eight independent feature correspondences to compute a well defined solution [17]. However, there are no analytical solutions for the number of samples required to estimate parameters of an arbitrary dynamical system. Furthermore, many samples may be degenerate due to repetitive excitation. As a solution, we propose to continue to randomly sample the observations until a well defined solution can be computed. The criteria that specifies whether a well defined solution is possible is dependent on the estimation method and three definitions are reviewed in Section 4.3.5. It is advantageous to limit the number of samples used in the estimate as the likelihood of randomly sampling only inlier observations decreases exponentially as noted in Section 4.3.4. In practice, we find that this number can be on the order of 30-50 samples for the 1-DOF simulation study reported in Section 4.4, but the number of samples depends greatly on the plant to be identified and the excitation involved.

Algorithm 1 DIRANSAC

Input:

- $\vec{\tau}_{ob}$ Vector of plant control inputs $[\tau_{ob}(t_0), \tau_{ob}(t_1), \dots, \tau_{ob}(t_n)] \in \mathbb{R}^{k \times \mathcal{T}}$
 \vec{v}_{ob} Vector of observed plant states $[v_{ob}(t_0), v_{ob}(t_1), \dots, v_{ob}(t_n)] \in \mathbb{R}^{q \times \mathcal{T}}$.
 ϵ Vector of inlier thresholds for each DOF.
 η Probability of success
 I Initial estimate of fraction of inliers.
 m Estimated number of samples required to fit model
 Γ_{kn} Known plant parameters.

Output:

- θ_p Parameter estimate with the lowest error
 I_e Fraction of inliers found with estimate
- 1: **function** DI_RANSAC($\vec{\tau}_{ob}, \vec{v}_{ob}, \epsilon, \eta, I, m, \Gamma_{kn}$)
 - 2: LowestError = inf
 - 3: $k_{min} \leftarrow$ ComputeIterationsRequired(η, I, m) // Section 4.3.4
 - 4: **while** $k < k_{min}$ **do**
 - 5: $S =$ Empty subset of observations
 - 6: **while** Solution is not well defined **do**
 - 7: $S = S +$ Randomly sampled observation from $\vec{\tau}_{ob}, \vec{v}_{ob}$
 - 8: $\overline{W}(\cdot, \mathbb{B}) \leftarrow$ ComputeDesignMatrix(S, Γ_{kn}) // Section 4.3.5
 - 9: Check if solution is well defined // Section 4.3.1
 - 10: **end while**
 - 11: $\hat{\theta}_p \leftarrow$ ComputeParameterHypothesis($\overline{W}(\cdot, \mathbb{B})$) // Section 4.3.5
 - 12: **if** PreliminaryTest($\hat{\theta}_p$) **then** // Section 4.3.2
 - 13: **try**
 - 14: $\vec{v}_{\hat{\theta}_p} \leftarrow$ ForwardSimulation($\hat{\theta}_p, \tau_{ob}(t_0), v_{ob}(t_0), \Gamma_{kn}$) // Section 4.3.3
 - 15: $e_{\hat{\theta}_p} \leftarrow$ ComputeModelError($\vec{v}_{\hat{\theta}_p}, \vec{v}_{ob}$) // Section 4.3.3
 - 16: **if** $e_{\hat{\theta}_p} <$ LowestError **then**
 - 17: LowestError = $e_{\hat{\theta}_p}$
 - 18: $\theta_p = \hat{\theta}_p$
 - 19: $I_e \leftarrow$ ComputeFractionOfInliers($\vec{v}_{\hat{\theta}_p}, \vec{v}_{ob}, \epsilon$) // Section 4.3.4
 - 20: $k_{min} \leftarrow$ ComputeIterationsRequired(η, I_e, m) // Section 4.3.4
 - 21: **end if**
 - 22: **catch** Numerical Integration Failure
 - 23: **continue**
 - 24: **end try**
 - 25: **end if**
 - 26: **end while**
 - 27: **return** θ_p, I_e
 - 28: **end function**
-

4.3.2 Preliminary Test

A preliminary test is used in an effort to save time by not attempting to verify hypothesized parameter estimates that are clearly wrong [34]. In dynamical plant applications some parameters such as mass terms are known to be positive while others like drag are known to be dissipative or negative. We can apply this knowledge by using a preliminary test to check if all the parameters of the hypothesized estimate $\hat{\theta}_p$ are the correct sign. If they are not, then the verification process is skipped and the hypothesized estimate is discarded.

4.3.3 Forward Simulation and Model Fit Error

Verification of the hypothesized estimate is performed by first attempting to complete a simulation of the dynamical plant using the hypothesized parameter estimate $\hat{\theta}_p$ subject to the same control inputs $\tau_{ob}(t)$, and initial condition $v_{ob}(t_0)$. This simulation is commonly performed using a numerical integration package, and if the error in the parameter estimate is significant, the simulation might fail to meet integration tolerances or otherwise not complete. For this reason the algorithm makes use of a try/catch framework. If the simulation fails then hypothesized estimate is assumed to not be correct and discarded.

In the event that the forward simulation does complete, the forward simulation will return the vector of plant velocities $\vec{v}_{\hat{\theta}_p}$ computed using the hypothesized estimate as $\vec{v}_{\hat{\theta}_p} = [v_{\hat{\theta}_p}(t_0), v_{\hat{\theta}_p}(t_1), \dots, v_{\hat{\theta}_p}(t_n)] \in \mathbb{R}^{q \times \mathcal{T}}$. The model fit error is computed as

$$e_{\hat{\theta}_p} = \sum_{j=1}^q \left(w_j (||[\vec{v}_{\hat{\theta}_p}]_j - [\vec{v}_{ob}(t)]_j||_2)^2 \right), \quad (4.1)$$

where w_j is the weight for the j^{th} degree of freedom.

Although it is more common to report the mean absolute error as a measure of parameter identification accuracy, this proposed error metric was found to better verify hypothesized estimates.

4.3.4 Inlier Classification and Early Exit Criteria

The inlier classification is computed from the simulated plant velocities $\vec{v}_{\hat{\theta}_p}$. The number of inliers is defined as the number of observations in \vec{v}_{ob} that are within some inlier threshold distance specified by ϵ of the corresponding computed plant velocities in $\vec{v}_{\hat{\theta}_p}$. The fraction of inliers I_e for a given hypothetical parameter estimate is simply the number of inliers divided by the total number of observations \mathcal{T} . If the plant has more than one degree of freedom, an individual inlier threshold for each degree of freedom can be used and thus $\epsilon \in \mathbb{R}^q$. In this case I_e is defined as some weighted average of all the fraction of inliers for each degree of freedom.

The number of iterations k_{min} required is computed as a function of the probability of success η and the estimated fraction of inliers I . This is adapted from the original RANSAC algorithm [11] as

$$k_{min} = \frac{\log(1 - \eta)}{\log(1 - I^m)}. \quad (4.2)$$

Where η is the probability of selecting a subset of observations \mathcal{S} with only inliers and m is the number of randomly selected samples required to compute a parameter estimate. As described in Section 4.3.1 the number of samples m required to estimate a solution is not constant and increases as needed to ensure that the solution is well defined. As a result we propose to compute k_{min} as defined in (4.2) using a high estimate for m and use the following criteria to exit early [1]. The minimum number of iterations k_{min} is recalculated each time a new best estimate is found using the inlier ratio of the new best estimate I_e . If the number of iterations performed is greater than the newly computed k_{min} then the algorithm exits.

We found that in practice for the 1-DOF system described in Section 4.4 that at least $m \geq 30$ samples are often drawn, and with “reasonable” inlier ratios of $w = 0.8$ the number of required iterations to achieve a good result with 0.95 probability was $\approx 2.5e3$.

4.3.5 Parameter Identification Methods

The DIRANSAC algorithm uses one of several types of least squares methods to compute the hypothesis. We will refer to the particular method used in DIRANSAC as the kernel of the algorithm. This section provide a brief overview of three least squares methods.

Ordinary Least Squares (OLS)

Overdetermined OLS problems have the form $Ax \approx b$ where the A is the input data, b is the output data, and x is a vector of parameters to be identified [21], [53]. OLS problems account for noise in b but assume no noise in A . Let $A_i \in \mathbb{R}^{m \times p}$ and $b_i \in \mathbb{R}^{m \times 1}$ be individual observations of the systems. We can define the design matrix \overline{W} as

$$\overline{W} = \begin{bmatrix} A_1 \\ A_2 \\ \vdots \\ A_i \end{bmatrix} \in \mathbb{R}^{nm \times p} \quad i = 1, 2, \dots, n, \quad (4.3)$$

where n is the number of observations. Likewise the observational vector is defined as

$$\mathbb{B} = \begin{bmatrix} b_1 \\ b_2 \\ \vdots \\ b_i \end{bmatrix} \in \mathbb{R}^{nm \times 1} \quad i = 1, 2, \dots, n. \quad (4.4)$$

Assuming $\overline{W}^T \overline{W}$ is full rank, and thus invertible, solutions to the OLS problem that minimize $\|Ax - b\|_2$ are

$$x = (\overline{W}^T \overline{W})^{-1} \overline{W}^T \mathbb{B} \in \mathbb{R}^{p \times 1}. \quad (4.5)$$

Solutions to the OLS problem are ill defined when $\overline{W}^T \overline{W}$ is not full rank, and thus not invertible.

Total Least Squares (TLS)

One class of overdetermined TLS problems has the form $Ax = b$ where the A is the input data, b is the output data, and x is a vector of parameters to be identified [21], [53]. TLS solutions assume noise in A and in b . Let $A_i \in \mathbb{R}^{m \times p}$ and $b_i \in \mathbb{R}^{m \times 1}$ be individual observations of the systems.

We can define the design matrix $\overline{\mathbb{W}}$ and the observational vector to be the same as in the OLS formulation. Solutions to the TLS problem can be found by using singular value decomposition. Let

$$[\overline{\mathbb{W}}, \mathbb{B}] = USV^T \in \mathbb{R}^{m \times p+1} \quad (4.6)$$

be a singular value decomposition where the diagonal matrix of ordered singular values is

$$S = \text{diag}(s_1, s_2, \dots, s_p, s_{p+1}), \quad (4.7)$$

where $s_i > s_{i+1}$, $i = 1, 2, \dots, p$. If we define the blocks of V to be

$$V = \begin{bmatrix} V_{11} & V_{12} \\ V_{21} & V_{22} \end{bmatrix}, \quad V_{12} \in \mathbb{R}^{p \times 1}, \quad V_{22} \in \mathbb{R}^1, \quad (4.8)$$

unique solutions for x can be computed as

$$x = -V_{12}/V_{22} \in \mathbb{R}^{p \times 1}. \quad (4.9)$$

Solutions to the TLS problem are ill defined when $s_p \approx s_{p+1}$

Nullspace Based Least Squares (NBLS)

We define NBLS problems to have the form $Ax = 0$ where the A is the input data, and x is a vector of parameters to be identified. Experimental results to be published by this author and others indicate that solutions to the NBLS are sensitive to noise in A . Let $A_i \in \mathbb{R}^{m \times p}$ be individual observations of the systems. We can define the design matrix \mathbb{W} as

$$\overline{\mathbb{W}} = \begin{bmatrix} A_1 \\ A_2 \\ \vdots \\ A_i \end{bmatrix} \in \mathbb{R}^{nm \times p} \quad i = 1, 2, \dots, n. \quad (4.10)$$

Given an $mn \times p$ matrix $\overline{\mathbb{W}}$ where $mn > p$, the unit vector x that minimizes

$$\min_x \|\overline{\mathbb{W}}x\|_2, \quad \|x\|_2 = 1 \quad (4.11)$$

is the unit eigenvector corresponding to the smallest eigenvalue of $\overline{\mathbf{W}}^T \overline{\mathbf{W}}$. Solutions to the NBLs are only defined up to scale. In practice the solutions are scaled such that they match one known parameter. If more than one eigenvalue of $\overline{\mathbf{W}}^T \overline{\mathbf{W}}$ is approximately zero, or equivalently if dimension of the nullspace of $\overline{\mathbf{W}}^T \overline{\mathbf{W}}$ is greater than one, then solutions are not well defined.

4.4 Simulated 1-DOF Experimental Setup

The performance of the new DIRANSAC algorithm was tested using observational data of a simulated 1-DOF UUV plant. The equations of motion (EOM) for a fully uncoupled 1-DOF UUV can be expressed as [12]

$$\tau(t) = m\dot{v}(t) + d|v(t)|v(t) - b \quad (4.12)$$

$$m\dot{v}(t) = -d|v(t)|v(t) + b + \tau(t). \quad (4.13)$$

We consider the case where available actuation consists of both a thruster and an actuated hydrodynamic control surface. A simple model for thruster force is

$$\tau_{prop}(t) = \beta_1 \omega(t)^2, \quad (4.14)$$

where β_1 is the quadratic propeller coefficient with units $(N * s^2) / rad^2$ and $\omega(t)$ is commanded angular speed of propeller in rad/s . A simple approximate model of the actuated hydrodynamic control surface is

$$\tau_{cs}(t) = -\beta_2 |v(t)|v(t)\alpha(t), \quad (4.15)$$

where β_2 is the hydrodynamic drag coefficient with units of $(N * s^2) / rad$ and α is the commanded deflection with units of *radians*.

Thus the EOM of a 1-DOF underwater vehicle with a thruster and control surface becomes

$$m\dot{v}(t) = -d|v(t)|v(t) + b + \beta_1\omega(t) - \beta_2|v(t)|v(t)\alpha(t) \quad (4.16)$$

$$0 = -m\dot{v}(t) - d|v(t)|v(t) + b + \beta_1\omega(t) - \beta_2|v(t)|v(t)\alpha(t). \quad (4.17)$$

All the unknown plant and actuator parameters enter linearly in (4.17). For this simulation we use NBLs as the kernel of DIRANSAC algorithm and we define a vector of unknown plant and actuator parameters as

$$\theta_p = [m \quad d \quad b \quad \beta_1 \quad \beta_2]^T. \quad (4.18)$$

Since all the unknown parameters enter linearly (4.17) can be written as

$$0 = \frac{\partial}{\partial \theta_p} [-m\dot{v}(t) - d|v(t)|v(t) + b + \beta_1\omega(t) - \beta_2|v(t)|v(t)\alpha(t)] \theta_p \quad (4.19)$$

$$0 = [-\dot{v}(t) \quad -|v(t)|v(t) \quad 1 \quad \omega(t) \quad -|v(t)|v(t)\alpha(t)] \theta_p \quad (4.20)$$

$$0 = \mathbb{W}\theta_p. \quad (4.21)$$

The following control signals were used to excite the system in simulation

$$\omega(t) = \sin(t * 0.25) \text{rad/s} \quad (4.22)$$

$$\alpha(t) = \sin(t * 0.028) \text{rad} \quad (4.23)$$

The following noise models were used:

- $v(t) = v_{true}(t) + \mathcal{N}(0, 0.04) + sp(0.05, 0.5, p)$ (m/s)
- $\dot{v}(t) = \dot{v}_{true}(t) + \mathcal{N}(0, 0.01) + sp(-0.01, 0.04, p)$ (m/s^2)
- $\omega(t) = \omega_{true}(t) + \mathcal{N}(0, 0.25) + sp(1.25, 6.25, p)$ (rad/s)
- $\alpha(t) = \alpha_{true}(t) + \mathcal{N}(0, 0.25) + sp(1.25, 6.25, p)$ (m)

Where $\mathcal{N}(\mu, \sigma)$ is white Gaussian noise with mean μ and standard deviation σ and $sp(\mu_s, a_0, p)$ is random “salt and pepper” noise with mean μ_s , amplitude a_0 and outlier probability of p such that:

$$sp(\mu_s, a_0, p) = \begin{cases} P(0) & = (1-p) \\ P(\mu_s + a_0) & = p/2 \\ P(\mu_s - a_0) & = p/2 \end{cases} \quad (4.24)$$

1-DOF parameter identification was performed in a sequence of simulations with increasing measurement error outlier ratios “ p ”. The true plant parameters were chosen to match those experimentally identified in [32]. The plant parameters were estimated using the standard NBLs method and the new DIRANSAC algorithm using the NBLs kernel. The simulation and identification for each outlier ratio was repeated 10 times, each iteration with the same noise model, but with different random noise values. No filtering was performed on any signal.

Parameter validation was performed by completing a simulation of the UUV plant dynamics using the same control input and initial condition, but using the estimated plant parameters. The error in parameter estimation is reported as mean absolute error (MAE) between the simulated plant velocities using the estimated parameters and the simulated plant velocities using the “true” parameters.

4.5 Results

4.5.1 Simulated 1-DOF Data

Figure 4.1 provides a plot of the MAE of plant parameters identified from observational datasets corrupted by an increasing ratio of outliers. Results from both NBLs and the DIRANSAC algorithm with the NBLs kernel are shown for comparison.

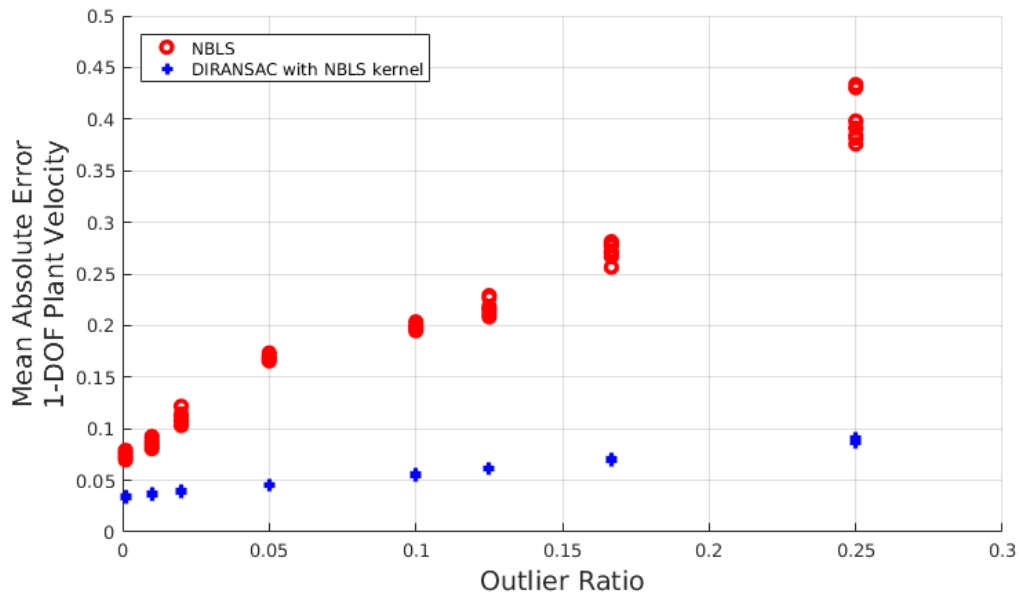


Figure 4.1: Mean absolute error of plant velocities when using parameters identified from data with an increasing ratio of measurement outliers

Figure 4.2 illustrates the improvement in parameter identification when using the DIRANSAC method. Figure 4.2 provides a plot of the plant velocity in simulation with parameters estimated from both the NBLs and DIRANSAC with the NBLs kernel methods. The outlier ratio of this particular simulation was 0.13 and the plot in Fig 4.2 includes the simulated noisy data with outliers for scale.

4.5.2 Discussion

These results suggest that the new DIRANSAC algorithm offers improvements over traditional least squares methods when estimating parameters from observational data corrupted by outliers. To confirm the performance of DIRANSAC the parameters of a simulated 1-DOF UUV were estimated using NBLs and DIRANSAC with a NBLs kernel. Results of parameter estimation using other least squares methods such as OLS and TLS were not reported, and is the subject of future work. However, the author believes that DIRANSAC with OLS and TLS kernels would offer similar improvements over traditional implementations of OLS and TLS respectively if the observational data is corrupted by non-Gaussian noise.

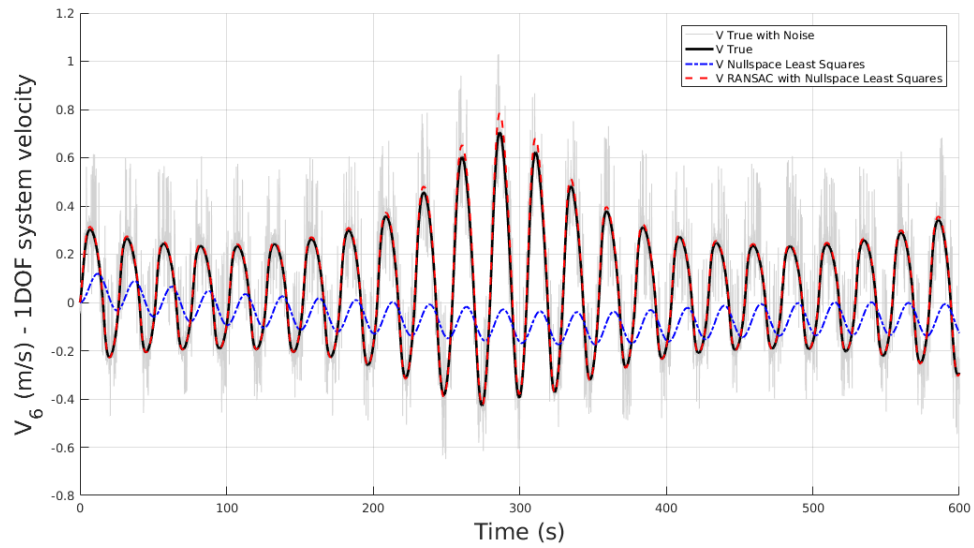


Figure 4.2: One degree of freedom plant velocity in forward simulation using parameters identified by each method. Fraction of outliers = 0.13

The estimation error of both NBLS and DIRANSAC with a NBLs kernel increases as the outlier ratio increases. However, these results indicate the estimation error using the DIRANSAC method is consistently lower than that of the NBLs method and the performance improvement over the traditional NBLs methods increases as the outlier ratio increases.

Chapter 5

Conclusion

Accurate identification of dynamical models for underwater robotic vehicles is useful for predictive simulation studies, model-based control algorithms, and model-based approaches to fault detection. The process of model identification or model estimation can be separated into two steps. First, the structure of the dynamical model can be developed using first principles. Chapter 2 accomplished this by reporting a derivation of the equations of motion (EOM) of underwater vehicles using Newtonian dynamics. The second step of model identification involves experimentally identifying the unknown parameters that enter into the dynamical model. Chapter 3 and Chapter 4 each reported new methods to accomplish this task.

Chapter 3 reported a simulation study with results that indicate the adaptive identifier (AID) reported in [36] can be extended to underactuated three degree of freedom (3-DOF) unmanned underwater vehicles (UUVs). Chapter 3 also reported an extension of the same AID to simultaneously identify plant and control parameters for six degree of freedom (6-DOF) UUVs. An additional extension of the AID to UUV plants of diagonal mass and drag matrices was reported.

Chapter 4 reported a new method for parameter identification of dynamical systems using the random sample consensus (RANSAC) framework. Simulation studies suggest that the new Dynamical Plant Identification using RANSAC (DIRANSAC) algorithm offers improvements over traditional least squares methods when estimating parameters of plants using observational data corrupted by non-Gaussian noise.

5.1 Future Work

- **Model-based fault detection:** Underwater vehicles may experience faults during deployment which could include thruster failure, chassis damage, and changes in buoyancy. These faults would result in large changes to model parameters such as thruster coefficients, drag, and mass. The AID reported in Chapter 3 can be implemented on board a UUV to run in real time. As a result, the AID may be able to detect significant changes in the adaptively identified parameter set during a mission. If the changes indicate a possible fault condition, the UUV could execute recovery behaviors.
- **Parameter Identification of Non-Traditional Underwater Locomotion:** The methods reported in Chapter 3 and Chapter 4 might be used to identify the control parameters of some non-traditional locomotion methods such as bio-inspired jet propulsion or fin undulation. The DIRANSAC algorithm was shown to be robust to non-Gaussian noise which may prove useful for fitting models that are finite approximations of perhaps infinite dimensional locomotion dynamics.

Appendices

Appendix A

On the Relationship Between “Derivative” and “Integral” Methods used in Least Squares Parameter Estimation of Dynamical Plant Models

This appendix reports a relationship between the “Integral Method” and the “Derivative Method” in Nullspace Based Least Squares (NBLS) parameter estimation. This result may have broader applicability to the relationships between “Integral Methods” and “Derivative Methods” in other least squares solutions such as Ordinary Least Squares (OLS) and Total Least Squares (TLS).

Section A.1 reports a definition of the “Derivative Method”. Section A.2 reports a definition of two different formulations of the “Integral Method”. Section A.3 reports a proof showing the relationship between the two methods when applied to NBLS parameter estimation.

A.1 Regressor Matrix Formulation using “Derivative Method”

Using the convention defined in [12] we consider six degree of freedom (6-DOF) underwater robotic dynamical plants of the form

$$\boldsymbol{\tau}(\boldsymbol{v}, \boldsymbol{\omega}, \boldsymbol{\eta}, \boldsymbol{\gamma}) = \boldsymbol{M} \begin{vmatrix} \dot{\boldsymbol{v}} \\ \dot{\boldsymbol{\omega}} \end{vmatrix} + (\boldsymbol{D}(\boldsymbol{v}, \boldsymbol{\omega}) + \boldsymbol{C}(\boldsymbol{v}, \boldsymbol{\omega})) \begin{vmatrix} \boldsymbol{v} \\ \boldsymbol{\omega} \end{vmatrix} + \boldsymbol{g}(\boldsymbol{\eta}, \boldsymbol{\gamma}), \quad (\text{A.1})$$

where the mass matrix \boldsymbol{M} is diagonal. $\boldsymbol{\tau}(\boldsymbol{v}, \boldsymbol{\omega}, \boldsymbol{\eta}, \boldsymbol{\gamma})$ is the control vector function where $\boldsymbol{\gamma}$ are the control inputs. In NBLS parameter estimation we define the vector $\boldsymbol{\theta}_p \in \mathbb{R}^n$ to be a vector of n unknown parameters to be estimated. Let the structure of $\boldsymbol{\theta}_p$ be defined as

$$\boldsymbol{\theta}_p = [\boldsymbol{m}_p^T \quad \dots]^T \in \mathbb{R}^n, \quad (\text{A.2})$$

where

$$\boldsymbol{m}_p = [m_{11} \quad m_{22} \quad m_{33} \quad m_{44} \quad m_{55} \quad m_{66}]^T \in \mathbb{R}^6 \quad (\text{A.3})$$

is a vector of unknown mass parameters. This appendix only considers dynamical plants with diagonal mass matrices for clarity, but this analysis can be extended to plants with mass matrices that are symmetric such as those found in [36].

Since all the unknown parameters in θ_p enter linearly into (A.1), the EOM can be rearranged and written in the form

$$0 = \frac{\partial}{\partial \theta_p} \left[M \begin{vmatrix} \dot{v} \\ \dot{\omega} \end{vmatrix} + (D(v, \omega) + C(v, \omega)) \begin{vmatrix} v \\ \omega \end{vmatrix} + g(\eta, \gamma) - \tau(v, \omega, \eta, \gamma) \right] \theta_p \quad (\text{A.4})$$

$$0 = W(\dot{v}, \dot{\omega}, v, \omega, \eta, \gamma) \theta_p,$$

where $W(\dot{v}, \dot{\omega}, v, \omega, \eta, \gamma)$ is the regressor matrix. Let W_{t_i} be the regressor matrix computed with observations made at time t_i . Each W_{t_i} matrix can be appended to the end of the matrix \overline{W} as

$$\overline{W} = \begin{vmatrix} W_{t_0} \\ W_{t_1} \\ \vdots \\ W_{t_i} \end{vmatrix} \quad t_i \in [t_0, t_n]. \quad (\text{A.5})$$

If the parameter vector $\theta_p \neq \mathbf{0} \in \text{NULL}(W_{t_i}) \quad \forall i$ then $\theta_p \in \text{NULL}(\overline{W}^T \overline{W})$. The basis for the proof of this statement is found in [19].

It follows directly in [19] that

$$\text{NULL}(\overline{W}^T \overline{W}) = \bigcap_{t_i \in [t_0, t_n]} \text{NULL}(W_{t_i}^T W_{t_i}). \quad (\text{A.6})$$

Each regressor W_{t_i} is at most rank 6 (for this 6-DOF system) and thus the product $W_{t_i}^T W_{t_i}$ must have a null space of at least dimension $n-6$. Although the structure of the regressor matrix W is constant and specific to the derivation above, the entries in (and thus the null space of) W_{t_i} will change as the plant (or vehicle) is subject to different excitation modes (maneuvers). Thus the plant should be excited in as many modes as possible. This will reduce the dimension of the intersection given in (A.6), or equivalently reduce the dimension $\text{NULL}(\overline{W}^T \overline{W})$. In theory over time more regressors with orthogonal null spaces are appended to \overline{W} and the dimension $\text{NULL}(\overline{W}^T \overline{W})$ will be one. When this occurs, θ_p will be in the image of a one dimensional subspace and thus defined up to scale.

A.2 Regressor Matrix Formulation using “Integral Method”

To avoid derivatives of signals v, ω both sides of (A.4) can be integrated from t_0 to some time step t_i as

$$\int_{t_0}^{t_i} 0 dt = \int_{t_0}^{t_i} \mathbf{W}(\dot{v}, \dot{\omega}, v, \omega, \eta, \gamma) \boldsymbol{\theta}_p dt \quad (\text{A.7})$$

$$0 = \int_{t_0}^{t_i} \left[\mathbf{W}(\dot{v}, \dot{\omega}, 0, 0, 0, 0) \right. \quad (\text{A.8})$$

$$\left. + \mathbf{W}(0, 0, v, \omega, \eta, \gamma) \right] dt \boldsymbol{\theta}_p \quad (\text{A.9})$$

$$0 = \left[\int_{t_0}^{t_i} \mathbf{W}(\dot{v}, \dot{\omega}, 0, 0, 0, 0) dt \right. \quad (\text{A.10})$$

$$\left. + \int_{t_0}^{t_i} \mathbf{W}(0, 0, v, \omega, \eta, \gamma) dt \right] \boldsymbol{\theta}_p. \quad (\text{A.11})$$

If the mass matrix is assumed to be diagonal, then $\widehat{\mathbf{W}}$ can be defined to be

$$\widehat{\mathbf{W}} \Big|_{t_i} = \int_{t_0}^{t_i} \mathbf{W}(\dot{v}, \dot{\omega}, 0, 0, 0, 0) dt \quad (\text{A.12})$$

$$\widehat{\mathbf{W}} \Big|_{t_i} = \begin{bmatrix} w_{11} & 0 & 0 & 0 & 0 & 0 & 0 & \dots & 0 \\ 0 & w_{22} & 0 & 0 & 0 & 0 & 0 & \dots & 0 \\ 0 & 0 & w_{33} & 0 & 0 & 0 & 0 & \dots & 0 \\ 0 & 0 & 0 & w_{44} & 0 & 0 & 0 & \dots & 0 \\ 0 & 0 & 0 & 0 & w_{55} & 0 & 0 & \dots & 0 \\ 0 & 0 & 0 & 0 & 0 & w_{66} & 0 & \dots & 0 \end{bmatrix},$$

where

$$w_{11} = u(t_i) - u(t_0) \quad w_{44} = a(t_i) - a(t_0) \quad (\text{A.13})$$

$$w_{22} = v(t_i) - v(t_0) \quad w_{55} = b(t_i) - b(t_0) \quad (\text{A.14})$$

$$w_{33} = w(t_i) - w(t_0) \quad w_{66} = c(t_i) - c(t_0). \quad (\text{A.15})$$

We substitute (A.12) into (A.11) and use Simpson's rule to numerically integrate the second term to obtain

$$0 = \left[\widehat{\mathbf{W}} \Big|_{t_i} + \int_{t_0}^{t_i} \mathbf{W}(0, 0, \nu, \omega, \eta, \gamma) dt \right] \boldsymbol{\theta}_p \quad (\text{A.16})$$

$$0 = \left[\widehat{\mathbf{W}} \Big|_{t_i} + \sum_{k=1}^i \int_{t_{k-1}}^{t_k} \mathbf{W}(0, 0, \nu, \omega, \eta, \gamma) dt \right] \boldsymbol{\theta}_p \quad (\text{A.17})$$

$$0 = \left[\widehat{\mathbf{W}} \Big|_{t_i} + \sum_{k=1}^i \left[\frac{\Delta t}{3n} \left[\mathbf{W} \Big|_{\dot{v}, \dot{\omega}=0, x=x(t_{k-1})} + 2 \sum_{j=1}^{n/2-1} \mathbf{W} \Big|_{\dot{v}, \dot{\omega}=0, x=x_{2j}} \right. \right. \right. \quad (\text{A.18})$$

$$\left. \left. \left. + 4 \sum_{j=1}^{n/2} \mathbf{W} \Big|_{\dot{v}, \dot{\omega}=0, x=x_{2j-1}} + \mathbf{W} \Big|_{\dot{v}, \dot{\omega}=0, x=x(t_k)} \right] \right] \boldsymbol{\theta}_p \quad (\text{A.19})$$

$$0 = \widetilde{\mathbf{W}} \Big|_{t_i} \boldsymbol{\theta}_p. \quad (\text{A.20})$$

where $x_j = x(t_{k-1}) + jh$, $h = \frac{1}{n}[x(t_k) - x(t_{k-1})]$, and n is the number of intervals used in Simpson's method. The formulation above assumes that $x(t)$ is a linear function between t_{i-1} and t_i i.e. $x(t) = \frac{x_{t_i} - x_{t_{i-1}}}{t_i - t_{i-1}} * t$, $t \in [t_{i-1}, t_i]$. We can use trapezoidal integration instead of Simpson's rule.

The result is the following alternate formulation

$$0 = \left[\widehat{\mathbf{W}} \Big|_{t_i} + \int_{t_0}^{t_i} \mathbf{W}(0, 0, \nu, \omega, \eta, \gamma) dt \right] \boldsymbol{\theta}_p \quad (\text{A.21})$$

$$0 = \left[\widehat{\mathbf{W}} \Big|_{t_i} + \sum_{j=1}^i \left[\mathbf{W} \Big|_{\dot{v}, \dot{\omega}=0, t=t_{j-1}} + \mathbf{W} \Big|_{\dot{v}, \dot{\omega}=0, t=t_j} \right] \frac{\Delta t}{2} \right] \boldsymbol{\theta}_p \quad (\text{A.22})$$

$$0 = \widetilde{\mathbf{W}} \Big|_{t_i} \boldsymbol{\theta}_p. \quad (\text{A.23})$$

Similar to the "Derivative Method" we can observe plant states during excitation and use the data to compute the regressor matrix $\widetilde{\mathbf{W}}$. Let $\widetilde{\mathbf{W}} \Big|_{t_i}$ be the regressor matrix computed at time t_i . Each

$\widetilde{\mathbf{W}}|_{t_i}$ matrix can be appended to the end of the matrix $\overline{\mathbf{W}}_{INT}$ as

$$\overline{\mathbf{W}}_{INT} = \left[\begin{array}{c} \widetilde{\mathbf{W}}|_{t_1} \\ \widetilde{\mathbf{W}}|_{t_2} \\ \vdots \\ \widetilde{\mathbf{W}}|_{t_i} \end{array} \right] \quad t_i \in [t_1, t_n]. \quad (\text{A.24})$$

If the parameter vector $\boldsymbol{\theta}_p \neq \mathbf{0} \in \text{NULL}(\widetilde{\mathbf{W}}|_{t_i}) \quad \forall i$ then $\boldsymbol{\theta}_p \in \text{NULL}(\overline{\mathbf{W}}_{INT}^T \overline{\mathbf{W}}_{INT})$. The proof, again in found in [19], is the same as before.

A.3 Relationship Between the Nullspaces of the “Derivative Method” and “Integral Method”

Claim: The nullspaces defined in the two Sections A.1 and A.2 are related by

$$\text{NULL}\left(\lim_{\Delta t \rightarrow 0} \frac{1}{\Delta t} [\overline{\mathbf{W}}_{INT}^T \overline{\mathbf{W}}_{INT}]\right) = \text{NULL}(\overline{\mathbf{W}}^T \overline{\mathbf{W}}). \quad (\text{A.25})$$

Proof: The proof is divided into three parts: first we show that the “Integral Method” can be expressed using discrete summations, secondly we show that each of these intermediate steps is basically differentiation with a larger Δt and, finally, we show that the null spaces of the two methods are related by (A.25).

For simplicity we chose the trapezoidal integration method described in (A.23).

$$\widetilde{\mathbf{W}}|_{t_i} = \widehat{\mathbf{W}}|_{t_i} + \sum_{j=1}^i \left[\mathbf{W}|_{\dot{v}, \dot{\omega}=0, t=t_{j-1}} + \mathbf{W}|_{\dot{v}, \dot{\omega}=0, t=t_j} \right] \frac{\Delta t}{2} \quad (\text{A.26})$$

We can express the first term on the right hand side which is defined in (A.12) as a sum of intermediate time steps defined as

$$\widehat{\mathbf{W}}|_{t_i} = \sum_{j=1}^i \widetilde{\mathbf{W}}|_{t_j}, \quad (\text{A.27})$$

where

$$\widetilde{\mathbf{W}} \Big|_{t_j} = \begin{bmatrix} \check{w}_{11} & 0 & 0 & 0 & 0 & 0 & \dots & 0 \\ 0 & \check{w}_{22} & 0 & 0 & 0 & 0 & \dots & 0 \\ 0 & 0 & \check{w}_{33} & 0 & 0 & 0 & \dots & 0 \\ 0 & 0 & 0 & \check{w}_{44} & 0 & 0 & \dots & 0 \\ 0 & 0 & 0 & 0 & \check{w}_{55} & 0 & \dots & 0 \\ 0 & 0 & 0 & 0 & 0 & \check{w}_{66} & \dots & 0 \end{bmatrix}, \quad (\text{A.28})$$

and

$$\check{w}_{11} = u(t_j) - u(t_{j-1}) \quad \check{w}_{44} = a(t_j) - a(t_{j-1}) \quad (\text{A.29})$$

$$\check{w}_{22} = v(t_j) - v(t_{j-1}) \quad \check{w}_{55} = b(t_j) - b(t_{j-1}) \quad (\text{A.30})$$

$$\check{w}_{33} = w(t_j) - w(t_{j-1}) \quad \check{w}_{66} = c(t_j) - c(t_{j-1}). \quad (\text{A.31})$$

This is true by inspection. For example the entry in the first row and column is

$$\widehat{\mathbf{W}}_{11} \Big|_{t_i} = [u(t_i) - u(t_{i-1})] + [u(t_{i-1}) - u(t_{i-2})] + \dots + [u(t_2) - u(t_1)] + [u(t_1) - u(t_0)] \quad (\text{A.32})$$

$$= u(t_i) - u(t_0). \quad (\text{A.33})$$

For convenience we define $\widetilde{\widetilde{\mathbf{W}}}_j$ as

$$\widetilde{\widetilde{\mathbf{W}}}_j = \widetilde{\mathbf{W}} \Big|_{t_j} + \left[\mathbf{W} \Big|_{\dot{v}, \dot{\omega}=0, t=t_{j-1}} + \mathbf{W} \Big|_{\dot{v}, \dot{\omega}=0, t=t_j} \right] \frac{\Delta t}{2} \quad (\text{A.34})$$

$$= \int_{t_{j-1}}^{t_j} \mathbf{W}(\dot{v}, \dot{\omega}, v, \omega, \eta, \gamma) dt. \quad (\text{A.35})$$

Substituting in (A.34) and (A.27) into (A.23) yields

$$\widetilde{\mathbf{W}} \Big|_{t_i} = \sum_{j=1}^i \widetilde{\mathbf{W}} \Big|_{t_j} + \sum_{j=1}^i \left[\mathbf{W} \Big|_{\dot{v}, \dot{\omega}=0, t=t_{j-1}} + \mathbf{W} \Big|_{\dot{v}, \dot{\omega}=0, t=t_j} \right] \frac{\Delta t}{2} \quad (\text{A.36})$$

$$= \sum_{j=1}^i \left[\widetilde{\mathbf{W}} \Big|_{t_j} + \left[\mathbf{W} \Big|_{\dot{v}, \dot{\omega}=0, t=t_{j-1}} + \mathbf{W} \Big|_{\dot{v}, \dot{\omega}=0, t=t_j} \right] \frac{\Delta t}{2} \right] \quad (\text{A.37})$$

$$= \sum_{j=1}^i \widetilde{\widetilde{\mathbf{W}}}_j. \quad (\text{A.38})$$

We note that

$$\widetilde{\mathbf{W}} \Big|_{t_i} = \widetilde{\widetilde{\mathbf{W}}}_i + \widetilde{\mathbf{W}} \Big|_{t_{i-1}}. \quad (\text{A.39})$$

Since each regressor matrix is now expressed as finite sum, we will see that when divided by an arbitrarily small Δt each summand is actually equivalent to the regressor matrix defined in (A.4). This is possible because the left hand side is 0 in the NBLs problem. Substitute (A.38) into (A.23) and note that $t_j = t_{j-1} + \Delta t$. The choice of Δt is arbitrarily small and thus we can take the limit of both sides and use the Fundamental Theorem of Calculus which states that $\lim_{\Delta t \rightarrow 0} \frac{1}{\Delta t} [\int_{t_{j-1}}^{t_j} \dot{x}(t) dt] = \dot{x}(t_j)$. These steps result in

$$0 = \left[\sum_{j=1}^i \widetilde{\widetilde{\mathbf{W}}}_j \right] \boldsymbol{\theta}_p \quad (\text{A.40})$$

$$\lim_{\Delta t \rightarrow 0} \frac{1}{\Delta t} 0 = \lim_{\Delta t \rightarrow 0} \frac{1}{\Delta t} \left[\sum_{j=1}^i \widetilde{\widetilde{\mathbf{W}}}_j \right] \boldsymbol{\theta}_p \quad (\text{A.41})$$

$$0 = \lim_{\Delta t \rightarrow 0} \left[\sum_{j=1}^i \left[\frac{1}{\Delta t} \left[\widetilde{\mathbf{W}} \Big|_{t_j} + \left[\mathbf{W} \Big|_{\dot{v}, \dot{\omega}=0, t=t_{j-1}} + \mathbf{W} \Big|_{\dot{v}, \dot{\omega}=0, t=t_j} \right] \frac{\Delta t}{2} \right] \right] \boldsymbol{\theta}_p \quad (\text{A.42})$$

$$0 = \lim_{\Delta t \rightarrow 0} \left[\sum_{j=1}^i \left[\frac{1}{\Delta t} \widetilde{\mathbf{W}} \Big|_{t_j} + \left[\mathbf{W} \Big|_{\dot{v}, \dot{\omega}=0, t=t_{j-1}} + \mathbf{W} \Big|_{\dot{v}, \dot{\omega}=0, t=t_j} \right] \frac{1}{2} \right] \right] \boldsymbol{\theta}_p \quad (\text{A.43})$$

$$0 = \sum_{j=1}^i \left[\lim_{\Delta t \rightarrow 0} \frac{1}{\Delta t} \left[\int_{t_{j-1}}^{t_j} \mathbf{W}(\dot{v}, \dot{\omega}, v, \omega, \eta, \gamma) \Big|_{t_j} dt \right] \right] \boldsymbol{\theta}_p \quad (\text{A.44})$$

$$0 = \sum_{j=1}^i \left[\mathbf{W}(\dot{v}, \dot{\omega}, v, \omega, \eta, \gamma) \Big|_{t_j} \right] \boldsymbol{\theta}_p. \quad (\text{A.45})$$

We use (A.39) and note that $\widetilde{\mathbf{W}}|_{t_0} = \mathbf{0}$ to express $\overline{\mathbf{W}}_{INT}$ as

$$\overline{\mathbf{W}}_{INT} = \begin{bmatrix} \widetilde{\mathbf{W}}|_{t_1} \\ \widetilde{\mathbf{W}}|_{t_2} \\ \widetilde{\mathbf{W}}|_{t_3} \\ \vdots \\ \widetilde{\mathbf{W}}|_{t_i} \end{bmatrix} = \begin{bmatrix} \widetilde{\mathbf{W}}_1 \\ \widetilde{\mathbf{W}}_2 + \widetilde{\mathbf{W}}|_{t_1} \\ \widetilde{\mathbf{W}}_3 + \widetilde{\mathbf{W}}|_{t_2} \\ \vdots \\ \widetilde{\mathbf{W}}_i + \widetilde{\mathbf{W}}|_{t_{i-1}} \end{bmatrix} = \begin{bmatrix} \widetilde{\mathbf{W}}_1 \\ \widetilde{\mathbf{W}}_2 + \widetilde{\mathbf{W}}_1 \\ \widetilde{\mathbf{W}}_3 + \widetilde{\mathbf{W}}_2 + \widetilde{\mathbf{W}}_1 \\ \vdots \\ \widetilde{\mathbf{W}}_i + \widetilde{\mathbf{W}}_{i-1} + \dots + \widetilde{\mathbf{W}}_1 \end{bmatrix} \quad i = 1, 2, 3, \dots n. \quad (\text{A.46})$$

We can use the structure in (A.46) to rewrite $\overline{\mathbf{W}}_{INT}$ as

$$\overline{\mathbf{W}}_{INT} = \begin{bmatrix} I_6 & 0 & 0 & \dots & 0 \\ I_6 & I_6 & 0 & \dots & 0 \\ I_6 & I_6 & I_6 & \dots & 0 \\ \vdots & \vdots & \vdots & \ddots & 0 \\ I_6 & I_6 & I_6 & \dots & I_6 \end{bmatrix} \begin{bmatrix} \widetilde{\mathbf{W}}_1 \\ \widetilde{\mathbf{W}}_2 \\ \widetilde{\mathbf{W}}_3 \\ \vdots \\ \widetilde{\mathbf{W}}_i \end{bmatrix} \quad (\text{A.47})$$

$$= A\overline{\mathbf{W}}, \quad (\text{A.48})$$

where I_n is the $n \times n$ identity matrix. From [19] we note that

$$NULL(\overline{\mathbf{W}}_{INT}^T \overline{\mathbf{W}}_{INT}) = NULL(\overline{\mathbf{W}}^T A^T A \overline{\mathbf{W}}) = NULL(A\overline{\mathbf{W}}), \quad (\text{A.49})$$

and similarly

$$NULL(\overline{\mathbf{W}} \overline{\mathbf{W}}^T) = NULL(\overline{\mathbf{W}}). \quad (\text{A.50})$$

Finally we need to show the following:

FACT: $NULL(A\overline{\mathbf{W}}) = NULL(\overline{\mathbf{W}})$

PROOF: A is triangular with non zero entries on the diagonal thus all eigenvalues of A are non zero and thus A is invertible. Let $x \in NULL(A\overline{\mathbf{W}})$ and therefore $A\overline{\mathbf{W}}x = \mathbf{0}$. Since A is invertible $A^{-1}A\overline{\mathbf{W}}x = A^{-1}\mathbf{0} \rightarrow \overline{\mathbf{W}}x = \mathbf{0}$ and $x \in NULL(\overline{\mathbf{W}})$. Therefore $NULL(A\overline{\mathbf{W}}) \subseteq NULL(\overline{\mathbf{W}})$. Now let $x \in NULL(\overline{\mathbf{W}})$ and thus $A\overline{\mathbf{W}}x = A\mathbf{0} = \mathbf{0}$ and therefore $x \in NULL(A\overline{\mathbf{W}})$ and $NULL(A\overline{\mathbf{W}}) \supseteq NULL(\overline{\mathbf{W}})$. Since $NULL(A\overline{\mathbf{W}}) \subseteq NULL(\overline{\mathbf{W}})$ and $NULL(A\overline{\mathbf{W}}) \supseteq NULL(\overline{\mathbf{W}})$ then $NULL(A\overline{\mathbf{W}}) = NULL(\overline{\mathbf{W}})$

As a consequence we can say that

$$NULL(\overline{\mathbf{W}}_{INT}^T \overline{\mathbf{W}}_{INT}) = NULL(A\overline{\mathbf{W}}) = NULL(\overline{\mathbf{W}}) = NULL(\overline{\mathbf{W}}^T \overline{\mathbf{W}}). \quad (\text{A.51})$$

Therefore we use the argument regarding arbitrarily small time steps as described in (A.45) to show that

$$NULL(\lim_{\Delta t \rightarrow 0} \frac{1}{\Delta t} [\overline{\mathbf{W}}]) = NULL(\overline{\mathbf{W}}). \quad (\text{A.52})$$

This completes the proof. The implication is that with arbitrary $\frac{1}{\Delta t'}$

$$NULL(\overline{\mathbf{W}}_{INT}^T \overline{\mathbf{W}}_{INT}) = NULL(\overline{\mathbf{W}}^T \overline{\mathbf{W}}) \approx NULL(\overline{\mathbf{W}}^T \overline{\mathbf{W}}), \quad (\text{A.53})$$

or the subspaces are equivalent.

Bibliography

- [1] D. P. Capel, "An effective bail-out test for ransac consensus scoring," in *British Machine Vision Conference*, Sep. 2005, pp. 629–638.
- [2] S. Choi and J.-H. Kim, "Robust regression to varying data distribution and its application to landmark-based localization," in *Systems, Man and Cybernetics, 2008. IEEE International Conference on*, IEEE, 2008, pp. 3465–3470.
- [3] S. Choi, T. Kim, and W. Yu, "Performance evaluation of ransac family," *Journal of Computer Vision*, vol. 24, no. 3, pp. 271–300, 1997.
- [4] O Chum, J. Matas, and S Obdrzalek, "Enhancing ransac by generalized model optimization," *Asian Conference on Computer Vision*, vol. 2, pp. 812–817, Jan. 2004.
- [5] O. Chum and J. Matas, "Matching with prosac-progressive sample consensus," in *Computer Vision and Pattern Recognition, IEEE Computer Society Conference on*, IEEE, vol. 1, 2005, pp. 220–226.
- [6] O. M. Curet, N. A. Patankar, G. V. Lauder, and M. A. MacIver, "Mechanical properties of a bio-inspired robotic knifefish with an undulatory propulsor," *Bioinspiration and Biomimetics*, vol. 6, no. 2, p. 026004, 2011.
- [7] O. Faltinsen, *Sea Loads on Ships and Offshore Structures*, ser. Cambridge Ocean Technology Series. Cambridge University Press, 1993.
- [8] S. Farahmand, G. B. Giannakis, and D. Angelosante, "Doubly robust smoothing of dynamical processes via outlier sparsity constraints," *IEEE Transactions on Signal Processing*, vol. 59, no. 10, pp. 4529–4543, 2011.
- [9] J Feldman, "Standard equations of motion for submarine simulation," US Department of Defense, Tech. Rep., 1979.
- [10] C. Feng and Y. Hung, "A robust method for estimating the fundamental matrix.," *Digital Image Computing: Techniques and Applications*, pp. 633–642, Dec. 2003.
- [11] M. A. Fischler and R. C. Bolles, "Random sample consensus: A paradigm for model fitting with applications to image analysis and automated cartography," *Communications of the Association for Computing Machinery*, vol. 24, no. 6, pp. 381–395, Jun. 1981.
- [12] T. I. Fossen, *Guidance and Control of Ocean Vehicles*. John Wiley and Sons, 1994.
- [13] M. Gertler and G. R. Hagen, "Standard equations of motion for submarine simulation," David W Taylor Naval Ship Research and Development Center Bethesda MD, Tech. Rep., 1967.
- [14] A. Goodman, "Experimental techniques and methods of analysis used in submerged body research," in *Proc. of the Third Symposium on Naval Hydromechanics*, 1960.

- [15] J. G. Graver, R. Bachmayer, N. E. Leonard, and D. M. Fratantoni, "Underwater glider model parameter identification," in *Proc. 13th Int. Symp. on Unmanned Untethered Submersible Technology (UUST)*, vol. 1, 2003, pp. 12–13.
- [16] E. Gray, *The Devil's Device: Robert Whitehead and the History of the Torpedo*. Naval Institute Press, 1991.
- [17] R. I. Hartley, "In defense of the eight-point algorithm," *IEEE Transactions on Pattern Analysis and Machine Intelligence*, vol. 19, no. 6, pp. 580–593, Jun. 1997.
- [18] O. Hegrenaes, O. Hallingstad, and B. Jalving, "Comparison of mathematical models for the hugin 4500 auv based on experimental data," in *2007 Symposium on Underwater Technology and Workshop on Scientific Use of Submarine Cables and Related Technologies*, Apr. 2007, pp. 558–567.
- [19] R. Horn and C. Johnson, *Matrix Analysis*. Cambridge University Press, 2012.
- [20] J. J. Hubbard, M. Fleming, V. Palmre, D. Pugal, K. J. Kim, and K. K. Leang, "Monolithic ipmc fins for propulsion and maneuvering in bioinspired underwater robotics," *IEEE Journal of Oceanic Engineering*, vol. 39, no. 3, pp. 540–551, Jul. 2014.
- [21] S. V. Huffel and J. Vandewalle, "On the accuracy of total least squares and least squares techniques in the presence of errors on all data," *Automatica*, vol. 25, no. 5, pp. 765–769, 1989.
- [22] D. Humphreys and K. Watkinson, "Prediction of acceleration hydrodynamic coefficients for underwater vehicles from geometric parameters," Naval Coastal Systems Lab Panama City FL, Tech. Rep., 1978.
- [23] F. H. Imlay, "The complete expressions for added mass of a rigid body moving in an ideal fluid," David Taylor Model Basin Washington DC, Tech. Rep., 1961.
- [24] T. R. Kane and D. A. Levinson, *Dynamics, Theory and Applications*. McGraw Hill, 1985.
- [25] M. Kang, L. Tang, and J. Gao, "Computational modeling of phagocyte transmigration for foreign body responses to subcutaneous biomaterial implants in mice," *BioMed Central: Bioinformatics*, vol. 17, no. 1, p. 111, 2016.
- [26] G. C. Karras, C. P. Bechlioulis, M. Leonetti, N. Palomeras, P. Kormushev, K. J. Kyriakopoulos, and D. G. Caldwell, "On-line identification of autonomous underwater vehicles through global derivative-free optimization," in *2013 IEEE/RSJ International Conference on Intelligent Robots and Systems*, Nov. 2013, pp. 3859–3864.
- [27] M. Krieg and K. Mohseni, "Thrust characterization of a bioinspired vortex ring thruster for locomotion of underwater robots," *IEEE Journal of Oceanic Engineering*, vol. 33, no. 2, pp. 123–132, May 2008.
- [28] S. Martin and L. Whitcomb, "Preliminary Results in Experimental Identification of 3-DOF Coupled Dynamical Plant for Underwater Vehicles," in *Proceedings of MTS/IEEE Oceans*, Quebec City, Quebec, Canada, 2008, pp. 1–9.
- [29] S. C. Martin and L. Whitcomb, "Experimental identification of six-degree-of-freedom coupled dynamic plant models for underwater robot vehicles," *IEEE Journal of Oceanic Engineering*, vol. 39, no. 4, pp. 662–671, Oct. 2014.
- [30] S. C. Martin and L. L. Whitcomb, "Preliminary experiments in underactuated nonlinear model-based tracking control of underwater vehicles with three degree-of-freedom fully-coupled dynamical plant models: Theory and experimental evaluation," *Proceedings of MTS/IEEE Oceans*, pp. 1–7, 2012.
- [31] S. C. Martin, "Advances in six-degree-of-freedom dynamics and control of underwater vehicles," PhD dissertation, The Johns Hopkins University, 2008.

- [32] S. C. Martin and L. L. Whitcomb, "Experimental identification of three degree-of-freedom coupled dynamic plant models for underwater vehicles," in *Sensing and Control for Autonomous Vehicles: Applications to Land, Water and Air Vehicles*, T. I. Fossen, K. Y. Pettersen, and H. Nijmeijer, Eds. Cham: Springer International Publishing, 2017, pp. 319–341.
- [33] S. C. Martin and L. L. Whitcomb, "Nonlinear model-based tracking control of underwater vehicles with three degree-of-freedom fully coupled dynamical plant models: Theory and experimental evaluation," *IEEE Transactions on Control Systems Technology*, vol. 26, no. 2, pp. 404–414, 2018.
- [34] J. Matas and O. Chum, "Randomized ransac with td,d test," *Image and Vision Computing*, vol. 22, no. 10, pp. 837–842, 2004.
- [35] J. Matas and O. Chum, "Randomized ransac with sequential probability ratio test," in *Computer Vision, 2005. ICCV 2005. Tenth IEEE International Conference on*, IEEE, vol. 2, 2005, pp. 1727–1732.
- [36] C. J. McFarland and L. Whitcomb, "Comparative experimental evaluation of a new adaptive identifier for underwater vehicles," in *2013 IEEE International Conference on Robotics and Automation*, May 2013, pp. 4614–4620.
- [37] C. J. McFarland, "Adaptive identification and control for underwater vehicles: Theory and comparative experimental evaluations," PhD dissertation, The Johns Hopkins University, 2013.
- [38] R. M. Murray, Z. Li, and S. S. Sastry, *A Mathematical Introduction to Robotic Manipulation*. CRC Press, 1994.
- [39] K. S. Narendra and A. M. Annaswamy, *Stable Adaptive Systems*. Dover, 1989.
- [40] S. Natarajan, C. Gaudig, and M. Hildebrandt, "Offline experimental parameter identification using on-board sensors for an autonomous underwater vehicle," in *Proceedings of MTS/IEEE Oceans*, Oct. 2012, pp. 1–8.
- [41] S. of Naval Architects, M. E. U. Technical, and R. C. H. Subcommittee, *Nomenclature for Treating the Motion of a Submerged Body Through a Fluid: Report of the American Towing Tank Conference*, ser. Technical and research bulletin. Society of Naval Architects and Marine Engineers, 1950.
- [42] P. Ridao, A. Tiano, A. El-Fakdi, M. Carreras, and A. Zirilli, "On the identification of non-linear models of unmanned underwater vehicles," *Control Engineering Practice*, vol. 12, no. 12, pp. 1483–1499, 2004, Guidance and control of underwater vehicles.
- [43] M. T. Sabet, H. M. Daniali, A. Fathi, and E. Alizadeh, "Identification of an autonomous underwater vehicle hydrodynamic model using the extended, cubature, and transformed unscented kalman filter," *IEEE Journal of Oceanic Engineering*, vol. 43, no. 2, pp. 457–467, Apr. 2018.
- [44] T. Salumäe and M. Kruusmaa, "Flow-relative control of an underwater robot," *Proceedings of the Royal Society of London A: Mathematical, Physical and Engineering Sciences*, vol. 469, no. 2153, 2013.
- [45] R. Schnabel, R. Wahl, and R. Klein, "Efficient ransac for point-cloud shape detection," *Computer Graphics Forum*, vol. 26, no. 2, pp. 214–226, Jun. 2007.
- [46] S.-G. Seo, "Safer and more efficient ship handling with the pivot point concept," *TransNav, the International Journal on Marine Navigation and Safety of Sea Transportation*, vol. 10, pp. 605–612, Jan. 2016.
- [47] D. Simpson, "Introduction to rousseeuw (1984) least median of squares regression," in *Breakthroughs in Statistics*, Springer, 1997, pp. 433–461.

- [48] D. A. Smallwood and L. Whitcomb, "Adaptive identification of dynamically positioned underwater robotic vehicles," *IEEE Transactions on Control Systems Technology*, vol. 11, no. 4, pp. 505–515, 2003.
- [49] A. Tiano, R. Sutton, A. Lozowicki, and W. Naeem, "Observer kalman filter identification of an autonomous underwater vehicle," *Control Engineering Practice*, vol. 15, pp. 727–739, Jun. 2007.
- [50] B. J. Tordoff and D. W. Murray, "Guided-mlesac: Faster image transform estimation by using matching priors," *IEEE Transactions on Pattern Analysis and Machine Intelligence*, vol. 27, no. 10, pp. 1523–1535, 2005.
- [51] P. H. Torr and A. Zisserman, "Mlesac: A new robust estimator with application to estimating image geometry," *Computer Vision and Image Understanding*, vol. 78, no. 1, pp. 138–156, 2000.
- [52] M. Uhercik, J. Kybic, H. Liebgott, and C. Cachard, "Model fitting using ransac for surgical tool localization in 3-d ultrasound images," *IEEE Transactions on Biomedical Engineering*, vol. 57, no. 8, pp. 1907–1916, Aug. 2010.
- [53] S. Van Huffel and J. Vandewalle, *The Total Least Squares Problem: Computational Aspects and Analysis*, ser. Frontiers in Applied Mathematics. Society for Industrial and Applied Mathematics, 1991.
- [54] P. W. van de Ven, T. A. Johansen, A. J. S. Åyrensen, C. Flanagan, and D. Toal, "Neural network augmented identification of underwater vehicle models," *Control Engineering Practice*, vol. 15, no. 6, pp. 715–725, 2007, Special Section on Control Applications in Marine Systems.
- [55] B. Wehbe, M. Hildebrandt, and F. Kirchner, "Experimental evaluation of various machine learning regression methods for model identification of autonomous underwater vehicles," in *2017 IEEE International Conference on Robotics and Automation (ICRA)*, May 2017, pp. 4885–4890.
- [56] N.-L. Wu, X.-Y. Wang, T. Ge, C. Wu, and R. Yang, "Parametric identification and structure searching for underwater vehicle model using symbolic regression," *Journal of Marine Science and Technology*, vol. 22, no. 1, pp. 51–60, 2017.

Vita

Tyler Paine was born in Seattle, Washington in 1989, and spent most of his youth in Montana. He graduated from Montana State University in 2011 with a degree in Mechanical Engineering. Tyler works as a design and manufacturing engineer at the Naval Undersea Warfare Center Division Keyport. In 2016 he received the Science, Mathematics and Research for Transformation (SMART) scholarship from the Department of Defense to pursue a Masters of Science in Engineering at the Johns Hopkins University.